ABSTRACT

This thesis is concerned with the measurement and interpretation of the thermophysical properties of certain simple molecules and their mixtures. The work has three main aims:

i) To provide further accurate measurements of shear viscosities for dilute gases and their mixtures at low temperature (below 300K) in order to provide the necessary data which is required in order to establish the appropriate intermolecular potential energy functions.

ii) The development of "data inversion" techniques for thermophysical properties which enable a unique potential to be established for simple species such as the inert gases.

iii) To carry out a preliminary investigation of anistropic molecules concentrating on model systems and the study of the way in which inversion methods can be applied to these anisotropic systems.

The measurement of shear viscosities has been performed by Clarke (1) and Gough (2) at low temperatures and by Dawe, Maitland and Matthews (3,5) at high temperatures. These measurements were made on a capillary viscometer for the inversion of viscosity data. It is necessary to have data over as wide a temperature range as possible from just above the boiling point of the gas up to at least 1600K. This wide range of temperature then enables a unique potential to be obtained from the inversion methods. In the present work, therefore, we measured the gaseous viscosities of Ar-Xe mixtures at temperatures in the range 180-300K in order to supplement the measurements made at high temperatures by Matthews. This work involved the reconstruction of a low temperature gas viscometer. Measurements were made at several temperatures for the argon-xenon mixtures and for a standard gas. From the ratios of the ratios of these flows, after several small though crucial corrections had been made, accurate viscosities for argon-xenon mixtures were determined. These results were in very good agreement with the previous measurements of Kestin, Khalifa and Wakeham (6), being within 1% of their measurements.

The second area of research involved the development of data inversion techniques. An inversion method is concerned with the calculation of potential functions from thermophysical properties such as viscosities and second virial coefficients. These inversion methods are, in general, very difficult to perform as the property

at any individual temperature is a complex function of the entire potential function over all separation and energies. However, in recent years an inversion method has been developed by Gough, Maitland and Smith (7) which yields the complete potential function from viscosity data. The methods of inverting second virial coefficients have until recently been more limited. Though able to produce the repulsive branch of the potential uniquely they were only able to produce in the attractive region the well depth as a function of well width (8). In the work described in this thesis, however, we were able to develop an inversion method for second virial coefficients which could reproduce the entire potential function (9,10), even though in principle, such a procedure was thought impossible (11). We attribute this success to the continuity of the potential function and its first derivative through $U(r) = 0$. In addition we showed that it was possible with data of high accuracy, as well as with data incorporating random errors, to obtain a very good estimate of the well depth parameter when no prior value of this parameter was known (10). However, when this method was applied to the experimental data for argon it indicated a potential well with a depth which was 5% too deep as compared with the best modern potentials for argon. This suggested that the data for argon may contain systematic errors at low temperatures.

Also in this area of the investigations, an inversion method was developed for thermal diffusion data which enabled the slope of the potential rather than the potential itself to be obtained. This method was applied to the experimental data for argon and krypton (12). The inversion methods for viscosity were applied to the argon-xenon viscosities and argon-nitrogen viscosities to yield potential energy functions for these unlike-interactions.

The final section of the thesis is concerned with a study of the inversion of properties from anistropic potentials. The results of these investigations were very interesting as they demonstrated that <u>one potential</u> of spherical form resulted from the inversion of both transport properties (calculated using the Mason Monchick approximation (13)) and second virial coefficients calculated for a model anisotropic system. This potential accurately reproduced the transport and gas imperfection data over the whole range of temperature investigated (14).

We investigated the way in which the averaging of the anisotropic function could give rise to the potential produced on inversion. This investigation of the properties for anisotropic systems is just beginning and this work suggests that this area of research could provide rich results in the future.

References

1. A.J. Clarke, D.Phil. Thesis., Oxford University, 1969.
2. D.W. Gough, D.Phil. Thesis, Oxford University, 1974.
3. R.W. Dawe, D.Phil. Thesis, Oxford University, 1968.
4. G.C. Maitland, D.Phil. Thesis, Oxford University, 1972.
5. G.P. Matthews, D.Phil. Thesis, Oxford University, 1976.
6. J. Kestin, H.E. Khalifa and W.A. Wakeham, Physica, 90A (1978) 215.
7. D.W. Gough, G.C. Maitland and E.B. Smith, Mol. Phys., 24 (1974) 151.
8. G.C. Maitland and E.B. Smith, Mol. Phys. 24 (1972) 1185.
9. H.E. Cox, F.W. Crawford, E.B. Smith and A.R. Tindell, Mol. Phys. 40 (1980) 705.
10. E.B. Smith, A.R. Tindell, B.H. Wells and F.W. Crawford, Mol. Phys. 42 (1981) 937.
11. H.L. Frisch and E. Helfand, J.Chem.Phys. 32 (1960) 269.
12 E.B. Smith, A.R. Tindell, B.H. Wells and J.L. Brun, Physica 106C (1981) 117.
13. L. Monchick and E.A. Mason, J.Chem.Phys. 35 (1961) 1676.
14. E.B. Smith, D.J. Tildesley, A.R. Tindell and S.J. Price, Chem. Phys. Lett. 74 (1980) 193.

SOME STUDIES ON MOLECULAR INTERACTIONS

A thesis submitted for the degree of

Doctor of Philosophy

by

ANDREW ROBERT TINDELL

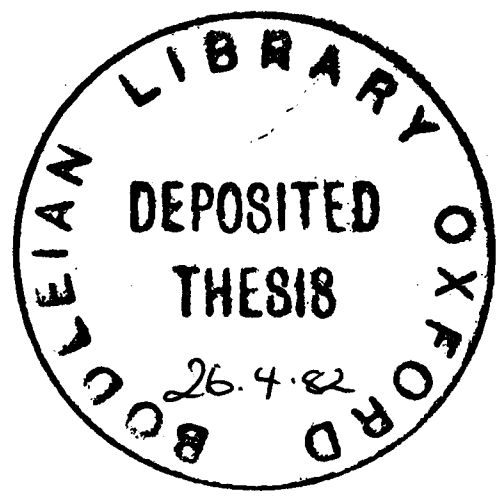
Physical Chemistry Laboratory

Oxford

St. Catherine's College

Oxford.

October 1981



The truth is rarely pure and never simple

The Importance of Being Earnest (1895)
Oscar Wilde

ACKNOWLEDGEMENTS

I would like to express my gratitude to the following people:

Dr E.B. Smith, my supervisor, for his enormous enthusiasm, not only in this project, but in all things.

Dr G.P. Matthews for help with the reconstruction of the viscometer, and many useful discussions concerning the experimental side of the work.

Mr B.H. Wells for many helpful discussions in sometimes difficult circumstances.

My wife, Deborah, for putting up with the trials and tribulations involved during the course of the work.

CONTENTS

	Page
CHAPTER ONE	
THE NATURE AND DETERMINATION OF INTERMOLECULAR FORCES	
A. Introduction	1
B. Theoretical Calculation	6
(a) Variational Calculations	7
(b) Perturbation Calculations	
(i) Long Range	9
(ii) Short Range	16
(iii) Very Long Range	16
(iv) Model Calculations	16
C. Experimental Sources of Information	17
(i) Gas Imperfection	18
(ii) Transport Properties of Dilute Gases	20
(iii) Spectroscopic Information	23
(iv) Molecular Beams	27
(v) Solid State Properties	30
D. The Representation of Pair Potential Energy Functions	33
CHAPTER TWO	
MOLECULAR THEORY OF GASES	39
A. Simple Kinetic Theory of Dilute Gases	39
(i) Viscosity	41
(ii) Thermal Conductivity	44
(iii) Diffusion	46
(iv) Comparison of Simple Kinetic Theory with Rigorous Kinetic Theory	47

(v) Application ot Real Gases 48

B. Rigorous Kinetic Theory 49

(i) The Dynamics of Molecular Collisions 49

(ii) Boltzmann Equation 53

(iii) Maxwell-Boltzmann equilibrium velocity distribution 59

C. Chapman-Enskog Solution 61

(i) The Zeroth Order Solution 66

(ii) First-Order Solution 66

(iii) Reduced Collision Integrals 68

(iv) Transport Coefficients for Binary Mixtures 70

D. Polyatomic Gases 72

(i) Semi Classical Theory 72

(ii) Classical Theory 73

(iii) Semi Classical Transport Coefficients 74

(iv) The Mason Monchick Approximation 75

E. Quantum Effects 76

CHAPTER THREE

THE MEASUREMENT OF VISCOSITY 77

A. Theory 77

(a) Theory of Capillary Flow 79

(i) Laminar or Poiseuillian Flow 79

(ii) Turbulent Flow 80

(iii) Slip Flow 80

(iv) Free Molecule Flow 80

(b) Corrections to Poiseuille's Equation 83
(i) Slip 83
(ii) Correction for Non-Ideality 86
(iii) Kinetic Energy Correction 87
(iv) Curve Pipe Flow Correction 88
(c) Theory of the Present Apparatus 90
B. Experimental Details 94
(a) Viscometer 94
(b) Control and Measurement of Temperature 97
(i) The Cryostat 98
(ii) Temperature Control 100
(iii) Temperature Measurement 102
(iv) The Gas Line 103
(v) The Measurement of Time 104
C. The Procedure for Carrying out a Run 105
(i) First Filling 105
(ii) Second Filling 105
D. Dimensions of the Apparatus 107

CHAPTER FOUR

THE INVERSION OF TRANSPORT PROPERTY AND GAS IMPERFECTION DATA 109
(a) Introduction 109
(b) Inversion of Viscosity Data 110
(c) The Inversion of Second Virial Coefficients 115
(i) Previous Techniques 115
(ii) A Complete Inversion Method for B(T) 118
(iii) Determination of the Well Depth parameter 123

(iv) Application of the Virial Inversion Method to Real Data 124

(v) Application of the Method to Argon 130

(d) The Inversion of Isotopic Thermal Diffusion Data 132

(i) Introduction 132

(ii) Inversion Procedure 133

(iii) The Direct Method 135

CHAPTER FIVE

EXPERIMENTAL VISCOSITIES FOR Ar-Xe MIXTURES 141

(a) Introduction 141

(b) Pressures at the Pointers 142

(i) First Filling 143

(ii) Second Filling 143

(c) Times of Flow and Correction Terms 147

(i) Curved Pipe Flow 147

(ii) Gas Imperfection 149

(iii) Slip 150

(iv) Kinetic Energy 150

(d) Final Accurate Ratios and Error Limits 151

(i) Temperature and Pressure Fluctuations 151

(ii) Other Sources of Error 155

(iii) Consistency Check of Ar-N_2 Ratios 156

(e) Final Viscosities of the Binary Mixtures 158

(i) Comparison with Other Workers 158

(f) Interaction Viscosities 159

CHAPTER SIX

THE APPLICATION OF THE INVERSION TECHNIQUES TO THE GASEOUS VISCOSITIES OF Ar-Xe AND Ar-N_2 163

A. An Intermolecular Potential for Ar-Xe 163

(i) Introduction 163

(ii) The Inversion of Ar-Xe Interaction Viscosities 164

(iii) Discussion 168

(a) Binary Diffusion Coefficients 168

(b) Comparison of Potential Functions 172

(c) Combining Rules 175

(iv) Conclusion 179

B. A Potential Function for Argon-Nitrogen Interactions 181

(i) Introduction 181

(ii) The Interaction Viscosities 181

(iii) Results of Inversion 185

(iv) Discussion 189

(a) The Diffusion Coefficients 189

(b) Comparison with Other Workers 190

(v) Conclusion 199

CHAPTER SEVEN

THE INVERSION OF THERMOPHYSICAL PROPERTIES FROM ANISOTROPIC POTENTIAL FUNCTIONS 200

(a) Introduction 200

(b) Application to a Model Anisotropic System 201

(c) Conclusion 205

(d) Investigation of the Effects of Anisotropy 207

(e) Discussion 209

(f) Conclusions 220

REFERENCES

CHAPTER 1

THE NATURE AND DETERMINATION OF INTERMOLECULAR FORCES

A. Introduction

The concept of intermolecular forces has a long history, the idea that molecules are point sources of attractive and repulsive forces being first formulated by Boscovich (1783). He recognised that molecules must repel each other at very small separations but assumed that the attraction and repulsion alternate a number of times as the separation increases. Later this idea was simplified to become the concept that molecules interact with attractive forces at long range and with repulsive ones at short range. This was stated by Clausius in 1857 (1).

Both Maxwell and Boltzmann (2,3,4,5) incorporated the concept of intermolecular forces into their models of the kinetic theory of gases. Maxwell used a model consisting of entirely repulsive forces and Boltzmann, used all attractive ones, each, however, produced from his model an acceptable description of the behaviour of viscosity. In 1873 Van der Waals developed an equation of state for a gas whose molecules were considered to consist of impenetrable rigid spheres surrounded by an

attractive force field. This led ultimately to the Van der Waals equation of state (6)

$$(P + \frac{a}{\tilde{V}^2})(\tilde{V}-b) = RT \qquad (1.1)$$

in which a is a parameter which characterizes the strength of the intermolecular attraction and the $a/\tilde{V}^2$ term allows for the reduction of the pressure at the walls, b represents the reduction in the available volume owing to the finite size of the molecules, R is the universal gas constant and $\tilde{V}$ is the molar volume of the gas. This equation is of great importance, as it predicts a gas-liquid transition and the presence of a critical point for a pure substance, neither of which occur in a perfect gas. The work of Van der Waals showed that the existence of condensed phases is due to the attractive forces between molecules and also that the small compressibility of these phases is due to the short range repulsive forces. Many of the foundations of the present knowledge of intermolecular forces were laid early in this century by Lennard-Jones, who concluded (7,8) that the same forces determine the behaviour of substances in each of the three states of matter.

The intermolecular pair potential describes the departure of the total energy of the two-atom system from its value when the two atoms are at infinite separation. This energy is equal to the work done in bringing the two atoms from infinite separation to

the separation r and is given by:

$$U(r) = -\int_{\infty}^{r} F(r)dr \qquad (1.2)$$

and hence $$F(r) = -dU/dr \qquad (1.3)$$

where F(r) is the force acting between the two atoms at the separation r. This description of intermolecular forces by means of a pair potential energy function relies on the Born-Oppenheimer approximation (9) for the separation of electronic and nuclear motions. The basis of this assumption is that the electron velocities are very high compared to those of the nuclei. This assumption was found (10) in the case of the hydrogen molecule to be accurate to 1 part in 10^4 in the energy, leading to negligible errors in heavier systems.
The use of pair potential functions is only valid in the dilute gas phase. In condensed phases the likelihood of many body interactions is much higher than in the gas phase, and leads to the inclusion of higher terms in the traditional concept of pair-wise additivity:

$$U_{total} = \sum_{i<j} U_{ij} \qquad (1.4)$$

where U_{ij} depends only on the coordinates of the two atoms. Axilrod and Teller (11) gave the form of the three body tripole-dipole interaction as

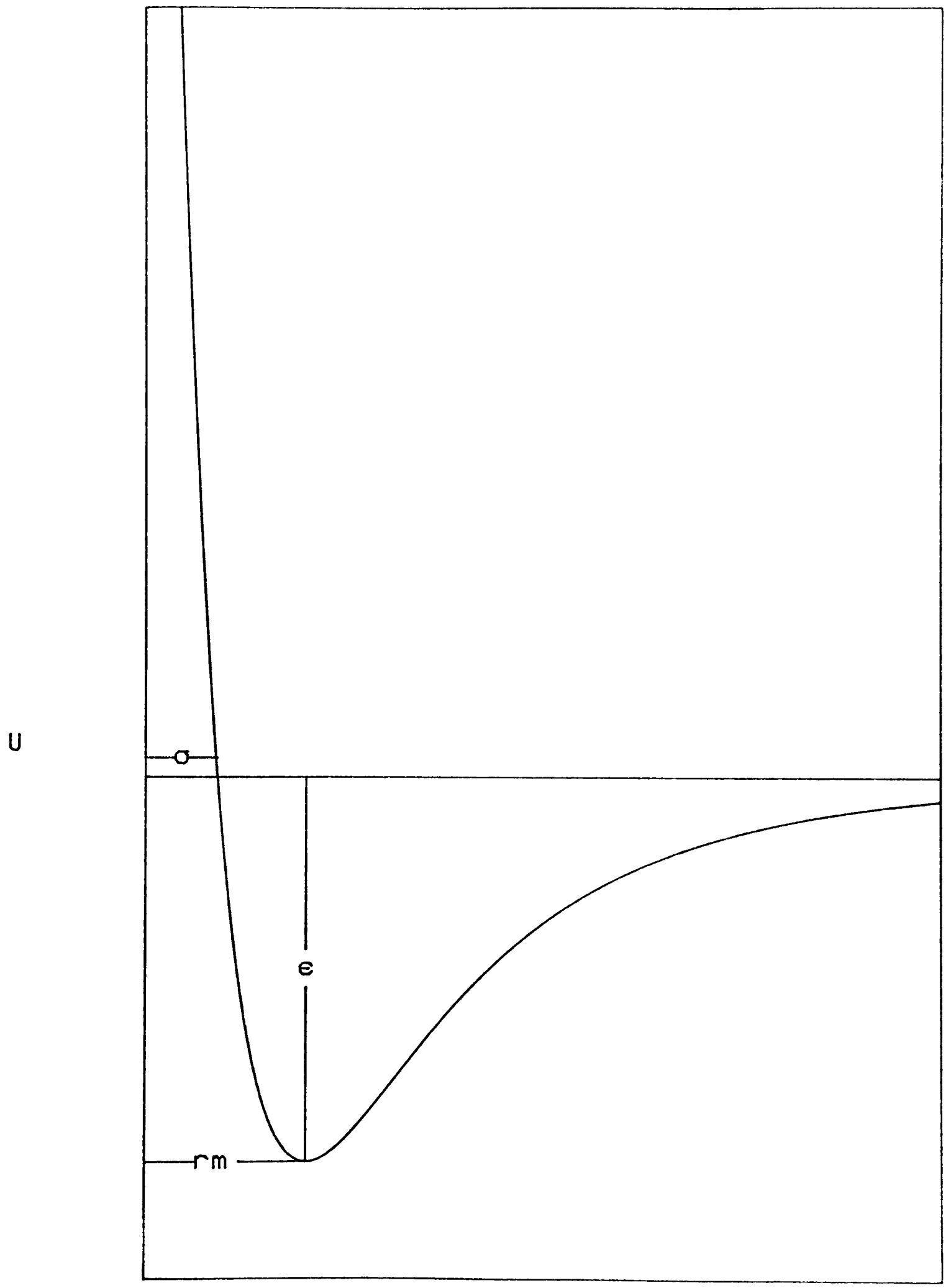
$$U_{ijk} = \frac{\nu(1 + 3\cos\theta_{12}\cos\theta_{23}\cos\theta_{13})}{(r_{12}r_{23}r_{13})^3} \qquad (1.5)$$

where θ_{12}, θ_{23}, θ_{13} are the angles formed by the three molecules, and r_{12}, r_{23}, r_{13} are the corresponding intermolecular distances. The coefficient ν may be estimated simply from the relation $\nu = -3/4\ \alpha C_6$ where α is the polarizability and C_6 is the leading coefficient in the dispersion energy. When many body terms are added to equation (1.4) it becomes

$$U_{total} = \sum_{i<j} U_{ij} + \sum_{i>j>k} \sum U_{ijk} + \ldots . \qquad (1.6)$$

The form of the pair potential energy function is shown in Figure 1.1. The shape of this function is determined by the relative magnitudes of repulsive and attractive contributions. At small separations the interaction is dominated by repulsive forces which arise from the Pauli exclusion principle. For closed-shell atoms or molecules, this reduces the internuclear charge density and hence decreases the screening of the nuclear charges by the electrons, giving rise to a net repulsion. At large separations, on the other hand, overlap of the electron orbitals is much smaller, and the dominant term is the long range attractive force resulting from electromagnetic interactions between the molecules. These two contributions lead to a minimum in the potential function

FIGURE 1.1



at some particular intermolecular separation, r_m. The value of the energy at this separation is - ε where ε is the well depth. The other characteristic parameter is the separation at which the potential energy is zero which is the collision diameter, σ. Throughout this work the well depth will be expressed in units of Kelvin (per molecule) by expressing this quantity as ε/k, where k is the Boltzmann constant.

The determination of the exact mathematical dependence of U(r) is a difficult task, partly because of the relatively low energies of the interaction. For example well depths are rarely greater than 500K (4 kJ mol^{-1}) compared to intramolecular chemical bonding interactions which are typically of the order of 2.5 - 5 x 10^4K (200-400 kJ mol^{-1}). Generally the measurement of intermolecular forces is accomplished by measuring some macroscopically observed quantity with some functional dependence on the intermolecular potential function. The success in analysing the data will depend on the accuracy of both the measurements and the theory connecting the forces to the macroscopic properties. However the reconstruction of a unique potential function poses an even more difficult task. The potential function can be regarded as having been mapped onto the property, however, if the mapping between these does not have a one-to-one correspondence then the inversion of the property to give a potential function

need not yield a unique potential. This problem and the various methods which have been developed to achieve a successful inversion are discussed in Chapter 4 of this thesis. Their application to the gaseous viscosities of argon-xenon and argon-nitrogen mixtures is described in Chapter 6 and the theory behind the determination of the viscosities is reviewed in Chapter 3. The theories connecting the transport properties and gas imperfection data to the potential functions are covered in Chapters 2 and 4. The present chapter will continue with a review of the theoretical and experimental studies of intermolecular forces.

B. Theoretical Calculations

In principle, it is possible by use of the Schrödinger wave equation to calculate the forces between particles. Ab initio calculations are possible but their accuracy is limited due to the mathematical complexities of such a procedure. The interaction energy represents only a small fraction of the total energy of the interacting molecules, and the many electron wavefunctions are difficult to calculate. Different pairs of atoms or different distances often require different approaches and approximations. There are, basically, three different approaches which may be adopted for these calculations. The full variational wavefunction is only viable for systems of 2-4 electrons. Perturbation theory

is suitable for atoms separated by large distances with weak attractions. For strong covalent bonds, on the other hand, self consistent molecular orbital theory may be employed.

Other theories which have been applied to this topic are the electron gas model which has been employed with success to the interactions between closed-shell atoms, ions and molecules at intermolecular separations of around bond distance. There is also the unified theory which combines perturbation theory and electron gas theory in such a way that the results are equally valid at both short and long distances for systems similar to those employing the electron gas model.

(a) Variational calculations

The interaction energy U(r) is given by

$$U(r) = E(r) - E(\infty) \qquad (1.7)$$

where E(r) is the total energy of the diatomic molecule, and E(∞) is the energy of the separated atoms. As the value of r increases then the interaction energy decreases towards zero and the method becomes increasingly inaccurate as the method is subject to increasing uncertainty in the total energy term. This method is in general, therefore, restricted to the repulsive short range region of the potential. Most calculations employ the Hartree-Fock

method which, in the single configuration formalism, leads to a purely repulsive potential due to the neglect of electron correlation. Many workers have concentrated on the helium diatom for which accurate atomic basis sets are available. Phillipson's calculations (12) and also those of Matsumoto et al (13) are generally accepted as being the most reliable for the description of the short range repulsive region. More recent calculations have tended to concentrate on the use of methods which go beyond the Hartree Fock limit in order to describe energies around the potential minimum. These calculations give potential functions which all have similar shapes and values of the collision diameter, but which differ in the depth of the potential minimum. For example, Bertoncini and Wahl (14) have employed a multi-configuration self-consistent field (MCSCF) method to calculate the change in correlation energy with separation. This gives a well depth for helium of 10.8K. This value for the well depth is reasonably close to that of McLaughlin and Schaefer (15) who used a configuration interaction (CI) method to yield a well depth of 12.0K.

Interaction energies for the heavier noble gases and their mixtures have also been determined by application of the variation method although the calculations for these heavier gases are lengthy and complex. Gilbert and Wahl (16) have performed single configuration SCF calculations for neon and argon diatoms which give repulsive energies at 10^5K and give an upper limit to the

potential due to an incomplete account being made of electron correlation.

Other more complex systems have been studied. Mixed interactions due to the interactions of Ne-He, He-Ar, and Ne-Ar have been investigated by Matcha and Nesbet (17) by SCF calculations using Hartree-Fock orbitals which were polarizable on collision. Very similar results were obtained for these systems by Hathaway and Krumhansl (18) using an extended Hückel method. Refined Hartree-Fock calculations were used to investigate the asymmetry of the He-H_2 system (19). Tsapline and Kutzelnigg found the system had a much larger asymmetry than predicted by perturbation theory. Catlow, Harker and Haynes (20) have studied H_2-H_2 and CH_4-CH_4 interaction with Hartree-Fock wave functions and fitted the repulsive interactions to bond centre models. For H_2-H_2, several basis sets were used and the results considered to be reliable, however, for the CH_4-CH_4 interactions, it was only feasible to employ two basis sets, and the results of these two sets gave interaction energies which differed by 10-20 percent.

(b) Perturbation Calculations

(i) Long range

At large separations, because the overlap of the wavefunctions of the separate atoms is very small, the interaction energy may be calculated by perturbation theory. The unperturbed system is that of the separated atoms, or molecules, with Hamiltonian $H^{(o)}$, and the total

operator H becomes:

$$H = H^{(o)} + H^{(1)} \qquad (1.8)$$

$H^{(1)}$ being a small perturbation. At sufficiently large separation, the electron exchange energy becomes negligible, and also $H^{(1)}$ may be expanded as a multipolar series. The first term is due to dipole-dipole interaction, the second to dipole-quadrupole interactions and so on. Each of the perturbation energies $U^{(n)}(r)$, contributing to the total interaction energy U(r),

$$U(r) = U^{(1)}(r) + U^{(2)}(r) + U^{(3)}(r) + \ldots \qquad (1.9)$$

can therefore be expressed as an inverse power series in r.

The first order energies $U^{(1)}(r)$, arise from interactions between the permanent multipole moments of the two molecules. In the case of two dipoles a Boltzmann averaging of these interactions over all orientations leads to a net attraction of (21)

$$U^{(1)}(r) = -\frac{2\,\mu_a^2\,\mu_b^2}{3kTr^6} \qquad (1.10)$$

where $\mu_{a,b}$ are the molecular dipole moments.

The second order term $U^{(2)}(r)$ may arise in two ways. The first <u>induction</u>, arises from one molecule being

polarized by the other. This leads to a dipole-induced dipole term which like the first order dipole-dipole terms has on r^{-6} dependence but unlike the latter the dipole-induced dipole term has no temperature dependence, the induction second order energy term obtained on Boltzmann orientational averaging being:

$$U_{ind}^{(2)} = - \frac{\mu_a^2 \alpha_b}{r^6} \qquad (1.11)$$

Where α_b is the dipole polarizability. Similar terms may be derived for higher order interactions, for example quandrupole/induced-dipole interactions give r^{-8} independent terms.

The second term which contributes to $U^{(2)}(r)$ is in fact the dominant term, arising from dispersion forces. These occur for both polar and non-polar molecules when the states of each of the two interacting molecules change. They cannot be analysed classically and their origins are purely quantum mechanical in nature. We can understand that although a molecule may possess no permanent dipole moment, its electrons are continuously in motion and therefore the electron density in a molecule may possess an instantaneous dipole moment which fluctuates according to the fluctuations in the electron density. This instantaneous dipole in one molecule is able to induce an instantaneous dipole in the second molecule. These two dipoles interact to produce the dispersion energy which is attractive in nature. In addition as might

be expected there are also contributions to the dispersion energy arising from instantaneous dipole-quadrupole, quadrupole-quadrupole interactions etc. The dispersion energy may therefore be written as

$$U_{disp}^{(2)} = \frac{C_6}{r^6} + \frac{C_8}{r^8} + \frac{C_{10}}{r^{10}} + \ldots \qquad (1.12)$$

where, for interactions between ground-state molecules, each coefficient is negative and hence each contribution is attractive.

There has been considerable investigation to obtain the magnitudes of these coefficients, particularly the first term C_6. London (22) first estimated the magnitude of C_6 by means of an oscillator model (23). He assumed that the frequency ω_o of the oscillator model was that corresponding to the energy required for ionization of the molecule from its ground state, $E_I = \hbar\omega_o$. This gives for C_6

$$C_6 = -\frac{3}{2} \frac{e^4 h^4}{m^2 (4\pi\varepsilon_o)^2} \sum_{k_u^a}{}' \sum_{k_v^b}{}' \frac{f_{ok_u^a} f_{ok_v^b}}{\{E_{ao}-E_{ak_u^a}\}\{E_{bo}-E_{bk_v^b}\}\{(E_{ao}-E_{ak_u^a}) + (E_{bo}-E_{bk_v^b})\}} \qquad (1.13)$$

where the subscripts, o, u and v represent quantum states for the isolated atoms a and b. The letters k_u^a and k_v^b represents the quantum numbers, other than angular momentum and magnetic, of the states u and v of atoms a and b.

This leads to the following expression for C_6

$$C_6 \approx -\frac{3}{2}\ \alpha_a\alpha_b\ \frac{\bar{\omega}_a\bar{\omega}_b}{2(\bar{\omega}_a+\bar{\omega}_b)} \qquad (1.14)$$

The $\bar{\omega}_{ab}$ energies may be approximated by ionization potentials and a semi-empirical value for C_6 obtained. In this way London obtained a value of C_6 for the di-argon interaction whose value of -5.03×10^{-78} Jm^6 is only 30% smaller than the most refined calculations performed over recent years.

Other early studied employed the variation principle to produce semi-empirical equations for C_6. Thus Slater and Kirkwood (24) derived the equation:

$$C_6 = -\frac{3}{2}\hbar\ \frac{e}{(m_e)^{\frac{1}{2}}} \cdot \frac{1}{(4\pi\varepsilon_o)^2} \cdot \frac{\alpha_a\alpha_b}{(\alpha_a/N_a)^{\frac{1}{2}}+(\alpha_b/N_b)^{\frac{1}{2}}} \qquad (1.15)$$

where N is the number of electrons contributing to the polarizability, which is normally those in the outer shell. Kirkwood (25) and Müller (26) developed a similar expression which involved diamagnetic susceptibilities χ rather than α. All these formulae tend to give the right order of magnitude for C_6, the Kirkwood Müller value usually being too large by a factor of two whereas the London value is usually too low.

More accurate calculations of C_6 were found by consideration of oscillator strengths and excitation energies which may be determined from spectral analysis (27). The accuracy of these could be confirmed by ensuring that they satisfied the sum rules S(k) of the form:

$$S(k) = \sum_n{}' f_n(\omega_n)^k \qquad (1.16)$$

where ω_n are the transition energies ($= E_i - E_o$). For example $S(o) = N_E$, the number of electrons in the atom, $S(-2) = \alpha(o)$, the static dipole polarizability. The sum values may be extracted for example from refractive indices, and polarizabilities. Refining the values to fit such summations enabled C_6 to be determined for many pairs of atoms to $\pm$ 5%. Bell (28) proposed an adaptation to this use of the sum rules which did not require a knowledge of the oscillator strengths.

The most recent calculations of C_6, however, are based on the limiting Casimir-Polder (29) equation which is valid for $r << C/\omega$.

$$C_6 = -\frac{3\hbar}{\pi(4\pi\varepsilon_o)^2} \int_o^\infty \alpha_a(i\omega)\alpha_b(i\omega)d\omega \qquad (1.17)$$

where $\alpha_a(i\omega)$ is the dipole polarizability of atom a at the imaginary frequency $i\omega$ (30).

$$\alpha_a(i\omega) = \frac{e^2}{m} \sum_{k_u^a=1}^{\infty} \frac{f_{ok_u^a}}{(\omega_{k_u^a}^2 + \omega^2)} \qquad (1.18)$$

with an equivalent expression for $\alpha_b(i\omega)$. The advantage of (1.17) is that it incorporates separated information about the individual atoms a and b and does not contain sums and products of quantities relating to the two atoms as (1.13) does. The imaginary frequencies $i\omega$ mean that the magnitude of the external polarizing field changes exponentially with time. Several methods have been used to relate the behaviour at imaginary frequencies to that at real frequencies. Langhoff and Karplus (31) have used a Pade approximant method, and Starkschall and Gordon (32) used methods based on moment theory and linear programming techniques. Both these latter approaches provide identical results given the same data as input, and many other calculations have been shown to be consistent with these (33). They have resulted in data accurate to about $\pm$ 3% for the noble gases.

The methods outlined above have been used to evaluate C_6 for some simple polyatomic systems (32) and similar techniques have been employed to estimate C_8 coefficients from quadrupole sum rules (34) and the anisotropy in C_6 for interaction between asymmetric molecules (33).

(ii) Short range

The repulsive force at short range, 'exchange' energy may be reasonably well represented by a Born-Mayer function:

$$U(r) = A \exp(-Br) \qquad (1.19)$$

Treatment of this by standard perturbation methods is complicated however since the theory of such techniques fails when the electron overlap is large. The various methods of treating the exchange energies have been reviewed by Certain and Bruch (35). More recent calculations (36) have been made for the noble gases in particular for all the mixtures of He, Ne and Ar. These potentials show a fair agreement with other functions proposed for these systems.

(iii) Very long range

At very large intermolecular separations, so-called retardation effects arise due to the finite time taken for the propagation of electromagnetic radiation between molecules. This leads to the dispersion energy varying as r^{-7} rather than r^{-6} (29).

(iv) Model calculations

Some success has been achieved using the electron gas model (37,38). These methods extended the Thomas-Femi-Dirac

statistical model of the atom. The method of Gordon and Kim (39) based their electron gas model on the Hohenberg-Kohn theorem, which shows that "the exact energy of a system is a functional of the electron density of the system". The unknown Hohenberg-Kohn functional required for this calculation is approximated by the known energy functional for a uniform electron gas. Rae has suggested (40) that the interaction energies should be modified by excluding "self-exchange" and that correlations between electrons with parallel spins should be included. These corrections improve the accuracy of the resulting potential functions. The model has been applied to xenon and its mixtures with the other noble gases by Schneider (41), and also to the mixtures of Ar-N_2 by Gordon and Kim (42,43).

C. Experimental Sources of Information

The theoretical calculations described in the preceding section have been useful in determining the outer bounds of the potential function at small and large separations, however, these methods except for systems with few electrons, have not been able to be applied to intermediate distances. In this section therefore we discuss the information which can be elucidated from experimental determinations. We will look at the various properties which have been used to obtain information about the intermolecular potential and in

particular what information each property contains in principle and what regions of separation are relevant to the experimental data.

(i) Gas imperfection

The theory of equilibrium statistical mechanics leads to the virial equation of state

$$\frac{PV}{RT} = 1 + \frac{B(T)}{\tilde{V}} + \frac{C(T)}{\tilde{V}^2} + \ldots \qquad (1.20)$$

where P is the pressure of the gas, T its temperature and $\tilde{V}$ its molar volume. In the limit as $\tilde{V} \to \infty$ this reduces to the perfect gas equation of molecules which are point masses. Then higher-order terms in the expansion, therefore, correspond to the effects of intermolecular forces. The second virial coefficient B accounts for the effects of interactions between pairs of molecules, the third virial coefficient C accounts for interactions of groups of three molecules and so on. The second virial coefficient is, for a spherically symmetrical interaction, given by:

$$B(T) = -2\pi N_A \int_o^\infty [e^{-U(r)/kT} - 1]r^2 dr \qquad (1.21)$$

Thus given U(r) it is a straightforward procedure to calculate B(T). This expression has been widely used to test suggested intermolecular potentials. As can

be seen from equation (1.21) it is clear, in principle, that B(T) must depend on the entire potential function over all separations. The range of temperature over which B(T) may be measured is for argon approximately $kT/\varepsilon = 0.5$ to $kT/\varepsilon = 5$ where ε is the depth of the potential well. This is determined by studying its low density (PVT) properties. In order to study the type of information which B(T) against temperature data contain it is instructive to write (1.21) in the alternative form:

$$B(T) = \frac{2\pi N_A e^{\varepsilon/kT}}{3T} \int_o^{\varepsilon} \Delta e^{-\phi/T} d\phi + \frac{2\pi N_A e^{\varepsilon/kT}}{3T} \cdot \int_{\varepsilon}^{\infty} r^3 \, e^{-\phi/T} d\phi \qquad (1.22)$$

where $\phi(r) = (U(r) + \varepsilon)/k$ and $\Delta = r_L^3 - r_R^3$, r_L and r_R being the left and right hand coordinates of the potential energy curve at energy ϕ. The first term corresponds to the contribution of the potential well to the virial coefficient at temperature T whereas the second term arises from the repulsive forces. At high temperatures the second term is dominant and hence B(T) depends only on the repulsive region of the potential. Thus, measurements of B(T) at high temperatures can give U(r) explicitly. The experimental measurements are, however, restricted to the low-energy repulsive region only. At low temperatures where the first term is dominant, measurements provide information about the width of the potential function as a function of energy. This analysis does not however take into account the

continuity of the potential function and its derivative through U(r) = 0 and recent treatments (44,45) indicate that because of this continuity B(T) is capable of providing explicit information about U(r) over a wide range of separations. This is discussed fully in Chapter 4.

(ii) Transport properties of dilute gases

The transport properties have played an important role in the search for realistic potential functions. As will be seen in Chapter 2 viscosity, thermal conductivity and isotopic, binary and thermal diffusion may be calculated from the potential energy function U(r) by the study of the dynamics of molecular collisions and integration over all possible trajectories and relative kinetic energies. The integrations perform averages over all these variables and so the reverse calculation, that is the process of inversion, must extract the potential function from the averaged properties of the gas!

Of all the transport properties which have been studied the viscosity is the most easily determined to high accuracy (1-2%) over a wide temperature range. It was, however, errors in early viscosity data at both high and low temperatures which considerably hindered investigations of intermolecular forces until remeasurement led to the discovery of the inaccuracy at the end of the 1960's

(46-48). The cause of these errors, despite considerable discussion were (49), however, never fully discovered. It is important to measure the viscosity data over as wide a temperature range as possible. This is because as was shown by Hanley and Klein (50) in order to differentiate between various proposed potentials the potentials had to be capable of reproducing experimental data to within 0.5% at temperatures greater than $kT/\varepsilon = 5.0$ and less than $kT/\varepsilon = 2.0$. Within the range 2.0 - 5.0 it was found that many potential functions could reproduce the experimental data. This underlines the difficulty involved in defining the realistic potential function by the procedure of curve fitting, and shows the great value of inversion techniques. At high temperatures, viscosities are almost entirely dependent on the repulsive region of the potential and a direct inversion method for this region has been developed by Dymond (51). A method of inversion over a wide temperature range in order to extract the full potential has been devised by Gough, Maitland and Smith (52) and this is discussed in further detail in Chapter 4.

Closely related to the viscosity coefficient, as will be seen later in Chapter 2, is the thermal conductivity coefficient λ. Simple kinetic theory yields $\lambda = F\eta C_v$ where C_v is the mass specific heat and F is a constant. As will be shown in Chapter 2, this expression is also true for rigorous kinetic theory. Thermal conductivity

data therefore give little additional information about the intermolecular forces and are also more difficult to measure. Typical accuracies are ± 4% and work by Springer and collaborators (53) agrees with the viscosity measurements to this level of accuracy at high temperature.

The coefficients of isotopic and binary diffusion have not generally been used for determination of intermolecular potentials since they are difficult to measure accurately over a wide temperature range. However recent measurements to ± 2% near room temperature may be used as a guide for consistency of viscosity data as will be seen in Chapter 6 for the work on argon-xenon. This is because they can be compared directly with the viscosity data without recourse to a potential energy function using a ratio of collision integrals $A^* = \Omega^{(2,2)} / \Omega^{(1,1)}$ which is insensitive to the detailed form of the potential function.

Thermal diffusion depends on the ratio of collision integrals. Two methods of inversion have been developed recently (54,55) the most recent during the present work. The inversion methods are described in detail in Chapter 4. Thermal diffusion is believed to be of particular value in the investigation of intermolecular forces since it is particularly sensitive to the shape of the potential energy function. It has been proposed that it may be used to differentiate model

potentials even when the thermal diffusion data is in error by 20% (56). When inverted directly we show that thermal diffusion gives the slope of the potential function rather than the function itself.

(iii) Spectroscopic information

Despite the fact that atoms such as the inert gases do not form chemically bound molecules, they form dimers under appropriate conditions. For example if three molecules approach each other at low energy one molecule may remove kinetic energy from the other two and leave them trapped in their potential well. At low temperatures the dimers may therefore be studied by spectroscopic techniques. It is possible by means of an inversion technique, the Rydberg-Klein-Rees analysis, to extract the potential function from the spectrum. If only the vibrational absorption bands are observed then the Rydberg-Klein-Rees (RKR) analysis yields the width of the potential well as a function of its depth. However if the rotational fine structure of the absorption spectrum can be resolved then the entire potential in the well region can be defined. In addition the dissociation energy of the van der Waals complex gives the well depth directly.

There are experimental problems, however, which mean that until recently this technique has not been used in intermolecular force determinations. First the dimers of

the inert gases possess no dipole moment and so are not active in the infrared region of the spectrum. Secondly the concentration is very small, typically 0.4% of atoms of argon at its boiling point are present as dimers. Finally the lifetime of such dimers is very short $\sim 10^{-10}$s at atmospheric pressure due to the effect of molecular collisions. Extremely refined techniques are necessary in order to observe the spectra.

The first successful spectroscopic study of inert gas dimers was by Tanaka and co-workers who observed a series of absorption bands due to Ne_2 (57), Ar_2 (58), Kr_2 (59) and Xe_2 (60) in the vacuum ultraviolet in the region of the characteristic atomic line spectra of the inert gases. To overcome the problem of low concentration Tanaka's apparatus had a path length of 6.65 m and the gas was cooled by liquid nitrogen at a partial pressure ranging from 1.3×10^{-6} to 0.1 bar. Similar results were obtained at room temperature with a path length of 13m. In the case of Ar_2 Tanaka and Yoshino (58) observed nine discrete band systems in the region 78-108 nm and identified six vibrational levels $\nu = 0$-5 for the ground state $^1\Sigma_g^+$ (formed from two ground state ^1S_o argon atoms). The rotational structure was poorly resolved and unassigned.

This information for argon was analysed in several ways in order to determine U(r). The determination of

dissociation energies (i.e. the well depth) had been determined in the past by the method of Birge and Spooner (61). This is based on the observation that the spacing between successive vibrational energy levels $\Delta G_{\nu+\frac{1}{2}} = G(\nu+1) - G(\nu)$ usually decreases monotonically as the dissociation limit is reached. This leads to the prediction that a plot of $\Delta G_{\nu+\frac{1}{2}}$ vs. ν (Birge-Spooner plot) should be linear and from this plot the dissociation energy may be calculated. However, Birge-Spooner plots are often curved and such a procedure can lead to large errors in dissociation energies calculated from it. In recent years more satisfactory methods have been proposed and one such method proposed by LeRoy and Bernstein (62) gives rise to the conclusion that the linear extrapolation which gives the dissociation energy is not $\Delta G_{\nu+\frac{1}{2}}$ against ν but $(\Delta G_{\nu+\frac{1}{2}})^{\frac{1}{2}}$ vs. ν. This analysis of LeRoy and Bernstein has been verified and their analysis leads to the correct results in a large number of cases (63). This analysis was applied by LeRoy to the Ar_2 data and leads to a value of $\varepsilon/k = 142.2 \pm 7.6$K (64). A value which has since been verified by other workers (65,66,67) using a wide range of thermophysical properties.

Colbourn and Douglas (68) have repeated Tanaka's work at higher resolution and obtained the rotational fine structure which enabled a full RKR analysis to be performed leading to a potential which is almost indistinguishable from the three of references 65, 66 and 67.

A more refined technique for the production of dimers has been in the expansion of a gas through a supersonic nozzle to give a molecular beam which is relatively collision free, thereby leading to an increased lifetime of the dimers. One such set of observations is for example on the Ar-HCl system by Klemperer (69). Ar-HCl has also been studied along with Xe-HCl (70) in the infrared portion of the spectrum by observation of the temperature dependence of lines caused by the dimer in the 'Q-branch' region. These observations gave the enthalpies of formation for Ar-HCl and Xe-HCl.

Another type of analysis which may be performed on systems such as Ar-H_2. In systems of the type X_2-Y rotation can occur both internally (by X_2 about its centre of mass), characterized by the quantum number j, and by relative end-over-end motion X_2 and Y, characterized by ℓ. The total rotational motion is characterized by a quantum number $J = j + \ell \ldots\ldots |j-\ell|$. These motions are coupled by the angular dependence of the intermolecular potential and the internal rotation is hindered by a potential energy barrier. The higher this barrier, the greater the degree of coupling between j and ℓ which leads to the J levels becoming shifted from the free rotation case. In the Ar-H_2 system as was shown by McKellar and Welsh (71) the vibrational and rotational features are in close agreement with those which would arise from a free hydrogen molecule (72). It therefore shows that the coupling is weak and that the

hydrogen molecule is almost freely rotating in the $Ar-H_2$ complex. Intermolecular potential functions which can account quantitatively for the observed features have been discussed by LeRoy and Van Kronendonk (73). Infrared spectra of dimers containing oxygen and nitrogen have been observed by Ewing and co-workers. The species $Ar-O_2$ (74) and $Ar-N_2$ (75) may be explained in terms of an equilibrium 'T' configuration and since the spectra features are not those which would be expected in free-rotation, one can conclude that unlike $Ar-H_2$ the O_2 and N_2 undergo hindered rotation.

(iv) Molecular beams

Molecular beams provide, in principle, a unique source of information in intermolecular forces since the effects under study are not obscured by thermal averaging of the collision processes. However, interpretation of the results of such experiments is subject to considerable problems.

Measurements involving molecular studies of isotropic interactions fall into two classes - those of total cross-section $\sigma_{Tot}(v)$ by primary beam attenuation and those of differential cross-section $\sigma(\chi)$. These latter measurements involve two crossed beams so that the angular scattering cross-sections can be measured as a function of collision energy from an accurately defined collision volume. The main features of such measurements

are the glory modulations and rainbow oscillations respectively. The rainbow oscillations are described in Chapter 2. The glory modulations arise from a quantum mechanical interference where two trajectories with the same collision energy and different impact parameters result in the same final trajectory, and since the trajectories are of different lengths this leads to interference. The spacing of the glory oscillations with energy are as detailed analysis shows (76) sensitive to the shape of the potential well.

The presence of anisotropy tends to damp out rainbow and diffraction oscillations in the total differential cross-sections and this makes it difficult even to obtain an effective isotropic potential with any accuracy. It is not possible to obtain quantitative information on the potential anisotropy from total differential cross-sections. Fully resolved state-to-state inelastic differential cross-sections would, in principle, contain the anisotropic information but these are difficult to obtain experimentally and are also very difficult to invert.

Measurements of noble gas interactions at thermal energies have been made possible by the use of supersonic nozzles. Determinations of argon total cross-sections by Baratz and Andres (77) have demonstrated glory oscillations. Improved data, giving exact positions of the glory extrema should yield a quantity $a_1.\varepsilon.r_m$

where a_1 is weakly model dependent (78) or rather more information if the amplitudes of the oscillations are also available (79).

The differential cross-sections for Ar-Ar at thermal energies have been determined by Scoles (80) using crossed supersonic beams, and rainbow maxima resolved. At greater resolution Lee observed both the rainbow and rapid quantum oscillations in the scattering of neon, argon, krypton and xenon. They have also published the differential cross-sections for all combinations of the noble gases (81,82,83,84). Their data analysed by the methods described below result in potential parameters which are in good agreement with those from other sources. Scoles has also done measurements on krypton out to the rainbow angle (85). His analysis of this data is similar to that of Lee et al. but also uses spectroscopic data to fix one of the parameters.

It is instructive at this point to consider the problems involved in the data inversion since the reliability of the interaction parameters obtained from the differential cross-sections depends critically on the method of interpretation of the experimental results. Firstly, if classical mechanics is valid at the energy of observation and the potential is monatomically repulsive, there is a (1:1) correspondence between the impact parameter and the angle of deflections. This means that the differential cross-sections can be

inverted to yield the potential (86). This approach will clearly be of greatest value at high energies. An inversion scheme which permits the deflection function to be both positive and negative has been put forward by Buck (87). He extended the scheme of Firsov which relates the classical deflection function to the potential. The deflection function has to be obtained by a fitting process based on a semi-classical approximation to χ in terms of the impact parameter b, and the potential may then be obtained pointwise. The quantum case has also been solved by Shapiro and Gerber (88) who proposed an iterative scheme which leads to successively better fits to the data in terms of phase shifts. All these schemes have an inherent problem, however, in that they require almost perfect experimental data. In practice they are at limited energies and angles and of course contain random noise. This leads to the formal schemes becoming unreliable and the analysis usually adopted involves the choice of an initial arbitrary analytical form for the potential function. ε and σ are then calculated by fitting of the experimental data.

(v) Solid state properties

The properties of solids have been of more uncertain value in the determination of pair potentials since they involve the simultaneous interaction of all molecules in the solid. Early workers measured crystal packing

parameters and sublimination energies, explaining them in terms of individual pair interactions or their sum over the whole lattice (86). For molecular crystals, their lattice energy, dimensions and other properties such as compressibility may be directly related to the intermolecular forces, this is simply because the stable arrangement of molecules in the lattice is a consequence of a balance between all the repulsive and attractive forces between the molecules. This can be illustrated as follows (87). If we assume a Lennard-Jones type interaction and assume that the total energy is given by the pairwise addition of all pairs in the lattice then the potential energy of the crystal is

$$\Phi = 2N_A \varepsilon \{ \sum_{i=1} (\frac{\sigma}{r_i})^{12} - \sum_{i} (\frac{\sigma}{r_i})^{6} \} \qquad (1.23)$$

where r_i denotes the separation of the i^{th} molecule from a particular reference molecule and the summations extend over all molecules around this selected molecule. For any particular structure the separation of every molecule from a particular molecule is known in terms of the nearest neighbour distance, a, and hence if we let

$$L_n = a^n \sum_{i} r_i^{-n} \qquad (1.24)$$

The sums L_n can be evaluated. For example for the face-centred cubic structure of the inert gas crystals the

sums $L_{12} = 12.13$ and $L_6 = 14.45$, so equation (1.23) becomes:

$$\Phi = 2N_A\varepsilon \{L_{12}(\frac{\sigma}{a})^{12} - L_6(\frac{\sigma}{a})^6\} \qquad (1.25)$$

Obviously for equilibrium the value of a must be such that $d\phi/da = 0$ i.e. Φ is a minimum. This is equivalent to

$$\frac{a}{\sigma} = (\frac{2L_{12}}{L_6})^{1/6} \qquad (1.26)$$

when the potential energy is $\Phi = -(N_a\varepsilon L_6^2/2L_{12})$. When the zero point energy, Φ_o, calculated from the Debye theory of a solid is included the total energy becomes

$$\Phi_E = -\frac{N_A\varepsilon}{2}\frac{L_6^2}{L_{12}} + \Phi_o \qquad (1.27)$$

Equations (1.26) and (1.27) demonstrate that if the assumption of pairwise additivity is valid then measurements of the nearest neighbour distance and sublimination energy will give σ and ε for the assumed 12-6 potential or any other potential used for calculation.

However, the assumption of pairwise additivity is not valid and in the case of argon the error in this assumption is about 7.5% for xenon it is 13%. Inclusion of the Axilrod-Teller (11) three body term however leads to a much more satisfactory agreement with

the experimental data. This suggests that the third-body term is the dominant non-additive contribution and also may imply fortuitous cancellation of higher order terms.

In conclusion we can say that the solid-state properties constitute a test of intermolecular potentials derived from other sources as well as providing a means of investigation of non-additive effects. Similar comments apply to the liquid-state properties although the molecular theory linking the properties to the inter-molecular potential function is less well developed.

D. The Representation of Pair Potential Energy Functions

In this section we discuss the various analytical forms which have been proposed in order to represent the potential energy function. Normally these analytical forms are written with adjustable parameters which are assigned values so that the properties calculated from the potential fit the experimental data. Two of these parameters are invariably ε and σ or r_m. These parameters, however, unlike the others only determine the scale and not the shape of the function.

Traditionally the most frequently used of these model potentials was probably that of Lennard-Jones (LJ) (8).

$$U(r) = \varepsilon[(\frac{m}{n-m})\ r^{*-n} - (\frac{n}{n-m})\ r^{*-m}] \qquad (1.28)$$

where $r^* = r/r_m$, and the collision diameter, σ, is given by:

$$\sigma = r_m(\frac{m}{n})^{1/(n-m)} \qquad (1.29)$$

This function has the rough general features of the true intermolecular potential energy function. It has a single minimum at r_m where the energy is $-\varepsilon$. The attractive exponent is of course usually 6 for the most commonly used n-6 form of this function which is theoretically based on the dispersion energy contribution. The repulsive term has, however, no theoretical justification. Most often the exponent n has been given the value of twelve resulting in the 12-6 potential.

$$U(r) = \varepsilon\{(\frac{r_m}{r})^{12} - 2(\frac{r_m}{r})^{6}\} \qquad (1.30)$$

which may also be written as

$$U(r) = 4\varepsilon\{(\frac{\sigma}{r})^{12} - (\frac{\sigma}{r})^{6}\} \qquad (1.31)$$

where $\sigma = (2^{-1/6}\ r_m)$ from (1.29). The Lennard-Jones potential has only two adjustable parameters and thus ε and σ may be changed to force fit experimental data. This leads to a poor representation of the potential

functions for the inert gases and gives values of C_6 which are too large by a factor of two and have well depths which are too small compared with those of recent studies (88). This leads to large errors in the predicted low temperature properties of the inert gases.

Following the recognition that the Lennard-Jones function was a poor representation of the true potential energy functions for the inert gases, a number of other simple potential energy functions were proposed. Many workers tried different values of n (89) and m (89,90) or more than two exponents of r (91). An exponential-6 function has also been proposed (92) which has the form

$$U(r) = \frac{\varepsilon}{(1-6/\alpha)} \left\{\frac{6}{\alpha} e^{\alpha(1-r^*)} - r^{*-6}\right\} \qquad (1.32)$$

and α is a measure of the steepness of the repulsive wall where $r^* = r/r_m$. This expression combines the functional forms suggested by theoretical calculations for both repulsive and long range energies. The exponential-6 potential has a spurious maximum at low values of r. All these analytical functions were tested to ascertain if they could reproduce both transport properties and gas imperfection data over a wide temperature range as well as spectroscopic data and proved to be unsatisfactory in this respect.

Kihara (93) introduced a function which incorporates a hard spherical core of radius $\gamma\sigma$ inside which $U(r) = \infty$,

and which represents the energy at greater distances based on core to core separations. This type of potential, however, was analysed by Smith et al (94) and it was shown that no such core potential could adequately represent the best modern potentials for argon and that it was therefore likely to be inadequate for the other noble gases.

It was obvious therefore that there was a need for more flexible functions and this flexibility has been achieved by introducing many disposable parameters whose values are determined by a fit to experimental data over a wide range of temperature. Such a function has been proposed by Barker and Pompe (95). This has the rather complex form:

$$U(r)/\varepsilon = \exp[\alpha(1-r^*)] \sum_{i=0}^{5} A_i (r^*-1)^i - \sum_{j=0}^{2} C_{2j+6}/(\delta+r^{*\,2j+6}) \qquad (1.33)$$

where $r^* = r/r_m$. Apart from the scaling parameters ε and r_m this function has eleven disposable form parameters which permit the shape of the potential to be varied. Such functions of this flexible form have been used with considerable success to describe the interactions of simple species, e.g. Barker-Fisher Watts potential (67) and BBMS potentials (65) for argon.

A final group of functions have been devised solely to provide a convenient analytic representation of directly determined pair potential functions. One of the simplest of these is the n(r^*)-6 function (96) which is effectively of the Lennard-Jones (n-6) type but the repulsive exponent n is a function of r.

$$U^*(r)/\varepsilon = \{(\frac{6}{n-6})r^{*-n} - (\frac{n}{n-6})r^{*-6}\} \qquad (1.34)$$

$$n = P + \gamma(r^* - 1) \qquad (1.35)$$

commonly P = 13.0. This simple three-parameter (γ, ε, and σ) function gives a remarkably accurate representation of the inert gas functions (96).

Finally we look at the representation which has been employed for non-spherical species. Here the energy is not only a function of distance but also of angle.

Two approaches have been widely used. In the first, the orientation-dependent function, $U(r, \omega_1, \omega_2)$ is expanded as a series

$$U(r,\omega_1,\omega_2) = U_o(r) + \sum_{n=1}^{\infty} U_n(r) f_n(\omega_1,\omega_2) \qquad (1.36)$$

where the angular terms $f_n(\omega_1,\omega_2)$ are known standard functions of the molecular orientations ω_1,ω_2 such as Legendre polynomials or spherical harmonics, and their coefficients $U_n(r)$ are functions only of separation.

$U_o(r)$ is the unweighted orientation average of the full potential. Expansions of this type are, in principle, exact although their practical utility assumes rapid convergence of the series which is not necessarily the case.

The second approach is that of a site-site potential in which it is attempted to separate the energy for a pair of molecules into a sum of interaction energies between interaction sites often corresponding with atomic nuclei. For example the N_2-N_2 interaction could be expressed as the sum of 4 such N-N interactions. One of the simplest of this type of model which has been extensively used is the diatomic Lennard-Jones 12-6 model where all interactions between sites are of the Lennard Jones (12-6) type. The potential function therefore becomes:

$$U = 4 \sum_{l=1}^{2} \sum_{m=1}^{2} \left\{ \left(\frac{\sigma}{r_{lm}}\right)^{12} - \left(\frac{\sigma}{r_{lm}}\right)^{6} \right\} \qquad (1.37)$$

where r_{lm} is the separation of the l^{th} and m^{th} interaction sites. This kind of potential will be used in the work discussed in Chapter 7 on anisotropic interactions.

CHAPTER 2

MOLECULAR THEORY OF GASES

A. Simple Kinetic Theory of Dilute Gases

In this section we consider a simple approach to the derivation of the transport coefficients of a gas and the physical principles which underlie the phenomena of viscosity, thermal conduction and diffusion. Although the treatment contains gross approximations, the results nevertheless show the correct functional dependence of the transport properties on the appropriate variables. The resulting expressions for the transport coefficients differ from those of exact kinetic theory for hard spheres only by constant numerical factors.

We consider a gas composed of identical hard spheres of diameter d and mass m. These particles exert no forces on one another other than on impact and are in a state of continuous random motion. We assume that their speeds are distributed according to the Maxwell-Boltzman distribution law:

$$dn_c = 4\pi N\left(\frac{m}{2\pi kT}\right)^{3/2} C^2\, e^{-mC^2/2kT}\, dC \qquad (2.1)$$

Where dn_c is the number of molecules whose speeds lie in the interval C to C + dC and N is the total number of molecules under consideration. The mean molecular speed is therefore given by:

$$\bar{C} = \left(\frac{8kT}{\pi m}\right)^{\frac{1}{2}} \qquad (2.2)$$

In order to evaluate the transport properties of gases we require an estimate of the fraction of gas molecules moving in each cartesian direction. If we take the very crude approximation that there are six equivalent directions in space then we can assume that there are 1/6 of the total number moving in any particular direction (e.g. in the direction of increasing x).

Another quantity which we need to evaluate is the mean free path length $\bar{\ell}$, that is the mean distance a molecule travels between collisions. As the mean speed of the molecules is $\bar{C}$, they sweep out, in unit time, a cylinder of length $\bar{C}$ and radius d. If the centre of another molecule falls within this cylinder then a collision will occur. Therefore, if there are n molecules per unit volume the number of collisions per unit time will be $\pi d^2 Cn$. The mean free path $\bar{\ell}$ is obviously given by:

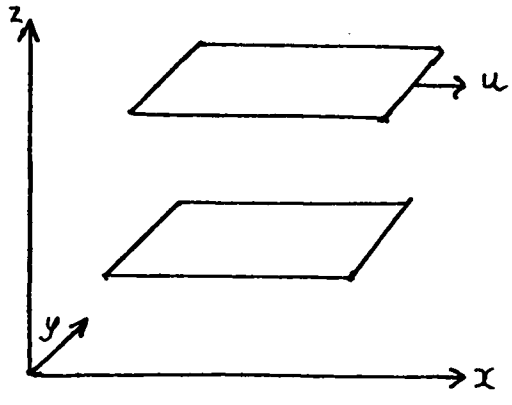
$$\bar{\ell} = \frac{\bar{C}}{nd^2\bar{C}\pi}$$

$$\text{i.e.} \quad \bar{\ell} = \frac{1}{\pi nd^2} \qquad (2.3)$$

having obtained these quantities we can now go on and calculate the expressions for the transport properties of the gas.

(i) Viscosity

In order to understand the principles of why viscosity arises let us consider the gas to be contained between two plates, (Figure 2.1a), the upper one of which is moving with



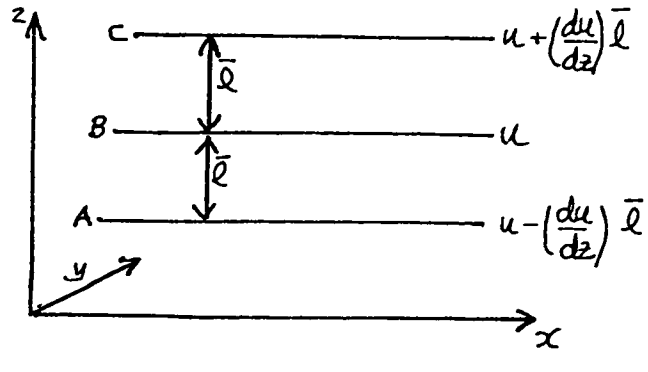


FIGURE 2.1(a) FIGURE 2.1(b)

a velocity u in the positive x-direction. The gas in contact with the lower stationary plate has no flow velocity in the x direction and therefore a velocity gradient is set up between the two plates which creates a drag on the upper plate. In order to maintain the velocity of the upper plate a force must be applied to overcome this drag.

Newton's law of viscosity defines the coefficient of shear viscosity, η, in terms of the viscous force, F, on a plate of area A and the velocity gradient (du/dz) by the equation

$$F = -\eta A \frac{du}{dz} \qquad (2.4)$$

Now we consider a reference layer in the gas lying in the xy plane in which the gas moves with a flow velocity u in the positive x-direction only. (Figure 2.1(b)). Those molecules which reach the reference plane B will on average, have travelled a distance $\bar{\ell}$, the mean free path, since their last collision. Those which arrive at plane B from above will have originated in plane C and will have a flow velocity in the positive direction of:

$$u + (\frac{du}{dz})\ \bar{\ell} \qquad (2.5)$$

and a positive x-direction flow momentum of

$$m\ \{u + (\frac{du}{dz})\ \bar{\ell}\} \qquad (2.6)$$

Where m is the mass of a molecule. Thus the number of molecules which will cross a unit area in the xy-plane in unit time will be all those contained in a column of height $\bar{C}$ and unit cross-sectional area which are moving in the correct direction, i.e. $n\bar{C}/6$.

The molecules reaching the reference plane B, from above will therefore transport downwards on amount of positive x-direction momentum

$$\frac{1}{6}\, nm\bar{C} \quad \{u + (\frac{du}{dz})\, \bar{\ell}\} \tag{2.7}$$

across unit area in unit time. Similarly the molecules which reach B from below will transport upwards

$$\frac{1}{6}\, nm\bar{C} \quad \{u - (\frac{du}{dz})\, \bar{\ell}\ \} \tag{2.8}$$

Hence the net transport of momentum across unit area of the reference plane B in the direction of positive velocity gradient in unit time is the frictional force F, on this plane in the positive x-direction

$$F = -\frac{1}{6}\, nm\bar{C}\ \{u + (\frac{du}{dz})\, \bar{\ell}\} + \frac{1}{6}\, nm\bar{C}\ \{u - (\frac{du}{dz})\, \bar{\ell}\ \}$$

$$= -\frac{1}{3}\, nm\bar{C}\ (\frac{du}{dz})\, \bar{\ell} \tag{2.9}$$

The frictional force per unit area for a unit velocity gradient is therefore according to (2.4), the coefficient of viscosity, η, so we may therefore define η as:

$$\eta = \frac{1}{3}\, nm\bar{C}\bar{\ell} = \frac{1}{3}\, \rho\bar{C}\ \bar{\ell} \tag{2.10}$$

where ρ is the mass density of the gas. Substituting for the mean free path from (2.3) and the mean molecular speed we obtain:

$$\eta = \frac{1}{3}\frac{m\bar{C}}{\pi d^2} = \frac{1}{3}\frac{m}{\pi d^2}\left(\frac{8kT}{\pi m}\right)^{\frac{1}{2}} \qquad (2.11)$$

This equation predicts somewhat surprisingly that the viscosity of a dilute gas consisting of hard spheres is independent of its density. This was first obtained by Maxwell who subsequently found it to be also true for real gases. The physical explanation for this independence is that in denser gases, though more molecules pass from one layer to another, the mean free path is shorter, and therefore, the momentum transferred by each molecule is less. In fact for real gases it is not exact but is a very good approximation at moderate densities. A less satisfactory conclusion of equation (2.11) is that the viscosity should be proportional to $T^{\frac{1}{2}}$. For real gases it is generally found that the viscosity varies more rapidly with temperature than this.

(ii) Thermal Conductivity

As already stated, gas viscosity arises from the transport of momentum across a momentum (velocity) gradient. A similar argument is applicable to thermal conductivity and to diffusion. The thermal conductivity of a gas is a consequence of the transport of kinetic energy across a temperature (i.e. kinetic energy) gradient. Diffusion in a gas is the transport of mass across a concentration gradient.

The law of heat conduction is given by

$$Q = -\lambda A(\frac{dT}{dz}) \qquad (2.12)$$

Where Q is the energy flow across an area A and λ is the coefficient of thermal conductivity. If we consider a similar argument to that used with viscosity we obtain for the net transport of energy across unit area in unit time in the direction of the energy gradient

$$-\frac{1}{3} n\bar{C}(\frac{dE}{dz})\ \bar{\ell} \qquad (2.13$$

But $$\frac{dE}{dz} = (\frac{dT}{dz}).(\frac{dE}{dT}) = C_v(\frac{dT}{dz}) \qquad (2.14)$$

Where C_v is the heat capacity of the gas per molecule. Hence the thermal conductivity coefficient λ is

$$\lambda = \frac{1}{3} n\ \bar{C}\ \bar{\ell}\ C_v \qquad (2.15)$$

substituting for $\bar{\ell}$ and $\bar{C}$ gives

$$\lambda = \frac{1}{3} \frac{C_v}{\pi d^2} (\frac{8kT}{\pi m})^{\frac{1}{2}} \qquad (2.16)$$

The thermal conductivity, is, therefore like viscosity independent of density and proportional to $T^{\frac{1}{2}}$. In addition from (2.16) and (2.11) it can be seen that:

$$\lambda = \eta\ C_v/m \qquad (2.17)$$

Despite the approximations made on obtaining this result

this relationship is found to be an extremely good approximation for real monatomic gases, although there is a different constant of proportionality.

(iii) Diffusion

Diffusion is the transport of mass along a concentration gradient. Since the argument for two gases diffusing into each other is complicated, let us imagine a gas composed of two isotopes, whose properties, including their molecular masses are sufficiently similar so that we can treat $\bar{C}$ and $\bar{\ell}$ as identical. We select one isotope as a reference and suppose that n is its number density in a reference plane which is situated in the gas normal to a concentration gradient of the isotope [d(nm)/dz].

Following the same type of argument as for viscosity and thermal conductivity, the net mass flow across unit area of the reference plane in the direction of the concentration gradient is

$$-\frac{1}{3}\,\bar{C}\,\bar{\ell}\,\frac{d(nm)}{dz} \qquad (2.18)$$

The transport coefficient for self-diffusion, D, is defined by the equation of Fick's Law.

$$J = -AD\,\frac{d(nm)}{dz} \qquad (2.19)$$

where J is the mass of flow of molecules of the reference isotope. We can obtain an expression for D by considering

transport of mass across unit area in Fick's Law and we find therefore

$$-\frac{1}{3}\,\bar{C}\,\bar{\ell}\,\frac{d(nm)}{dz} = -\,AD\,\frac{d(nm)}{dz} \qquad (2.20)$$

i.e. $$D = \frac{1}{3}\,\bar{C}\,\bar{\ell} \qquad (2.21)$$

$$\therefore \quad D = \frac{1}{3}\left(\frac{8kT}{\pi m}\right)^{\frac{1}{2}}\,\frac{1}{n\pi d^2} \qquad (2.22)$$

Therefore, the diffusion coefficient is inversely proportional to the number of molecules per unit volume. Furthermore applying the expression for a perfect gas

$$n = P/kT \qquad (2.23)$$

(2.22) becomes

$$D = \frac{1}{3}\left(\frac{8kT}{\pi m}\right)^{\frac{1}{2}}\,\frac{kT}{P\pi d^2} \qquad (2.24)$$

The self-diffusion coefficient of a hard-sphere gas is therefore predicted to be inversely proportional to pressure and proportional to $T^{3/2}$.

(iv) Comparison of Simple Kinetic Theory with Rigorous Kinetic Theory

The rigorous kinetic theory for hard-sphere molecules gives the same general form of the expressions for transport properties as defined above except due to the assumptions

made in the simple kinetic theory derivation, the numerical constants are different. The solutions given by rigorous kinetic theory to a first approximation are shown below:

$$\eta = {}^{5}/_{16}\ (\pi mkT)^{\frac{1}{2}}/\pi d^2 \qquad (2.25)$$

$$\lambda = {}^{25}/_{32}\ \{(\pi kT/m)^{\frac{1}{2}}/\pi d^2\}\ C_v \qquad (2.26)$$

$$D = {}^{3}/_{8}(\pi k^3T^3/m)^{\frac{1}{2}}/\pi d^2P \qquad (2.27)$$

(v) Application to Real Gases

The equations above derived from rigorous kinetic theory only apply to hard sphere gases and contain a cross-section πd^2 derived from the mean free path which is independent of temperature. However for real gases with intermolecular forces which are both attractive and repulsive according to separation, the situation is more complex as the cross-sections now are a function of temperature. The rigorous kinetic theory for real gases therefore introduces a term which may be thought to be a correction to the hard-sphere cross-section which allows for the effects of intermolecular forces.

$$\eta = \frac{5}{16}\ \frac{(\pi mkT)^{\frac{1}{2}}}{\pi d^2\Omega_\eta^*} \qquad (2.28)$$

$$\lambda = \frac{25}{32}\ \frac{(\pi kT/m)^{\frac{1}{2}}C_v}{\pi d^2\Omega_\lambda^*} \qquad (2.29)$$

$$D = \frac{3}{8}\ \frac{(\pi k^3T^3/m)^{\frac{1}{2}}}{8P\pi d^2\Omega_D^*} \qquad (2.30)$$

Where the dimensionless factors Ω_{η}^{*}, Ω_{λ}^{*} and Ω_{D}^{*} introduce into the equations the effects of the intermolecular forces on the binary collisions in the gas.

B Rigorous Kinetic Theory

This discussion of the kinetic theory will be restricted to single component gases of monatomic molecules which have spherically symmetric force fields and between which collisions are perfectly elastic and are governed by classical mechanics. In addition we only consider the situation where the molecules undergo many more collisions with each other than they do with the walls of the container. Moreover the density is such that the majority of collisions occur between two molecules. The first condition implies that the mean free path is very much smaller than the dimensions of the vessel and the second implies that the thermodynamic state of the gas can be described by the virial series up to the second virial coefficient.

(i) The Dynamics of Molecular Collisions

In order to obtain expressions for the transport properties of real gases it is necessary to consider the dynamics of molecular encounters. In addition it is necessary to consider a system in which the molecules may experience both attractive and repulsive forces depending on their separations. This analysis is for a system of spherical molecules in which the electronic state of the molecules does not change on collision.

Expressions may be obtained for the collision by a consideration of the collisional invarients and classical equations of motion. By changing the variables and the axis system, the problem may be reduced to a two-body system in a plane, then to a one-body system in a plane, and finally to the one-dimensional motion of a hypothetical single particle.

The present summary will begin at the two dimensional one-body stage which is illustrated in Figure (2.2)

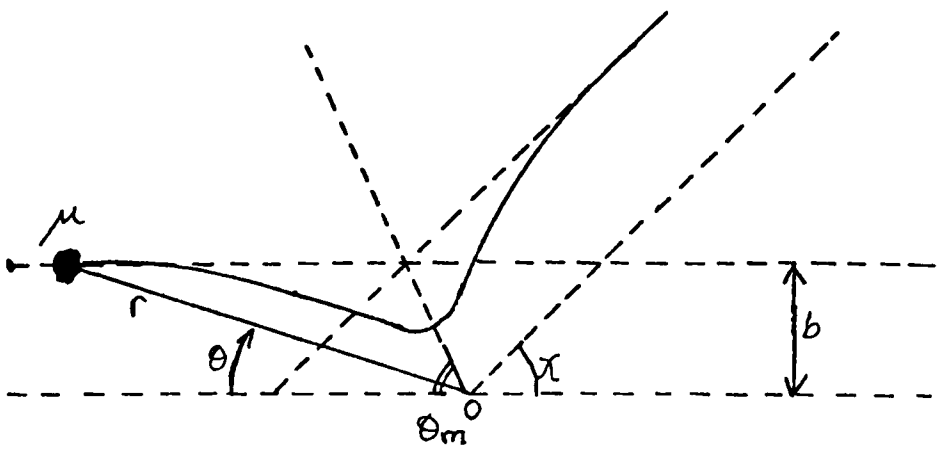


FIGURE 2.2

Where θ = angle specifying the orientation,

θ_m = value of θ at the distance of closest approach

r : intermolecular separation

χ : angle of deflection

b, the impact parameter, is the distance of closest approach in the absence of the potential U(r), χ_m is related to θ_m by:

$$\chi_m = \pi - 2\theta_m \qquad (2.31)$$

From a consideration of the summational invariants, one may derive the expression for the angle of deflection:

$$\chi(b,g) = \pi - 2b \int_{r_m}^{\infty} \frac{dr/r^2}{(1-U(r)/\frac{1}{2}\mu g^2 - b^2/r^2)^{\frac{1}{2}}} \qquad (2.32)$$

where g is the initial relative velocity and μ the reduced mass is equal to $m_i m_j/(m_i+m_j)$.

For a realistic potential function χ as a function of b and g has the form shown in Figure 2.3. Collisions with a large positive χ can be attributed to the repulsive part of the potential acting at small impact parameters, as b increases χ decreases until at b_1 the net force is zero and there is no deflection. For $b > b_1$ χ passes through a minimum χ_m at b_2 and converges to zero as b tends to infinity. For small values of g, χ_m goes to - infinity and b_o is then the 'orbiting value'. It should be noticed

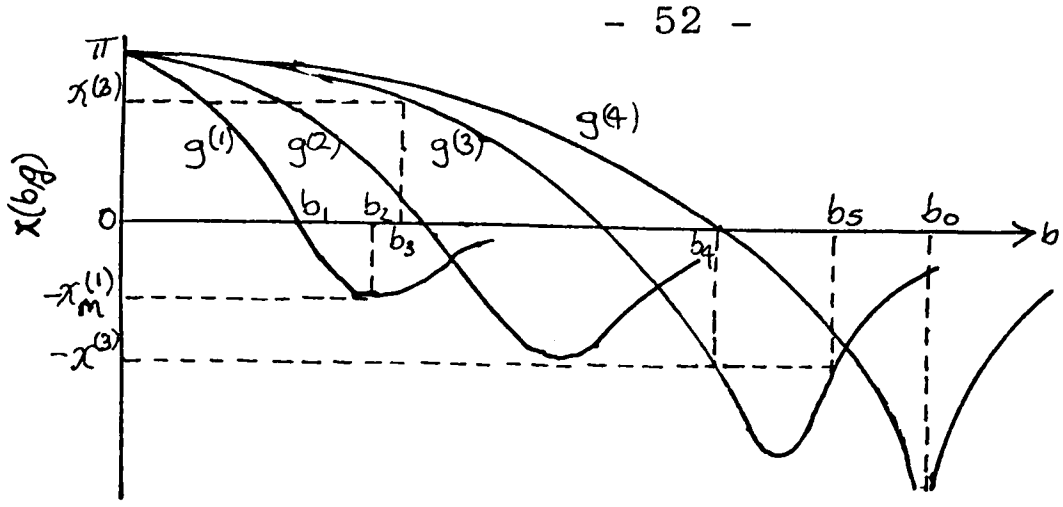


FIGURE 2.3 : Typical deflection functions. Relative initial speeds $g^{(1)} > g^{(2)} > g^{(3)} > (2E_4/\mu)^{\frac{1}{2}} > g^{(4)}$. ($E^4$ is the critical orbiting energy.

that as long as $\chi <+ \chi_m$ several values of the impact parameter (usually three) can lead to the same value of $|\chi|$ at the same relative velocity. $|\chi|$ is important as in scattering experiments only the magnitude of χ may be determined and not its sign. On the diagram b_3, b_4 and b_5 all lead to $|\chi|$. This means it is necessary when calculating the classical differential cross section to sum all these contributions to the scattering

$$\sigma(\chi,g) = \sum \left| \frac{b}{\sin\chi(d\chi/db)} \right| \qquad (2.33)$$

The χ function is concerned with the collsion integrals $\Omega^{(\ell,s)}$ as will be seen later.

(ii) Boltzmann Equation

A complete treatment of the state of a gas containing N molecules would aim to describe the positions and velocities of all molecules in the gas as a function of time by classical mechanics. Since N is so large $\approx 10^{20}$ this treatment is not possible and consequently the problem must be solved statistically to seek the probable behaviour of the N molecule system. This is a simpler approach. The assumption that only binary collisions occur implies that the position and velocity of a typical molecule are independent of the positions and velocities of the other (N-1) molecules. Since the same statement applies to any of the N molecules it is obvious that an adequate description of the probable behaviour of the N molecules is given by specifying the probable behaviour of a single molecule. This reduces the analysis to the search for a function $f(\underline{r},\underline{c},t)$ which is defined that $f\ \underline{dr}\ \underline{dc}$ is the probable number of molecules which will be found in the range $\underline{dr}$ about $\underline{r}$ with velocities in the range $\underline{dc}$ about $\underline{c}$.

This function f completely determines the property of a gas. The function f as defined above, for example, shows that the number density, the mean velocity $\underline{u}$ and the mean thermal kinetic energy E which may all be functions of $\underline{r}$ and t but not $\underline{c}$, are given by:

$$n(\underline{r},t) = \int f(\underline{r},\underline{c},t)d\underline{c} \qquad (2.34)$$

$$n(\underline{r},t)\underline{u}(\underline{r},t) = \int \underline{c}f(\underline{r},\underline{c},t)d\underline{c} \qquad (2.35)$$

$$n(\underline{r},t)E(\underline{r},t) = \int \tfrac{1}{2}m(\underline{c}-\underline{u})^2 f(\underline{r},\underline{c},t)d\underline{c} \qquad (2.36)$$

where the integrations are over all molecular velocities. For a gas whose molecules are not subject to external forces, the only mechanism available by which a molecule can change its velocity is that of collision with other molecules. Therefore in the absence of collisions if we consider a group of molecules located at $\underline{r}$ with velocities c at time t, then at the end of a small interval dt the molecules will be located at $\underline{r} + \underline{c}dt$ with identical velocities, so that

$$f(\underline{r},\underline{c},t)d\underline{r}d\underline{c} = f(\underline{r} + \underline{c}dt,\underline{c},t+dt)\underline{drdc} \qquad (2.37)$$

However, if collisional processes occur in the gas, then in the time dt some of the original molecules may be lost and others may be gained due to collision. If we denote the the number of molecules joining the group in time dt by $\Gamma^+ \underline{dr}\ \underline{dc}\ dt$ and those leaving the group $\Gamma^- \underline{dr}\ \underline{dc}\ dt$ then we can write

$$f(\underline{r}+\underline{c}dt,\ \underline{c},\ t+dt) - f(\underline{r},\underline{c},t) = (\Gamma^+ - \Gamma^-)dt \qquad (2.38)$$

Expanding the first term on the left of equation (2.38) in a Taylor series and taking the limit as dt tends to zero

we have:

$$(\frac{\partial}{\partial t} + \underline{c}.\frac{\partial}{\partial \underline{r}})f(\underline{r},\underline{c},t) = \Gamma^{+} - \Gamma^{-} \qquad (2.39)$$

Evidently, in order to complete this equation to yield the time and positional charge of f we must compute explicitly the number of gains and losses by the original group of molecules. Figure 2.4 shows a collision which results in a loss of one molecule (labelled 2) from the initial group

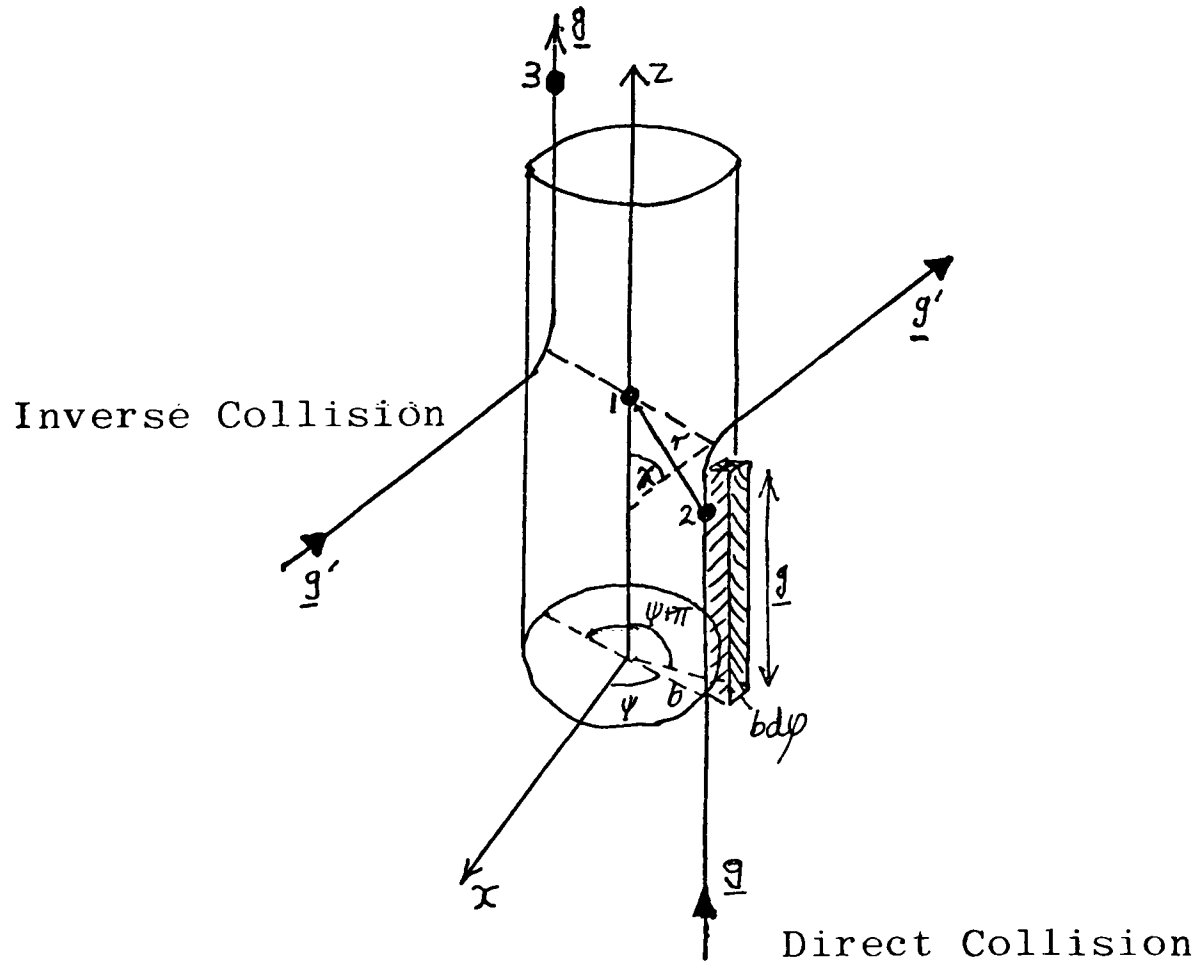


FIGURE 2.4 : Direct and Inverse binary collisions. The collision is drawn so that molecule 1 is at rest. The angle χ is the angle of deflection of the relative velocity of molecule 2. The angle ψ defines the orientation of the plane of the collision in space.

having a velocity $\underline{c}$. Before collision molecule 1 has a velocity $\underline{c}_1$, the velocity of molecule 2 being $\underline{c}$. Thus, molecule 2 is of the initial group whereas molecule 1 is not. The relative velocities before and after collision are defined by

$$\underline{g} = \underline{c} - \underline{c}_1 \tag{2.40}$$

$$\underline{g}' = \underline{c}' - \underline{c}_1' \tag{2.41}$$

respectively, where c_1' and c' are the velocities of molecules 1 and 2 respectively after collision. Because the collision is elastic, $|\underline{g}| = |\underline{g}'|$ and the effect of the collision is simply to rotate the velocity through an angle χ where $\underline{g}.\underline{g}' = g^2 \cos\chi$. Furthermore, because the centre of mass of the two body system moves at a constant velocity $\underline{G}$, throughout the encounter we have

$$\underline{G} = \tfrac{1}{2}\underline{c}_1 + \tfrac{1}{2}\underline{c} = \tfrac{1}{2}\underline{c}' + \tfrac{1}{2}\underline{c}_1' \tag{2.42}$$

so that

$$\underline{c}_1 = \underline{G} - \tfrac{1}{2}\underline{g}, \quad \underline{c} = \underline{G} + \tfrac{1}{2}\underline{g} \tag{2.43}$$

$$\underline{c}_1' = \underline{G} - \tfrac{1}{2}\underline{g}', \quad \underline{c}' = \underline{G} + \tfrac{1}{2}\underline{g}' \tag{2.44}$$

In addition to the relative velocity of the two molecules, the geometry of the collision is defined by the impact parameter b and the azimuthal angle ψ which defines the orientation of the plane in which the collision takes place. This collision changes the velocity of molecule 2

so that after collision it is no longer part of the original group. The number of collisions in time dt of molecules with initial velocities in the range $\underline{c}$ and $\underline{c} + d\underline{c}$ with a single molecule of velocity $\underline{c}_1$, such that the impact parameter lies between b and b + db and the azimuthal angle is between ψ and $\psi + d\psi$ is given by the number of molecules with velocity $\underline{c}$ which lie somewhere in a 'cylinder' of volume $gbdbd\psi dt$ at the beginning of the interval and by definition is equal to

$$bdbd\psi gf(\underline{r},\underline{c},t)d\underline{c}dt \qquad (2.45)$$

Now the number of molecules with velocities near $\underline{c}_1$ in a volume $d\underline{r}$ near $\underline{r}$ is $f(\underline{r},\underline{c}_1,t)d\underline{r}d\underline{c}_1$, so that the number of collisions between molecules with a velocity $\underline{c}$ and molecules with any velocity $\underline{c}_1$ at any impact parameter and any azimuthal angle in unit time is

$$\underline{dr}\ \underline{dc} \int_o^\infty d\underline{c}_1 \int_o^\infty bdb \int_o^{2\pi} d\psi gf(\underline{r},\underline{c},t)f(\underline{r},\underline{c}_1,t) \qquad (2.46)$$

This is equal to $\Gamma^- d\underline{r}\ d\underline{c}$ since each of these collisions results in the loss of a molecule from the initial group. This assumes only binary collisions occur and the condition of molecular chaos (1). This is that the probable number of molecules at $\underline{r}$ with velocities $\underline{c}$ is independent of the positions and velocities of other molecules.

Figure 2.4 also contains a diagram of the collision between molecules 1 and 3, which is said to be the inverse of that between molecules 2 and 1 in that after collision, molecule 3 has velocity $\underline{c}$ and consequently represents a gain of a molecule to the group f $d\underline{r}\ d\underline{c}$. Such an inverse collision occurs if molecule 3 has a velocity prior to collision of $\underline{c}'$ whereas molecule 1 has velocity $\underline{c}_1'$, so that the relative velocity prior to collision is $\underline{g}' = (\underline{c}' - \underline{c}_1')$. Furthermore it is necessary that the inverse collision occurs with the same impact parameter b and an azimuthal angle of $\psi + \pi$. By a similar argument to that for the previous direct collision, the number of inverse collisions occurring in a volume $d\underline{r}$ near $\underline{r}$ in unit time, each of which leads to a gain of a molecule to the group is

$$\Gamma^+ d\underline{r}\ d\underline{c} = d\underline{r}\ d\underline{c} \int_o^\infty d\underline{c}_1 \int_o^\infty bdb \int_o^{2\pi} d\psi g f(\underline{r},\underline{c}',t) f(\underline{r},\underline{c}_1',t \tag{2.47}$$

Here we have used the fact that the collision is elastic and so using the results of classical mechanics (2) $|\underline{g}| = |\underline{g}'| = g$ and $d\underline{c}d\underline{c}_1 = d\underline{c}'d\underline{c}_1'$.

Thus we can write a final equation of change for the function f as

$$\frac{\partial f}{\partial t} + \underline{c} \cdot \frac{\partial f}{\partial \underline{r}} = J(ff) \qquad (2.48)$$

$$J(ff) = \int_o^\infty d\underline{c}_1 \int_o^\infty bdb \int_o^{2\pi} d\psi g \{f(\underline{r},\underline{c}',t)f(\underline{r},\underline{c}_1',t) - f(\underline{r},\underline{c},t)f(\underline{r},\underline{c}_1,t)\} \qquad (2.49)$$

This non-linear integro-differential equation is the Boltzmann equation. The solution of this equation $f(\underline{r},\underline{c},t)$ should enable the calculation of all the macroscopic properties of a dilute gas. The intermolecular forces can be seen to influence the solution of the equation and hence the properties of the gas through their determination of the relationship between $\underline{c}$ and $\underline{c}_1$ and $\underline{c}'$ and $\underline{c}_1'$ according to classical mechanics.

(iii) Maxwell-Boltzmann equilibrium velocity distribution

In order to solve the Boltzmann equation for $f(\underline{r},\underline{c},t)$ in a general case we first consider a gas in equilibrium, that is a gas whose parameters of state and properties do not change with time or position. We can deduce from this that the solution of the Boltzman equation f_E is itself not a function of position or time, but only of velocity. This means that the left hand side of equation (2.49) is zero. It is then evident that in order for this to be true

$$f_E(\underline{c})f_E(\underline{c}_1) = f_E(\underline{c}')f_E(\underline{c}_1') \qquad (2.50)$$

for all possible values of $\underline{c}$, $\underline{c}_1$, b and ψ. Taking logarithms of both sides leadsto

$$\ell n f_e(\underline{c}) + \ell n f_e(\underline{c}_1) = \ell n f_e(\underline{c}') + \ell n f_e(\underline{c}_1') \qquad (2.51)$$

Since the only independent quantities in a collisional process for which this result is true are the number of molecules, the three components of linear momentum and kinetic energy, this leads to the conclusion that $\ell n f_e$ must be a linear combination of these five collisional invariants.

Hence

$$\ell n f_e(\underline{c}) = a_1 + \underline{a}_2 . \underline{c} + \tfrac{1}{2} a_3 mc^2 \qquad (2.52)$$

or
$$f_e(\underline{c}) = a_4 \exp\{-\tfrac{1}{2}a_6(\underline{c} - \underline{a}_5)^2\} \qquad (2.53)$$

where $a_1 - a_6$ are constants. The values of these constants may be deduced following application of the equations

$$n = \int f_E(\underline{c})d\underline{c} \qquad (2.54)$$

$$n\underline{u} = \int f_E(\underline{c})\underline{c}\, d\underline{c} \qquad (2.55)$$

$$nE = \frac{3}{2}nkT = \int f_E(\underline{c})\tfrac{1}{2}m(\underline{c} - \underline{u})^2 d\underline{c} \qquad (2.56)$$

Here, n is the number of density, $\underline{u}$ the average velocity and T the temperature. Equation (2.56) also defines

the kinetic theory temperature T, in terms of the average translational kinetic energy of the molecules which arises by virtue of their motion relative to the mean velocity of the gas. This definition renders the kinetic theory temperature identical with the thermodynamic temperature. The solution for $f_E(\underline{c})$ from these equations is:

$$f_E(\underline{c}) = n(\frac{m}{2\pi kT})^{3/2} \exp(-\frac{mC^2}{2kT}) \qquad (2.57)$$

where

$$C = \underline{c} - \underline{u} \qquad (2.58)$$

is the velocity relative to the mean velocity of the gas. It is called the peculiar velocity. For a gas at equilibrium one is often interested not in distribution of velocities but distribution of speeds, i.e. without regard to direction. To obtain this result equation (2.58) is integrated over all directions to give the Maxwell-Boltzmann distribution Law.

$$F(C) = 4\pi n \left(\frac{m}{2\pi kT}\right)^{3/2} C^2 \exp(-\frac{mC^2}{2kT}) \qquad (2.59)$$

C. Chapman-Enskog Solution

Chapman (3) and Enskog (4) independently solved the Boltzmann equation by means of a perturbation method. The solution of the Boltzmann equation in a more general

case is begun by studying the processes whereby an initially non-uniform gas approaches equilibrium. We shall consider only the case which corresponds to the most usual practical situation where the non-uniformities in the quantities $n(\underline{r},t)$, $\underline{u}(\underline{r},t)$ and $T(\underline{r},t)$ do not change significantly over a mean free path length $\bar{\ell}$. i.e.

$$\delta^* = \frac{\bar{\ell}}{x} \frac{\partial x}{\partial \underline{r}} \ll 1 \qquad (2.60)$$

where $x = n$, $\underline{u}$ or T, and δ^* is a measure of the deviation from a uniform state.

If we consider three time scales in the gas, t_1, corresponding to the motion of a molecule through the intermolecular potential of another $t_1 \approx 10^{-12}$s. t_2 is the average time between collisions, $t_2 \approx 10^{-9}$s and t_3 the time taken for a molecule to travel a distance corresponding to that of the container, $t_3 \approx 10^{-4}$s. For times $t << t_2$ $f(\underline{r},\underline{c},t)$ must be obtained from the general solution of the Boltzmann equation. For $t_3 > t >> t_2$ many collisions occur in a volume element $d\underline{r}$ at $\underline{r}$ and $f(\underline{r},\underline{c},t)$ changes rapidly with time due to velocity changes at each collision. However the total number of molecules, their total momentum and total energy remain constant since they are conserved in each collision. This means that f can rapidly adjust itself to the essentially constant values of $n(\underline{r},t)$, $\underline{u}(\underline{r},t)$ and $T(\underline{r},t)$ which exist in $d\underline{r}$ at $\underline{r}$: that is the quantity is independent of position within $d\underline{r}$, and also independent of time on the time scale $t_3 > t >> t_2$.

This process rapidly establishes local equilibrium within $d\underline{r}$ so that to a first approximation $f(\underline{r},\underline{c},t)$ is the function characteristic of the constant values of n, $\underline{u}$ and T. On a larger time scale than t_3, the non-uniformities in n, $\underline{u}$, T decay when every molecule has transversed the container many times. This second process leading to equilibrium is much slower so that the changes in $n(\underline{r},t)$, $\underline{u}(\underline{r},t)$ and $T(\underline{r},t)$ occur at a rate such that the rapid changes in $f(\underline{r},\underline{c},t)$ always allow it to keep up with them and maintain the local equilibrium to at least a first approximation.

This leads to a simplification of the solution providing we restrict ourselves to the slower equilibrating process, that is to the hydrodynamic regime. In these circumstances it is possible to regard f as dependent on t only through the dependencies of n, $\underline{u}$, and T on t since f always changes almost sufficiently rapidly to keep up with the changes. In addition we may assume that the explicit dependence of f on $\underline{r}$ is not greater than its indirect dependence via the dependence of n, $\underline{u}$ and T on $\underline{r}$. If we consider the time dependence of f, for $t >> t_2$

$$\frac{\partial f(\underline{r},\underline{c},t)}{dt} = \frac{\partial f}{\partial n}\frac{\partial n}{\partial t} + \frac{\partial f}{\partial \underline{u}}\cdot\frac{\partial \underline{u}}{\partial t} + \frac{\partial f}{\partial T}\cdot\frac{\partial T}{\partial t} \qquad (2.61)$$

Now we have established that if the frequency of collisions is very high the solution for f would approximate to a local equilibrium solution at each point in the gas. This

suggests a perturbative solution in terms of successive approximations which describe increasingly large departures from equilibrium. That is a solution of the form

$$f = f_o + \xi f_1 + \xi^2 f_2 + \ldots\ldots \qquad (2.62)$$

where $1/\xi$ measures the collision frequency. Therefore in the case of infinite collision frequency the solution becomes f_o. Arbitrary variation of ξ alters the total number of collisions occuring in unit volume in unit time, but does not affect the fraction of collisions with particular values of molecular velocities, impact parameter and orientation. The introduction of ξ implies a modification of the Boltzmann equation to allow for varying collision frequency and since the right hand side only of the Boltzmann equation (2.49) introduces the effect of molecular collisions, and since it is proportional to the collision frequency,this leads to:

$$\frac{\partial f}{\partial t} + \underline{c}.\ \frac{\partial f}{\partial \underline{r}} = \frac{1}{\xi}\ J(ff) \qquad (2.63)$$

Substituting for f (2.62) into (2.63) leads to the right hand side of the modified Boltzmann equation as

$$\frac{1}{\xi}\ J(f_o f_o) + \{J(f_o f_1) + J(f_1 f_o)\} + \ldots \qquad (2.64)$$

From this expression it is possible to obtain the following equations for the conservation of mass, momentum and energy.

$$\frac{\partial n}{\partial t} = - \sum_j u_j \frac{\partial n}{\partial x_j} - n \sum_j \frac{\partial u_j}{\partial x_j} \qquad (2.65)$$

$$nm \frac{\partial u_i}{\partial t} = - nm \sum_j u_j \frac{\partial u_i}{\partial x_j} - \sum_j \frac{\partial p_{ij}}{\partial x_j} \quad i = 1,2,3 \qquad (2.66)$$

$$\frac{3}{2} nk \frac{\partial T}{\partial t} = - \frac{3}{2} nk \sum_j u_j \frac{\partial T}{\partial x_j} - \sum_i \frac{\partial q_i}{\partial x_i} - \sum_i \sum_j p_{ij} \frac{\partial u_i}{\partial x_j} \qquad (2.67)$$

$$\text{where } p_{ij} = \int f(mC_iC_j)d\underline{c} \qquad i,j = 1 \text{ to } 3 \qquad (2.68)$$

$$q_i = \int f(\tfrac{1}{2}mC^2)C_i d\underline{c} \qquad i = 1 \text{ to } 3 \qquad (2.69)$$

In (2.67) the time dependence of the energy at a point arises from three contributions: convective, conductive and viscous dissipative processes corresponding to the three terms on the right hand side. The elements p_{ij} and q_i have a physical significance. For example p_{11} is the x_1-direction momentum (mC_1) of all the molecules crossing a plane of unit area perpendicular to the x_1-direction in unit time. It is therefore the force exerted on this plane in the x_1 direction (i.e. the normal stress). On the other hand p_{21} is the x_2-direction momentum (mC_2) of all the molecules crossing the same plane perpendicular to the x_1-direction in unit time. It is therefore the force per unit area in the x_2-direction, a shear stress. The element q_1 represents the amount of thermal kinetic energy transported across unit area perpendicular to the x_1-direction in unit time. This is the heat flux in the x_1-direction

(i) The zeroth-order solution

This is essentially solved in a similar way to the equilibrium case which leads to the expression:

$$f_o(\underline{r},\underline{c},t) = n\left(\frac{m}{2\pi kT}\right)^{3/2} e^{-C2} \qquad (2.70)$$

where C is a dimensionless velocity:

$$C = \left(\frac{m}{2kT}\right)^{\frac{1}{2}} \underline{c} \qquad (2.71)$$

This solution corresponds to the Euler equations of hydrodynamics for an inviscid gas. That is an ideal gas with zero coefficients of viscosity and thermal conductivity. This is due to

$$q_i^{(o)} = 0 \qquad i = 1,2,3 \qquad (2.72)$$

$$p_{ii}^{(o)} = P=nkT \qquad i = 1,2,3 \qquad (2.73)$$

and $$p_{ij}^{(o)} = 0 \qquad i \neq j \qquad (2.74)$$

(ii) First-order solution

If the first-order expressions for the heat flux vector $\underline{q}^{(1)}$ and the elements of the stress tensor $p_{kj}^{(1)}$ are substituted into the general conservation equations (2.65) to(2.67)) we obtain the Navier-Stokes equations of hydrodynamics. The solution of these which involves an expansion in Sonine polynomials (5) leads to the following

definition of the transport coefficients and introduces the collision integrals $\Omega^{(\ell,s)}(T)$.

$$[\lambda]_1 = \frac{25}{32}\left(\frac{kT\pi}{m}\right)^{\frac{1}{2}} \frac{C_v}{\Omega^{(2,2)}(T)} \tag{2.75}$$

$$[\eta]_1 = \frac{5}{16} \frac{(m\pi kT)^{\frac{1}{2}}}{\Omega^{(2,2)}(T)} \tag{2.76}$$

The quantity $\Omega^{(2,2)}(T)$ is defined by:

$$\Omega^{(2,2)}(T) = \frac{1}{6}\int_o^\infty Q^{(2)}(g)e^{-\gamma^2}\gamma^6 d(\gamma^2) = \frac{1}{6}(kT)^{-4}\int_o^\infty$$

$$\gamma = \left(\frac{m}{2kT}\right)^{\frac{1}{2}} g \qquad Q^{(2)}(E)e^{-E/kT}E^3 dE \tag{2.77}$$

Here $E = \gamma^2 kT = \frac{1}{4} mg^2$ the relative kinetic energy of collision and the transport cross-section $Q^{(2)}(E)$ is defined by

$$Q^{(2)}{}_E = 3\pi\int_o^\infty (1 - \cos^2\chi)bdb \tag{2.78}$$

The classical deflection angle is related to the intermolecular potential for spherical molecules as discussed earlier (equation (2.32)).

$$\chi(E,b) = \pi - 2b\int_{r_o}^\infty \frac{dr/r^2}{\{1-b^2/r^2-U(r)/E\}^{\frac{1}{2}}} \tag{2.79}$$

where r_o is the classical distance of closest approach in a collision.

The viscosity and thermal conductivity both contain the $\Omega^{(2,2)}(T)$ collision integral since the transport of momentum and energy are dominated by binary molecular collisions of the same type. Hence to a first-order approximation

$$[\lambda] = \frac{5}{2m} [\eta]_1 C_v \qquad (2.80)$$

(iii) Reduced collision integrals

For rigid spherical molecules of diameter d, it may be shown that the deflection angle χ is given by the expression $\cos \frac{1}{2}\chi = b/d$. Substitution of this leads to the following expression for $\Omega^{(2,2)}_{rs}(T)$ which is

$$\Omega^{(2,2)}_{rs}(T) = \pi d^2 \qquad (2.81)$$

For an intermolecular potential of the form $U(r) = \varepsilon f(r/\sigma)$ it is convenient to define reduced collsion integrals $\Omega^{(2,2)*}(T^*)$ by

$$\Omega^{(2,2)*}(T^*) = \Omega^{(2,2)} / \Omega^{(2,2)}_{rs}(T) \qquad (2.82)$$

$T^* = kT/\varepsilon$. By defining additional reduced variables

$$r^* = r/\sigma, \quad b^* = b/\sigma, \quad U^* = U/\varepsilon, \quad E^* = E/\varepsilon$$

and equations (2.77 - 2.79) become

$$\Omega^{(2,2)*}(T^*) = \frac{1}{6T^{*4}} \int_o^\infty e^{-E^*/T^*} E^{*3} Q^{(2)*}(E^*) dE^* \quad (2.83)$$

where $$Q^{(2)*}(E^*) = 3\int_o^\infty (1-\cos^2\chi) b^* db^* \quad (2.84)$$

and $$\chi(E^*, b^*) = \pi - 2b^* \int_{r_o^*}^\infty \frac{dr^*/r^{*2}}{\left\{1 - \frac{b^{*2}}{r^{*2}} - \frac{U^*(r^*)}{E^*}\right\}^{1/2}} \quad (2.85)$$

The equations for thermal conductivity and viscosity now become

$$[\lambda]_1 = \frac{25}{64} \left(\frac{kT\pi}{m}\right)^{\frac{1}{2}} \frac{C_v}{\sigma^2 \Omega^{(2,2)*}(T^*)} \quad (2.86)$$

and $$[\eta]_1 = \frac{5}{16} \left(\frac{mkT}{\pi}\right)^{\frac{1}{2}} \frac{1}{\sigma^2 \Omega^{(2,2)*}(T^*)} \quad (2.87)$$

The higher order corrections to these expressions are given in the form

$$[\eta]_m = [\eta]_1 f_\eta^{(m)} \quad (2.88)$$

where $f_\eta^{(m)}$ is a factor close to unity and which is a function of the generalized collision integrals $\Omega^{(\ell,s)}(T)$ given by:

$$\Omega^{(\ell,s)}(T) = [(s+1)!(kT)^{s+2}]^{-1} \int_o^\infty Q^{(\ell)}(E) e^{-E/kT} E^{s+1} dE \quad (2.89)$$

where the transport cross section $Q^{(\ell)}(E)$ is

$$Q^{(\ell)}(E) = 2\pi\left[1-\frac{1+(-1)^{\ell}}{2(1-\ell)}\right]^{-1}\int_{o}^{\infty}(1-\cos^{\ell}\chi)bdb \qquad (2.90)$$

χ given by equation (2.79) and similarly for the reduced collision integrals.

The self diffusion coefficient is a function of a different collision integral $\Omega^{(1,1)}$ and is given by

$$[D_{11}]_1 = \frac{3}{8n}\left(\frac{kT}{\pi m}\right)^{\frac{1}{2}}\frac{1}{\sigma_{11}^2\,\Omega_{11}^{(1,1)*}(T_{11}^*)} \qquad (2.91)$$

(iv) <u>Transport coefficients for binary mixtures</u>

In a binary gas mixture there are three types of two-body collisions possible, each characterized by a different intermolecular potential function $U_{11}(r)$, $U_{22}(r)$ and $U_{12}(r)$ having parameters ε_{11}, σ_{11}, ε_{22}, σ_{22}, ε_{12} and σ_{12} respectively. By arguments similar to those presented for pure gases it is possible to obtain expressions for the viscosity and thermal conductivity of a binary mixture, e.g. the viscosity of a binary gas mixture to a first approximation may be written:

$$[\eta_{mix}]_1 = \frac{1 + Z_\eta}{X_\eta + Y_\eta} \qquad (2.92)$$

where

$$X_\eta = \frac{x_1^2}{[\eta_1]_1} + \frac{2x_1x_2}{[\eta_{12}]_1} + \frac{x_2^2}{[\eta_2]_1}$$

$$Y_\eta = \frac{3}{5} A_{12}^* \left[\frac{x_1^2}{[\eta_1]_1} \left(\frac{m_1}{m_2}\right) + \frac{2x_1x_2}{[\eta_{12}]_1} \left\{ \frac{(m_1+m_2)^2}{4m_1m_2} \right\} \left(\frac{[\eta_{12}]_1^2}{[\eta_1]_1[\eta_2]_1} \right) + \frac{x_2^2}{[\eta_2]_1} \left(\frac{m_2}{m_1} \right) \right]$$

$$Z_\eta = \frac{3}{5} A_{12}^* \left[x_1^2 \frac{m_1}{m_2} + 2x_1x_2 \left\{ \frac{(m_1+m_2)^2}{4m_1m_2} \left(\frac{[\eta_{12}]_1}{[\eta_1]_1} + \frac{[\eta_{12}]_1}{[\eta_2]_1} \right) - 1 \right\} + x_2^2 \left(\frac{m_2}{m_1} \right) \right]$$

where $[\eta_1]_1$ and $[\eta_2]_1$ are the first order expressions for the viscosities of pure components 1 and 2, $[\eta_{12}]$ is the interaction viscosity which corresponds to the viscosity of a hypothetical gas of molecules with a mass equal to twice the reduced mass of the two components and whose intermolecular potential is $U_{12}(r)$. A_{12}^* is the ratio of two collision integrals:

$$A_{12}^*(T_{12}^*) = \Omega_{12}^{(2,2)}(T_{12}^*)/\Omega_{12}^{(1,1)*}(T_{12}^*) \qquad (2.93)$$

D. Polyatomic Gases

In obtaining the transport coefficients for a dilute, monatomic gas we solved the Boltzmann equation for f the distribution function. In the case of polyatomic species such a distribution function is not adequate since the distribution of the molecules among their various internal states is not described by such a function.

One treatment uses the Wigner distribution function (6) which describes the probability of finding molecules in a particular region of configuration velocity space and in specified internal states. This leads to a Boltzmann-type equation, the Waldmann-Snider equation (7,8). This equation has been solved and expressions for some of the transport coefficients have been produced (9-11). The quantum mechanical kinetic theory is extremely complex and for the usual transport coefficients only small corrections are required to expressions produced by the purely classical approach of Taxman (12) and the semi-classical treatment of Wang Chang and Uhlenbeck (13).

(i) Semi Classical Theory

In this theory of Wang Chang and Uhlenbeck a distribution function f_i is defined for each possible quantized internal state of the molecule. The binary collisions are treated quantum mechanically which allows the concept of inverse collisions to be invoked but otherwise the treatment

is classical. The solution for f_i is similar to that used for the Boltzmann equation although conservation of angular momentum which needs to be considered for the quantum mechanical kinetic theory is not considered. This is a limitation of the semi-classical theory and the treatment is unable to account for all the transport properties of rotating molecules since the semi-classical argument requires the molecules to be in definite internal states before and after collision. According to the uncertainty principle this is only valid if ΔE_{int} the energy difference between two internal states of a molecule and the time between molecular collisions t_{coll} satisfy the inequality

$$\Delta E_{int}\ t_{coll} \geqslant \hbar \qquad (2.94)$$

For degenerate rotational levels $\Delta E_{int} = 0$ and so this inequality is not valid. Therefore strictly the Wang Chang Uhlenbeck theory cannot be applied to molecules with rotational energy states. In practice, however, the numerical errors arising from this are small (14).

(ii) Classical Theory

In the approach of Taxman collision dynamics and the internal energy of molecules are treated classically. In a classical analysis inverse collisions cannot be assumed to exist, however, Taxman showed that by a finite

set of collisions molecules can return to their former states before a direct collision from those after the collision. The theory gives a classical Boltzmann equation which may be solved to give the transport coefficients.

(iii) Semi-classical transport coefficients

To an approximation equivalent to first order Chapman Couling the shear viscosity of a dilute polyatomic gas may be written (15):

$$[\eta]_1 = \frac{5}{16} \frac{(m\pi kT)^{\frac{1}{2}}}{Z(T)} \qquad (2.95)$$

Z(T) incorporates all the information about binary collisions for a particular temperature. It is considerably more complex than $\Omega^{(2,2)}(T)$ the corresponding function for a monatomic species.

$$Z(T) = \frac{1}{2} [\sum_i \exp(-\varepsilon_i)]^{-2} \sum_{ijk\ell} \exp(-\varepsilon_i - \varepsilon_j) \; x$$

$$\int_o^\infty \int_o^{2\pi} \int_o^\pi [\gamma^4 \sin^2\chi + \frac{1}{3}(\Delta\varepsilon)^2 - \frac{1}{2}(\Delta\varepsilon)^2 \sin^2\chi]\gamma^3 \; x$$

$$\exp(-\gamma^2) I_{ij}^{k\ell} \sin\chi d\chi d\psi d\gamma \qquad (2.96)$$

$$\gamma \simeq \left(\frac{m}{4kT}\right)^{\frac{1}{2}} \underline{g} \qquad \varepsilon_i = \varepsilon_i'/kT \text{ and}$$

$$\Delta\varepsilon = \varepsilon_k + \varepsilon_\ell - \varepsilon_i - \varepsilon_j \tag{2.97}$$

ε_i' = energy of ith internal quantum state. i, j, are initial internal quantum states. $I_{ij}^{k\ell}$ is the degeneracy-averaged differential scattering cross-section (16). The accurate evaluation of these cross-sections is very expensive in terms of computer time and approximations have been made in order to simplify the evaluations. One such evaluation which has been used is that due to Mason and Monchick the results of which are used in Chapter 7.

(iv) <u>The Mason Monchick approximation</u> (15)

The Mason Monchick approximation starts from the recognition that the change in internal energy $\Delta\varepsilon$ for a binary encounter usually involves only a few quanta of internal energy, and that at moderate temperatures the significant internal energy is in rotational modes. The quanta of internal energy for rotation are in general $<<$ kT hence $\Delta\varepsilon << 1$. The reduced relative kinetic energy γ^2 is of order unity so to a first approximation $\Delta\varepsilon$ may be neglected compared to γ^2.

This implies that the trajectories of colliding molecules are insignificantly distorted by exchange of $\Delta\varepsilon$

between translational and internal energies. Hence the inelastic differential cross-section may be replaced by its value for elastic scattering I_{el}. This leads to the following expression for shear viscosity.

$$\eta = \frac{5}{16} \frac{(mkT\pi)^{\frac{1}{2}}}{<\Omega^{(2,2)}(T)>} \qquad (2.98)$$

where $<\Omega^{(2,2)}(T)>$ is the collision integral averaged over all orientations. This averaging will be discussed in more detail later.

E. Quantum effects

It is possible to modify the collision process to include quantum effects. (17). In this the collision processes are described in terms of phase shifts which are obtained through solution of the radial wave equation:

$$\frac{d^2}{dr^{*2}} + \frac{4\pi^2}{\Lambda^{*2}} [E^* - U^*(r^*)] - \frac{\ell(\ell+1)}{r^{*2}} r^* R_e(r^*) = 0 \qquad (2.99)$$

$r^* = r/\sigma$, $R_e(r^*)$ is the radial wavefunction, ℓ is the angular momentum quantum number $E^* = E/\varepsilon$ and

$$\Lambda^* = h/[\sigma(2\mu\varepsilon)^{\frac{1}{2}}] \qquad (2.100)$$

is the reduced de Broglie wavelength which governs the magnitude of quantum effects. In this work Λ^* is sufficiently small so that the effects of quantum effects on the collision integrals has been shown (18,19) to be negligible. They have therefore been ignored in this work.

CHAPTER 3

THE MEASUREMENT OF VISCOSITY

A. Theory

There are two types of method which may be used to measure gas viscosity. These are absolute methods where no external viscosity data are required to calculate the results, and relative methods where external data must be used to calibrate the apparatus. The experimental methods for carrying out these measurements have been known, in general, for at least fifty years. However, only in the last ten to fifteen years have reliable measurements been made over a wide range of temperatures. The reasons for this are principally poor apparatus design and an inadequate knowledge of the theory underlying the experimental measurements. Accurate absolute determinations have been made by placing a gas between two concentric cylinders and measuring the torque experienced by one cylinder when the other is rotated. The most notable measurement of this type was that of Beardøn(1) who made an accurate determination of the viscosity of air at room temperature upon which most relative measurements are based (2).

Kestin and his group (3) have employed an oscillating disc viscometer which involves the observation of the damping effect of a gas on the oscillations of a thin disc placed close to a stationary plate. Both relative

and absolute determinations are possible by this method which is more easily adapted to the measurement of viscosities over a wide range of temperature than the cylinder method and a judicious choice of the characteristics of the suspension system permits absolute viscosity measurements to be made. The oscillatory disc method is capable of producing results to high accuracy typically of the order of 0.1 - 0.3%. It is possible by use of suitable torsion fibres for the suspension of the discs to make measurements up to 1000K. The disadvantages of the method are that measurements above 1000K are limited by lack of suitable suspension materials, and that the dimensions of the apparatus and their variation with temperature must be known with very high accuracy.

The other principle method which has been extensively employed by this group and also in work by Guevara and his collaborators (4) is that of the capillary flow type. In this method the time taken for a known volume of gas to pass from a closed vessel through a capillary tube may be related to the viscosity of the gas at the temperature of the tube by the Hagen-Poiseuille equation for laminar flow: the capillary flow method which has been used in this work is unsuitable for absolute viscosity determinations since the flow rate of a gas through a capillary tube is proportional to the fourth power of its radius, as well as to the gas viscosity. Uncertainties, therefore, in the radii of the capillary tubes, which in this work are

of the order of a few percent seriously limit the accuracy of the measurements. This lack of uniformity introduces a geometric factor Γ into the equations derived later. However, the theory of capillary flow viscometry is now well adapted to give relative determinations based on a single room temperature standard of viscosity. A further very important feature, is that measurements on such an apparatus may be made over a wide temperature range, thus providing data which may be used in inversion methods (see Chapter 4) to give the intermolecular pair potential energy function. In this work the capillary flow method was used to provide viscosity data in the temperature range 120-1600K to an accuracy which was estimated to be $\pm$ 1%.

a) Theory of Capillary Flow

As a gas passes through a capillary tube, it may do so by one of four types of flow:

(i) Laminar or Poiseuillian Flow

This is normal streamline viscous flow; the flow is parallel to the axis of the pipe, i.e. the fluid velocities are symmetrically distributed about the axis. In addition the velocity at the walls is zero. The flow rate is then governed by Poiseuille's equation. One may define a Knudsen number $K = \bar{l}/d$ where $\bar{l}$ is the mean free path and d is the tube diameter. In this region $K \sim 10^{-5}$.

(ii) Turbulent flow

This occurs when the fluid velocity increases to an extent such that the flow becomes full of eddies. The onset of such flow can be considered to occur at a critical value of the Reynold's number (5) $R_e = 2r\rho v/\eta$ (ρ = density of the gas). This value is usually of an order 2300-4000 being towards 2000 for straight pipes and increasing to the higher value for curved pipes. In the present work the Reynolds number lies in the range 0.3 - 270 so turbulent flow is absent.

(iii) Slip Flow

This type of flow occurs at pressures such that $K \approx 10^{-2} - 10^{-1}$ i.e. when the mean free path is between 1-10% of the capillary diameter. In such circumstances the fluid velocity at the walls cannot be ignored.

(iv) Free molecule flow (6)

This occurs at extremely low pressures, where $K > 5$ and hence molecule-wall collisions govern the flow rate. The work described here has $K \approx 10^{-2} - 10^{-4}$, corresponding to slip and laminar flow.

Initially we will consider the flow of an incompressible fluid, the solution will then be modified for gases.

Let us consider the laminar flow of such an incompressible fluid through a capillary tube.

For a short cylinder of this fluid of radius a, length dx, one can equate the force arising from the pressure difference (dP) between its ends with the viscous shearing stress acting over its surface:

$$\pi a^2 dP = 2\pi a.\eta dx \frac{dv}{da} \qquad (3.1)$$

On integrating, since dP/dx is independent of a (laminar flow), using the boundary conditions that v = 0 at the walls (i.e. no slip) where a = r we obtain:

$$v = - \frac{1}{4\eta} \frac{dP}{dx} (r^2 - a^2) \qquad (3.2)$$

The distribution of velocities is therefore parabolic, with the maximum being in the centre and decaying to zero at the walls.

Now the volume swept out in unit time by an annulus of width da is given by $2\pi a.v.da$. The total volume flowing per second through the cross-section at x is thus:

$$\frac{dV}{dt} = \int_o^r 2\pi a.v.da = - \frac{\pi r^4}{8\eta} \frac{dP}{dx} \qquad (3.3)$$

This expression for dv/dt (3.3) gives the original Poiseuille equation on integration along the length of the tube - since the volume flow rate is independent of pressure.

$$\frac{dv}{dt} = \frac{\pi r^4 \Delta P}{8L\eta} \qquad (3.4)$$

In order to use equation (3.3) for gases we need to convert the volume flow rate to a molar flow rate dn/dt which is constant along the tube. Assuming the gas to be ideal:

$$\frac{dv}{dt} = \frac{RT}{P} \cdot \frac{dn}{dt} \qquad (3.5)$$

Where P is the mean pressure of a small volume dv containing dn moles of gas. Since dn/dt is independent of position along the tube then combining equations (3.3) and (3.5) gives:

$$RT. \frac{dn}{dt} = -\frac{\pi r^4 P}{8\eta} \frac{dP}{dx} \qquad (3.6)$$

Integrating along the tube and introducing the boundary conditions $P = P_f$ at $x = 0$, and $P = P_b$ at $x = L$

$$\frac{dn}{dt} = \frac{\pi r^4}{16\eta LRT} (P_f^2 - P_b^2) \qquad (3.7)$$

This equation is the basis for capillary flow viscometry . although it only applies when all the conditions used in its derivation are met. Usually, therefore, corrections need to be made and these are discussed in the next section.

b) Corrections to Poiseuille's equation

(i) Slip

The derivation of Poiseuille's equation assumes that the flow velocity of the layer of fluid at the wall is zero. In fact this layer must be considered to have a small but finite velocity. Molecules near the wall of the tube consist of 50% moving towards the surface with a mean flow momentum characteristic of the layer where they made their last collision and 50% moving away from the surface with zero mean flow momentum. Thus the net momentum of all these molecules cannot be zero. The correction to the flow rate takes the form of a constant $(1 + 4\xi/r)$ where $\xi = \eta/\varepsilon$ where ε is a constant called the external coefficient of friction. This quantity ξ represents the imaginary distance the surface must be moved back in order that the wall velocity should be truly zero. The factor is negligible when r is large compared to ξ, but when r is small the flow is controlled by slip, becoming proportional to r^3 instead of r^4. There have been many attempts to derive theoretical expressions for ξ. Meyer (7) using simple kinetic theory, deduced that $\xi = \bar{l}$, the mean free path. Maxwell (8) developed a model in which only a fraction f of the molecules are diffusely reflected from the surface, the remaining molecules being specularly reflected retaining their initial tangential momentum.

This led to the relation $\xi = \frac{(2-f)\bar{l}}{f}$, but the value of f remained undetermined. However Knudsen (9), determined experimentally that $\xi = 4/3\ \bar{l}$, corresponding to f ≈ 85% and this formulahas been used by many subsequent workers. Recent theoretical calculations try to investigate the perturbation of the distribution function at the surface but are still confined to simplified models. They deduce that ξ is directly proportional to $\bar{l}$ but constants of proportionality have ranged from 1.0 to 1.33 (10,11). In this work therefore it was considered to be more accurate to correct for slip by utilising its dependence on pressure.

Since η/ε is proportional to $\bar{l}$, the factor $(1 + 4\eta/\varepsilon r)$ may be written $(1 + K\bar{l}/r)$ where K is a constant. Equation (3.7) therefore becomes

$$\frac{dn}{dt} = -\frac{\pi r^4 P}{8\eta RT} \frac{dP}{dx} [1 + K\bar{l}/r] \qquad (3.8)$$

in the slip region. Using the simple kinetic theory expression for η (Chapter 2):

$$\eta = {}^1/3\ \rho\ \bar{c}\ \bar{l}$$

and $\bar{c} = (8RT/\pi M)^{\frac{1}{2}}$ along with $\rho = PM/RT$ where M is the molecular weight of the gas gives:

$$\frac{K\bar{l}}{r} = \frac{3K\eta}{r\rho\bar{c}} = \frac{3K\eta}{r\bar{P}} \left(\frac{\pi RT}{8M} \right)^{\frac{1}{2}} \qquad (3.9)$$

hence the slip coefficient k_s becomes:

$$k_s = 1 + \frac{4\xi}{r} = 1 + \frac{K_s \eta}{r\bar{P}} \left(\frac{T}{M}\right)^{\frac{1}{2}} \qquad (3.10)$$

where $\bar{P}$ is the average pressure in the capillary tube, $\frac{1}{2}(P_f+P_b)$ and K_s is a constant which can be determined if the true viscosity is known. Hopefully K_s would be independent of the nature of the gas and the temperature. However, this assumption is not borne out by experiment (12,13) and indicates a need to determine K_s experimentally as a function of temperature and gas, or to work under conditions such that the slip coefficient is negligible (at high pressures). In this work which involved the measurement of viscosities at temperatures less than 300K where slip is not as important as it is at high temperatures we adopted the expression found for K_s by Gough (14).

$$K_s/J^{\frac{1}{2}}K^{-\frac{1}{2}} = 18.0 - 0.03\ (T_c - 290) \qquad (3.11)$$

i.e. K_s is temperature dependent but independent of the nature of the gas. K_s thus varies linearly with temperature. For mixtures the average molecular weight was taken for M. This is not strictly correct since the mean free path does not vary in a simple manner with composition (15). However, for the small corrections employed in the present work, this simplification was considered to be justifiable.

(ii) Correction for non-ideality

The perfect gas law was assumed in our derivation of equation (3.5) hence if we apply instead the virial equation of state, up to the second virial coefficient B, for our small volume of gas we get:

$$PV = nRT\ (1 + \frac{Bn}{V})$$

$$= nRT\ (1 + \frac{BP}{RT}) \qquad (3.12)$$

assuming the correction is small, this gives for the molar flow rate:

$$RT\ \frac{dn}{dt} = \frac{P}{1 + BP/RT}\ \frac{dV}{dt} \qquad (3.13)$$

Substituting in equation (3.3) including the geometrical factor Γ referred to earlier, and expanding the demonimator by the binomial theorem:

$$\frac{dn}{dt}\ .dx = -\frac{\Gamma\pi r^4}{8\eta RT}\ P(1 - \frac{BP}{RT})\ dP \qquad (3.14)$$

which after integating along the length of the capillary and applying the boundary conditions gives:

$$\frac{dn}{dt} = \frac{\Gamma\pi r^4}{8\eta LRT}\left[\frac{1}{2}(P_f^{\,2} - P_b^{\,2}) - \frac{B}{3RT}\ (P_f^{\,3} - P_b^{\,3})\right] \qquad (3.15)$$

The correction for non-ideality, k_B, is therefore:

$$k_B = 1 - \frac{2B}{3RT} \frac{(P_f^3 - P_b^3)}{(P_f^2 - P_b^2)} \qquad (3.16)$$

(iii) Kinetic energy correction

A small correction is needed to take into account the supply of kinetic energy required to accelerate the fluid as it enters the capillary and which is dissipated into the reservoir at the end of the tube as heat. This correction is the Hagenbach correction and is very important for liquids (16), where the mass flow rate is much higher than that for gases. The correction to the viscosity is of the form:

$$- m \frac{\rho}{8\pi L} \cdot \frac{dv}{dt}$$

where m is a constant of approximate value 1.1, and which can be determined experimentally by plotting the apparent viscosity against flow rate. We thus apply a correction of the form:

$$k_H = 1 - \frac{1.1M}{8\pi\eta L} \cdot \frac{dn}{dt} \qquad (3.17)$$

Where dn/dt may be expressed to sufficient accuracy in terms of experimental quantities to be defined later as $\Delta(P_f V_f)/RT_f t$.

There are two other effects which occur at the entrance of the capillary. These can, however, be ignored in the capillary used in the present work due to its length ($L/r \approx 10^4$). These are the energy used to establish the parabolic velocity profile required by Poiseuille's equation and also in the convergence of the streamlines (The Couette correction). The latter has the effect of introducing an effective length $L' = L + nr$, $n \approx 0.8$, whilst the former changes the value of m from 1.1 to 1.12. Both these effects are negligible in the present work.

(iv) Curve pipe flow correction

The capillary used in this work is coiled in the form of a helix. This curvature introduces an increased resistance to flow which was first investigated by W.R. Dean in 1911 (17) for the case of liquids. He showed that superimposed on the stream-line flow parallel to the axis of the pipe, there is a secondary flow such that fluid at the centre of the pipe is forced to the outside, returning along the upper and lower walls, and thus any particular portion of the fluid moves in an elongated spiral motion along the pipe. Now Poiseuille's equation is no longer strictly valid, however under certain conditions the deviations are small. Dean found that the increased resistance for a curved pipe over that in a straight pipe of similar dimensions is related to the fourth power of a dimensionless parameter called the Dean number (De) defined as:

$$(De) = R_e \left(\frac{r}{R_c}\right)^{\frac{1}{2}} \qquad (3.18)$$

Where R_c is the radius of curvature of the pipe and (R_e) is the Reynold's number defined earlier. This was verified experimentally by White (18) using the flow of water through pipes of varying radii of curvature. In the case of gases the situation is less straightforward as no theoretical treatment of the flow of compressible fluids in curved pipes has yet been given. However, it is possible to obtain information on the effect from experiment, in the manner suggested by Dawe (13) and this was carried out by Clarke (19) for this particular apparatus. The study confirmed the conclusions of Larrain and Bonilla (20) in that significant curved-pipe effects (a correction of 0.1%) appeared around a Dean number of 5. Although the corrections tend to cancel out for relative viscosity measurements, it was decided to only use measurements with Dean numbers less than 5 in our experiments. The Dean number was calculated from the formulae:

$$(R_e) = \frac{2r\rho v}{\eta} = \frac{2r\rho}{\eta} \frac{M}{\pi r^2 \rho} \frac{dn}{dt} = \frac{2M}{\pi r \eta} \cdot \frac{dn}{dt} \qquad (3.19)$$

$$(D_e) = (R_e) \left(\frac{r}{R_c}\right)^{\frac{1}{2}} = \frac{r^3 M(p_f^2 - P_b^2)}{8\eta^2 LRT} \left(\frac{r}{R_c}\right)^{\frac{1}{2}} \qquad (3.20)$$

Although the Dean number increases as the temperature decreases this could be overcome by decreasing the pressures P_f and P_b and so very few times of flow were affected.

We thus have a working equation for the flow of a real gas through a coiled capillary tube under present experimental conditions ($D_e < 5$)

$$\frac{dn}{dt} = \frac{\Gamma\pi r^4}{16\eta LRT}(P_f^2-P_b^2)\left(1 + \frac{K_s\eta}{r\bar{p}}\left(\frac{T}{M}\right)^{\frac{1}{2}}\right)\left(1 - \frac{2B}{3RT}\frac{(P_f^3-P_b^3)}{(P_f^2-P_b^2)}\right) \times \left(1 - \frac{1.1M}{8\pi\eta L}\cdot\frac{dn}{dt}\right) \qquad (3.21)$$

$$= \frac{\Gamma\pi r^4}{16\eta LRT}(P_f^2-P_b^2)\, k_S k_B k_H \qquad (3.22)$$

Now we consider the application of equation (3.22) to the experiments carried out in this work.

c) Theory of the Present Apparatus

No attempt was made in the present work to obtain absolute viscosities via equation (3.21). Instead, the relative method was adopted, i.e. ratios of viscosities were determined to high accuracy. The experimental set-up is shown schematically below.

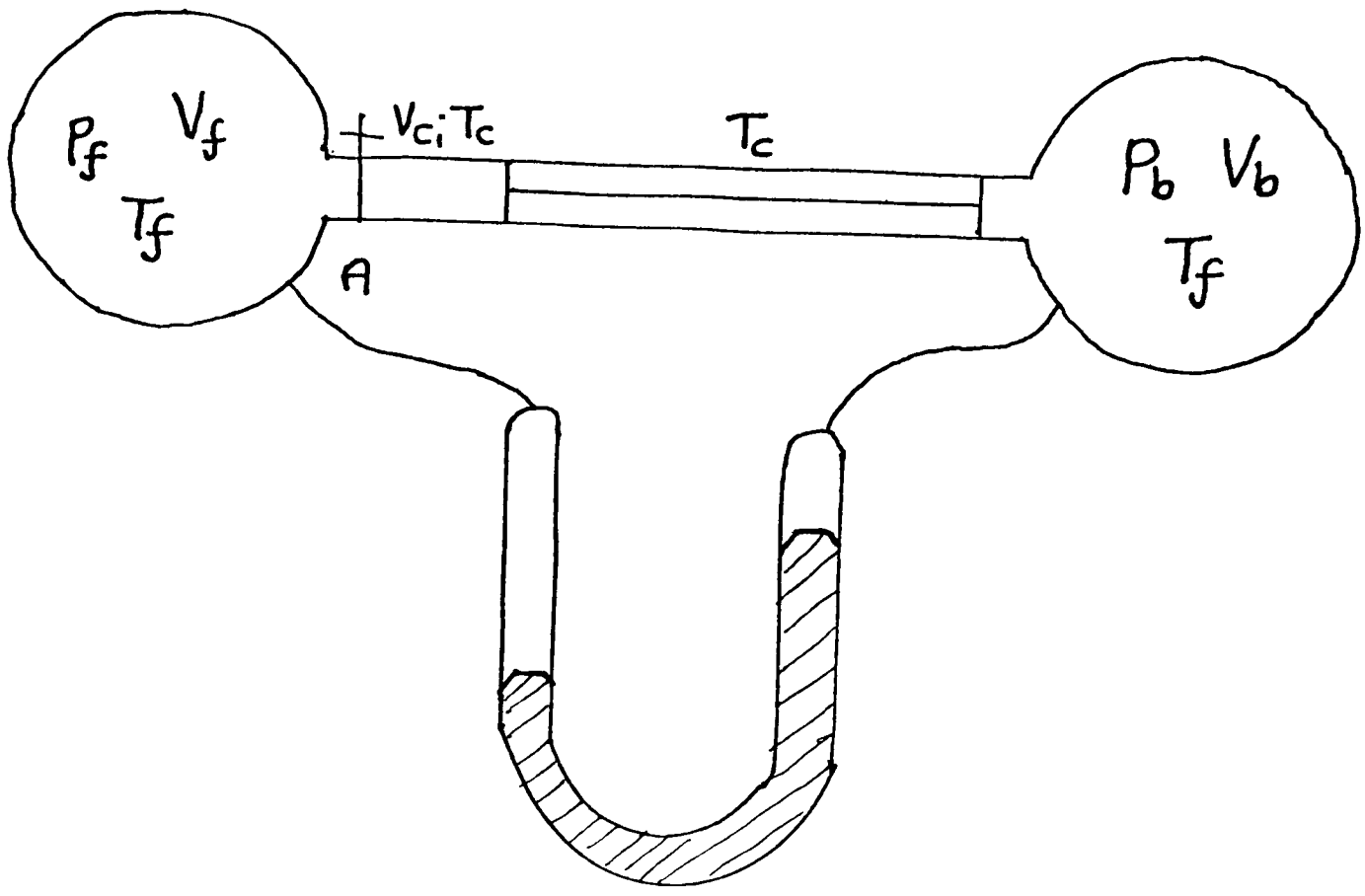


Figure 3.1

Gas flows from the left hand globe at pressure p_f via the capillary, at a temperature $T = T_c$, to the right hand globe where the pressure is P_b, the volume of the capillary is negligible and the pressure difference $P_m = P_f - P_b$ is monitored using a mercury manometer. Both the front vessel (volume V_f) and back vessel (V_b) are thermostatted at the constant temperature T_f. As the run proceeds, the pressure difference P_m slowly decreases and the time taken for the mercury surface in limb A of the manometer to fall between fixed points is recorded. If this procedure is then repeated for another gas under identical conditions, then the ratio of the viscosities of the two gases is, subject to several small, though

crucial, corrections equal to the ratio of the two flow times. The ratio of the viscosities of one gas between two temperatures to a first approximation is given by:

$$\frac{\eta_T}{\eta_o} = \frac{t_T}{t_o} \cdot \frac{T_o}{T} \qquad (3.23)$$

Where T, T_o are the absolute temperatures and t represents the time of flow Hence the only parameters which are required are the times of flow and the absolute temperature of the capillary. The volumes of the two vessels V_f and V_b are also required but only approximately for the calculation of correction terms.

Consider there to be n moles of gas in the volume V_f. Applying the virial equation of state to this volume, where $B_f = B(T_f)$ gives:

$$P_f V_f = nRT_f(1 + B_f n/V_f) \qquad (3.24)$$

$$\frac{d(P_f V_f)}{dt} = -\frac{dn}{dt} RT_f\left(1 + \frac{2B_f n}{V_f}\right) \qquad (3.25)$$

$$= -\frac{dn}{dt} RT_f\left(1 + \frac{2B_f P_f}{RT_f}\right)$$

the negative sign is necessary since $P_f V_f$ decreases with time and a second order term has been neglected on the right hand side of (3.25) from dV_f/dt. Hence substituting dn/dt from (3.22) gives

$$- \frac{d(P_f V_f)}{dt} = \frac{\Gamma \pi r^4 T_f}{16 \eta L T_c} (P_f^2 - P_b^2) k_S k_B k_H \left(1 + \frac{2B_f P_f}{RT_f}\right) \qquad (3.26)$$

Therefore, for a pressure drop from pointer i at t = 0 to pointer j where t = t,

$$I = \int_j^i \frac{d(P_f V_f)}{(P_f^2 - P_b^2)} = \frac{\Gamma \pi r^4 T_f t}{16 \eta L T_c} \left(1 + \frac{2B_f \bar{P}_f}{RT_f}\right) \bar{k}_S \bar{k}_B \bar{k}_H \qquad (3.27)$$

Where the correction terms are now evaluated at the mean pressure in the interval i to j. This separate integral for dn/dt from that for dp/dx (Eqn. 3.7) is possible since the rate of flow of gas through the capillary is very much greater than the rate of change of pressure P_f. For the present apparatus the ratio of the two rates is of the order of 3000 and hence we can integrate over the length of the capillary while assuming dn/dt to be constant.

Now rewriting equation (3.27) and denoting the first correction term for gas imperfection as $\bar{k}_b$

$$\eta = \frac{\Gamma \pi r^4 T_f t}{16 I L T_c} \cdot \bar{k}_b \bar{k}_S \bar{k}_B \bar{k}_H \qquad (3.28)$$

Hence we can, if we measure the time of flow for two gases 1 and 2 under identical conditions of pressure and volume (i.e. identical I) and at the same capillary temperature T_c obtain, ignoring correction terms.

$$\eta_1 / \eta_2 = t_1 / t_2 \qquad (3.29)$$

In addition if the time of flow of a single gas is measured at two different capillary temperatures T_o and T

$$\frac{\eta_T}{\eta_{T_o}} = \frac{t_T}{t_o} \frac{T_o}{T} \frac{I_o}{I_T} \left[1 + 3\alpha(T-T_o)\right] \qquad (3.30)$$

where the temperature dependence of I is due to the change in the temperature of the small volumes V_{fc} acting as a heat exchanger, and α is the coefficient of linear expansion of the capillary material. These two equations (3.29) and (3.30) are the basic working equations for the present apparatus.

B Experimental Details

a) Viscometer

The low-temperature capillary viscometer used for the present experiments was originally designed and built by A.G. Clarke in 1966 and is described in full detail in his Part II thesis (19). The apparatus has since been rebuilt in parts and before the current work the manometer and front and back vessels were replaced along with the manometer controlling the constant gas volume thermometer. The viscometer is shown in Figure 3.2. The front vessel VF, which was of cylindrical shape and the spherical back vessel VB, both of capacity approximately 1 litre, were contained in a large tank WB containing water acting as a thermostat.

The front vessel rested on the bottom of the tank

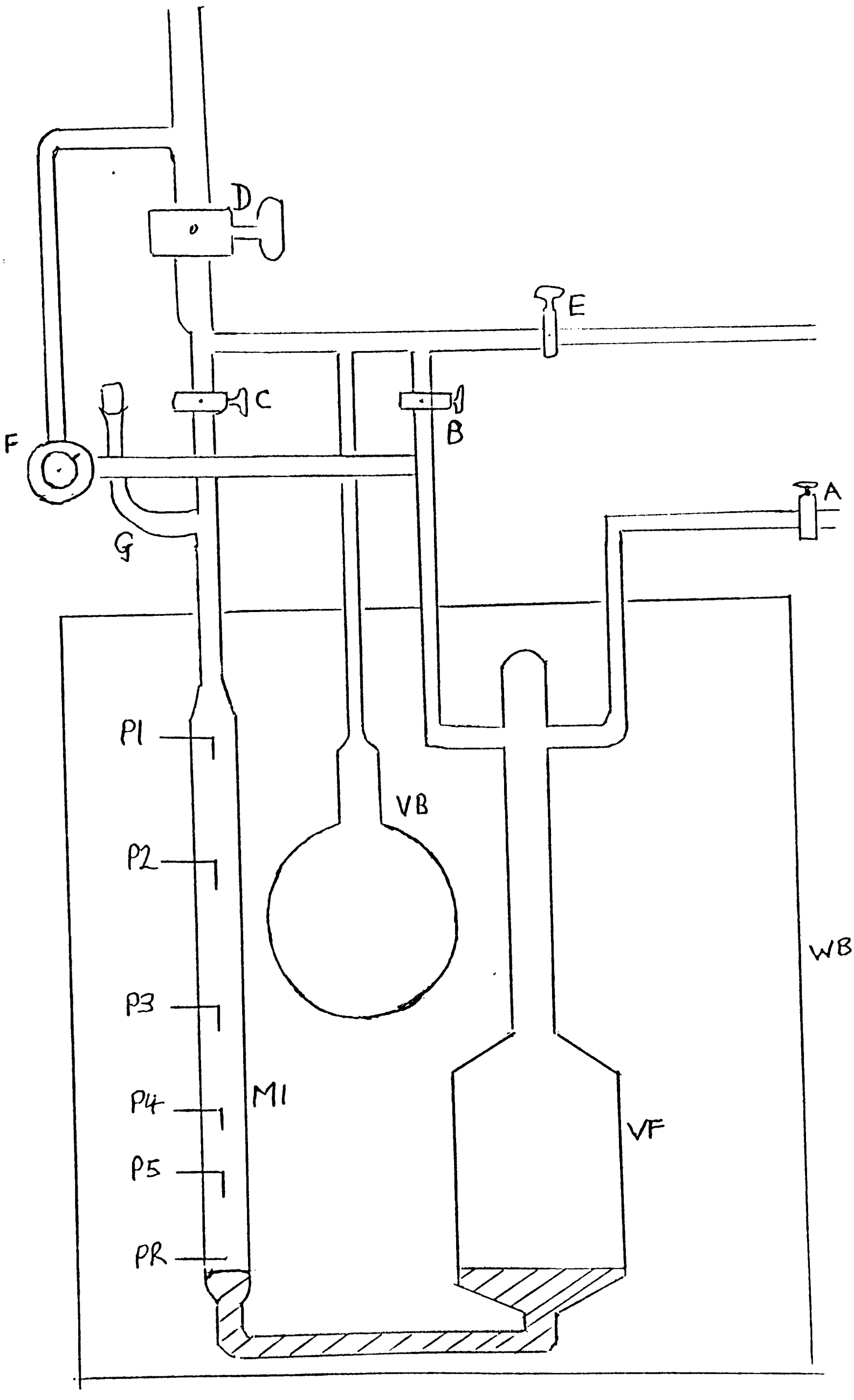


FIGURE 3.2 : THE VISCOMETER

on a cork support and was connected through its base to a vertical tube M1 of 15 mm bore and height 350 mm which acted as a manometer and which contained approximately 200 cm^3 of doubly-distilled mercury. The tube M1 contained 5 pointers P1-P5 which consisted of a 10 mm length of 0.7 mm diameter platinum wire, turned down to a fine tip and spot-welded to short tungsten rods which were sealed through the glass such that the tips of the pointers pointed vertically downwards. In addition there was a sixth tungsten rod which was situated at the base of the manometer and which allowed a small A.C. current to be passed through the mercury to the pointers. The figure also shows the arrangement of taps which were connected to the viscometer and by which gas could be admitted to various parts of the apparatus. Tap E was always open in the experiments except at night when taps A and E were closed in order to isolate the capillary from the mercury in VF so that mercury vapour could not distil into the capillary if the cold trap leading to the capillary warmed up.

The water bath WB, which also held themanostat buffer globe and mercury U-tube which were part of the temperature control system consisted of a glass-fronted metal tank of side 450 mm, lagged with expanded polystyrene sheeting, containing water to which anti-rusting and anti-bacterial agents had been added. The water was thermostatted at $25.00 \pm 0.05^{o}C$ by means of a 750W immersion heater controlled by a contact thermometer, efficient stirring being achieved by means of a TEP water pump external to

to the apparatus which also helped to reduce vibration of the mercury in M1. The water level in the tank was topped up regularly with a packed layer of 10 mm diameter polythene spheres on the surface helping to reduce evaporation losses.

The viscometer was separated from the cryostat by means of two lead-tubes, part of whose length had been bent into the form of a U of depth 200 mm. This was surrounded by a small Dewar vessel containing crushed solid carbon dioxide intimately mixed with ethanol which helped to prevent mercury vapour from the viscometer being carried into the capillary. After passing through the mercury trap, the gas entered the cryostat and was brought to the required temperature T_c by means of a heat exchanger which consisted of a part of the lead-tube of internal diameter 6mm and length 120mm. From the heat exchanger the gas flowed through the capillary and then passed out of the cryostat into the back vessel. The capillary itself was of Pyrex-glass with smoothly-tapered orifices. It consisted of two 1.2m lengths of precision bore capillary tubing of nominal radius 0.15mm joined smoothly together and coiled into a helix of average radius 37.5mm and pitch 5 mm. The arrangement of the heat exchanger and capillary in the cryostat will now be described.

It was necessary to ensure that the heat exchanger was of sufficient length for thermal equilibrium to be reached before the gas passed into the capillary. The

analysis of this problem is given by McCullough and Scott (21). They show that the temperature difference between the gas and its surroundings decreases exponentially with distance along the heat exchanger, the length L_e over which the difference falls to e^{-1} of its initial value being given approximately by:

$$L_e = \frac{C_p R_h^2 \rho v}{4\lambda} \qquad (3.31)$$

where C_p is the mass specific heat, R_h is the radius of the tube, ρ is the density of the fluid, v is its mean speed and λ is the thermal conductivity. The very slow flow of gas in the present experiments ensured that this length was always very short, and even in the worse case amounted to only 1 mm. Thus after a distance of 10 mm, the temperature difference will have fallen to e^{-10} of its original value, and therefore temperature equilibration will have been reached. Since the length of the heat exchanger was 120mm the conclusion is that thermal equilibrium will always be reached before the gas passes into the capillary.

b) Control and measurement of temperature

The cryostat, together with its control system was designed to maintain the capillary at a uniform but arbitrarily adjustable temperature in the range 120-320K for periods of time up to a week, to within a variation of not more than $\pm$ 0.1K, and to measure the temperature with similar

accuracy. The design is shown in Figure 3.3. It consists of two brass cans fitting one inside the other, being separated by a highly insulating material and surrounded by a large Dewar, which contained the coolant. The coiled capillary and heat exchanger are situated inside the inner can, immersed in the cryogenic fluid which is well stirred to maintain uniformity of temperature.

A heating coil wound round the outside of the inner can maintains the uniform temperature, being controlled by the pressure fluctuations of a constant-volume gas thermometer bulb situated centrally inside the capillary helix. The temperature is measured using a platinum resistance thermometer. The various parts will now be described in further detail.

(i) The cryostat

The outer brass can, of outer diameter 0.16m and height 0.22m and inner can, of outer diameter 0.112m and height 0.142m , were suspended from a Dexion frame by means of four strips of non-conducting Tufnal. The vertical space between them was filled with thick expanded polystyrene and polythene sheeting to cut down conduction and convection. The inner can rested on a circular base of 25mm thick expanded polystyrene to cut down heat losses. The heating coil consisted of nichrome wire wound non-inductively around the outside of the inner can and held in place with bakelite varnish. The ends of the coil were soldered to

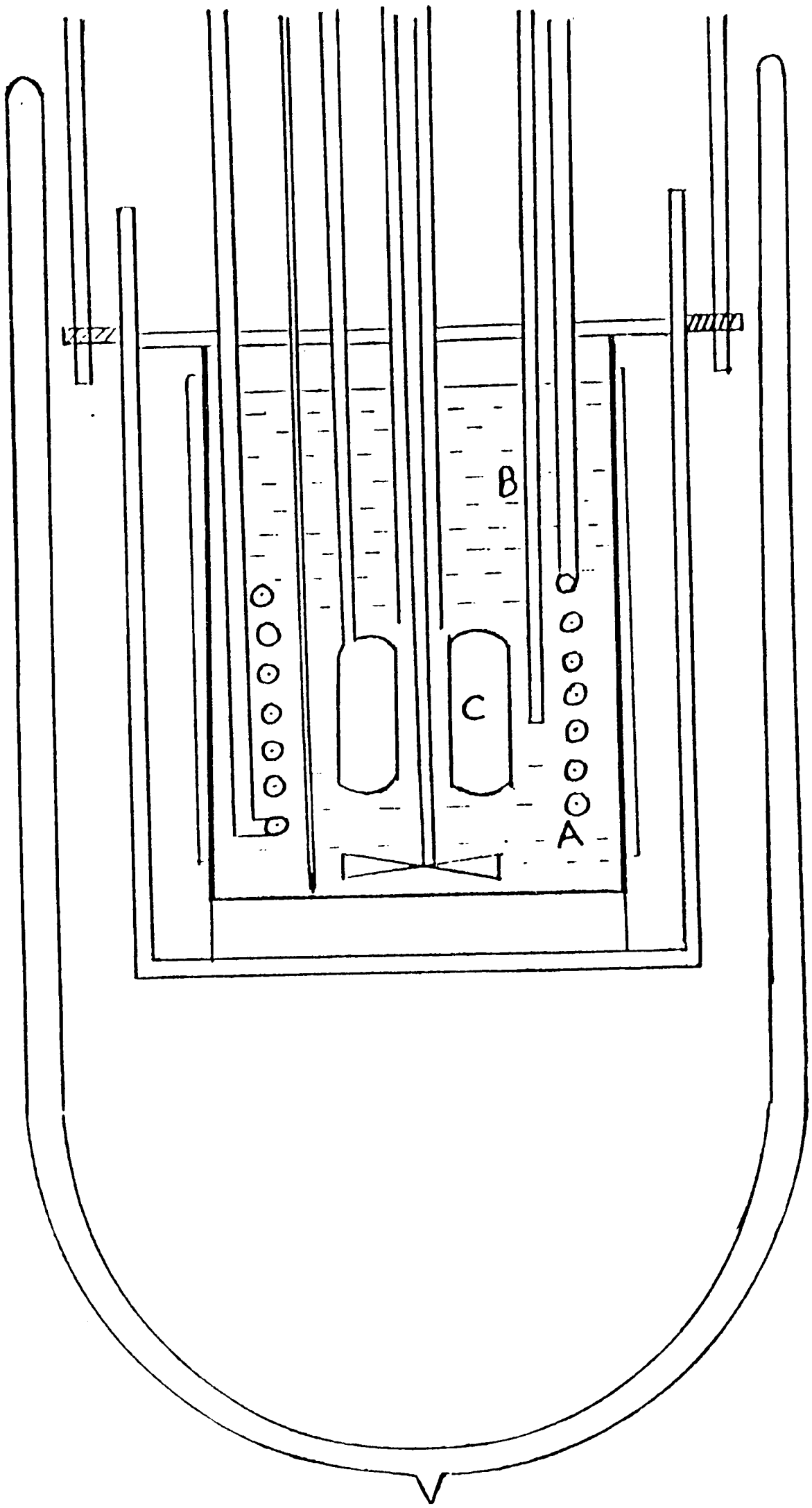


FIGURE 3.3 : The Cryostat

A Capillary; B platinum resistance thermometer; C Gas thermometer bulb

a wire which led vertically out of the cryostat and connected with the temperature control circuit.

The capillary, gas thermometer, stirrer and platinum resistance thermometer were arranged inside the inner can, the lead tubes emerging across a diameter. The can had a well-fitting lid made of 3mm sheet perspex which was cut into halves joining along the diameter and which rested on the rim of the inner can. The cryostatic fluid used depended on the temperature range required. For the ranges 120-200K, 200-290K and 290K upwards, isopentane, absolute ethanol and ethylene glycol were used respectively. Approximately 860 cm^3 of cryostatic fluid being required. The fluid could be added without removing the lagging by means of a thin-walled tube of 5mm outside dimaeter which ran from the bottom of the inner can right out of the cryostat. This device was of particular value in keeping the level of the extremely volatile isopentane constant. The stainless-steel stirrer lay inside a glass guide tube and was surrounded by the gas thermometer bulb of annular design.

The large Dewar vessel, which surrounded the cryostat was of internal diameter 0.2m and depth 0.42m and was supported on an adjustable stand so that it could be raised and lowered easily. When working above room temperature the Dewar was not used, the necessary cooling provided by the laboratory air. For the cryostat temperature from 220-300K a mixture of industrial ethanol and an excess of crushed solid carbon-dioxide, equilibrium temperature 200K

was used as the coolant, whilst for lower temperatures liquid nitrogen (78K) was employed. The solid carbon dioxide was added manually, but the liquid nitrogen was added using an automatic system consisting of a 25 litre storage Dewar on top of which rested a cryostatic pump (British Oxygen Co. Ltd.) which was controlled by means of a pair of metal capillary sensors (K.D.G. Instruments Ltd) positioned alongside the cryostat. A well-insulated copper tube fed the liquid nitrogen from the pump into the main Dewar. The pump operated at 12V D.C. and was activated whenever the liquid nitrogen level round the cryostat fell below the lower bulb, the upper bulb halting the flow. The level of liquid nitrogen was thus kept fixed about half-way up the outer can which aided temperature control in the cryostat. About 10-15l of liquid nitrogen were used per day and the system was run continuously during low-temperature measurements.

(ii) Temperature control

It was very important to ensure that the capillary remained at constant temperature during the measurement of the times of flow of the gases. This is because the times of flow are very sensitive to temperature, the percentage error in the viscosity being approximately twice that in any temperature fluctuations. The temperature control system is shown in Figure 3.4. The pressure variations of the gas thermometer bulb which, because of its large volume, sampled temperature gradients over the whole of the

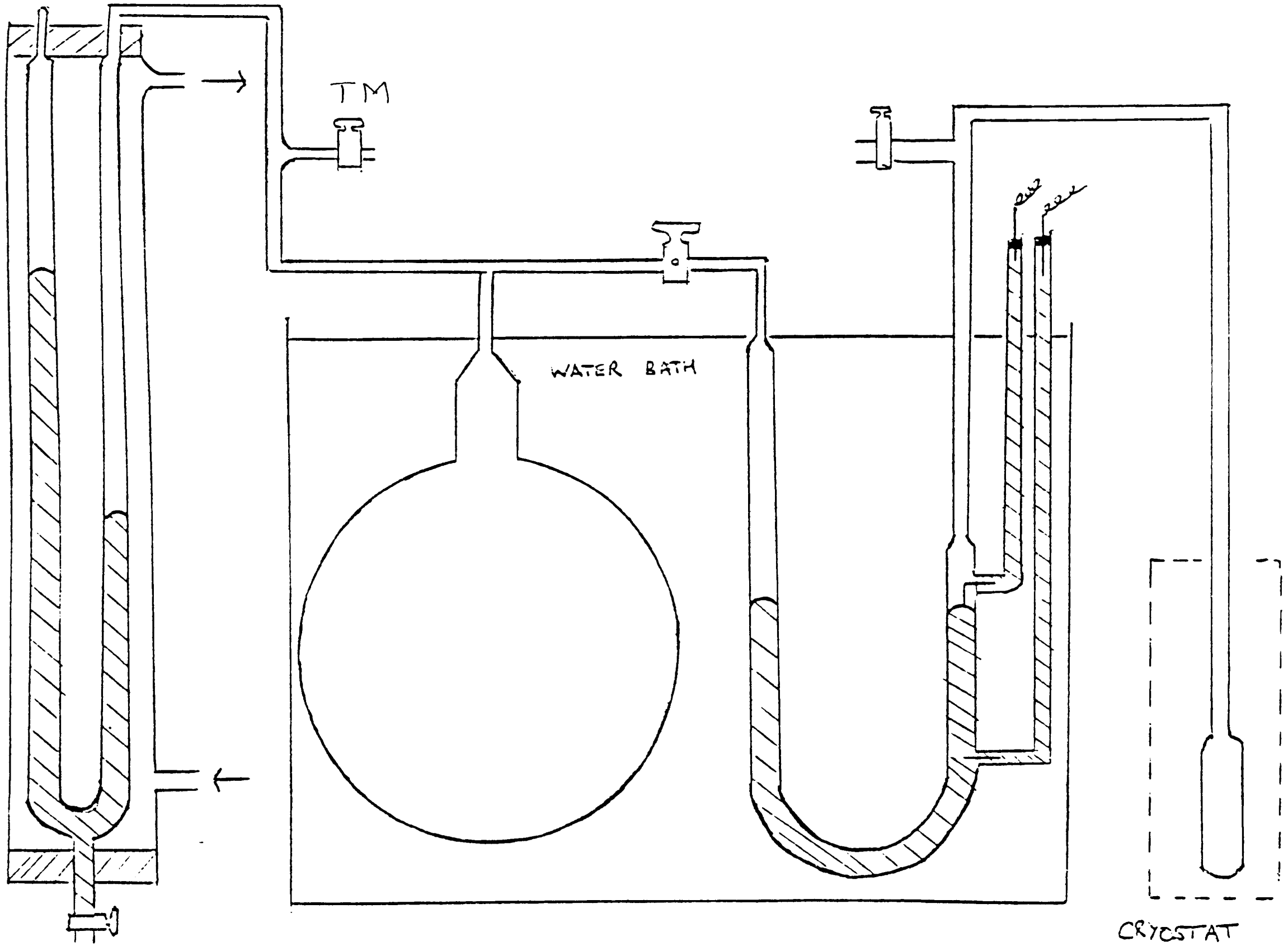


FIGURE 3.4

cryostat were transmitted via helium gas to the right-hand side of a U-tube containing mercury. The pressure on the other side of the U-tube was kept constant by means of a manostat which consisted of a 3 litre globe and a mercury manometer of height 0.85m kept at constant temperature. The movement of the mercury level in the U-tube was monitored by means of two platinum pointers sealed through the wall at the base of two small side-arms filled with mercury. The making and breaking of a circuit at the upper of these pointers controlled the cryostat heater by means of a relay.

The manostat globe and mercury U-tube were in the water bath WB and the mercury manometer, which gave a rough guide to the temperature of the cryostat at which thermostatting would occur, was surrounded by a water jacket through which water circulated from the water-bath by means of a second TEP pump, this also aided circulation of the water in the bath. The pressure of the gas in the manostat could be altered by means of a tap TM connected to the gas line. This allowed the temperature in the cryostat to be controlled over a wide range of temperature.

The heating circuit is shown in outline in Figure 3.5

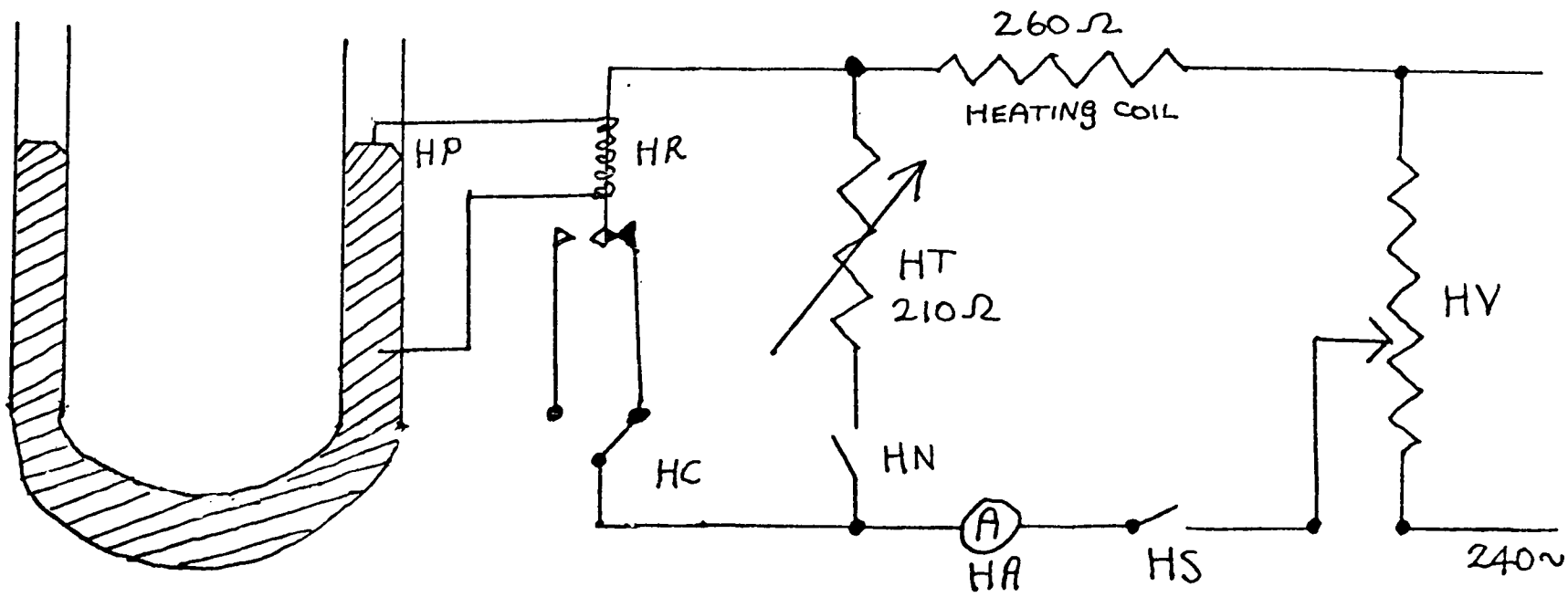


Figure 3.5

The heating coil, of resistance 260Ω, was connected in series with three 70Ω rheostats HT, a switch HS and ammeter HA. The variable resistors could be shorted out by means of a relay HR controlled by the fluctuations of the mercury level at pointer HP: the current flowing in the heater coil was controlled by the variac HV. The effect of the relay could be reversed by means of the cross-over HC, and the cooling current, which was operative when the contact at HP was broken, could be reduced to zero when switch HN was open rather than being controlled by the rheostats. Switch HN was opened when there was a dnager of the coolant running low, e.g. overnight; the cross-over switch facilitated the setting of the heating and cooling current for a particular temperature. The heating current, which was controlled by the setting of HV and the cooling current; controlled by the rheostats HT were adjusted such that the cryostat warmed or cooled at the rate of approximately 2 Kelvin per hour under the appropriate experimental conditions. This gave good temperature thermostatting for the capillary, stability of the order of $\pm$ 0.1 Kelvin being typical.

(iii) Temperature measurement

The temperature was measured to an accuracy of at least $\pm$ 0.05K using a Tinsley 5187H platinum resistance thermometer calibrated by the N.P.L. The value of the constants in its calibration formula

$$\theta = \frac{R_\theta - R_o}{\gamma R_o} + \delta\left(\frac{\theta}{100} - 1\right)\left(\frac{\theta}{100}\right) + \beta\left(\frac{\theta}{100} - 1\right)\left(\frac{\theta}{100}\right)^3 \qquad (3.32)$$

where $R_o = 23.393$ ohm

$\gamma = 3.925 \times 10^{-3}$

$\delta = 1.491$

$\beta = 0$ $(\theta/^oC > 0)$

$= 0.111$ $(\theta/^oC < 0)$

and values of $\theta/^oC$ as a function of the measured resistance R_θ/ohm had been produced. The temperature scale used was the International Practical Scale of 1948 and T/K was given by

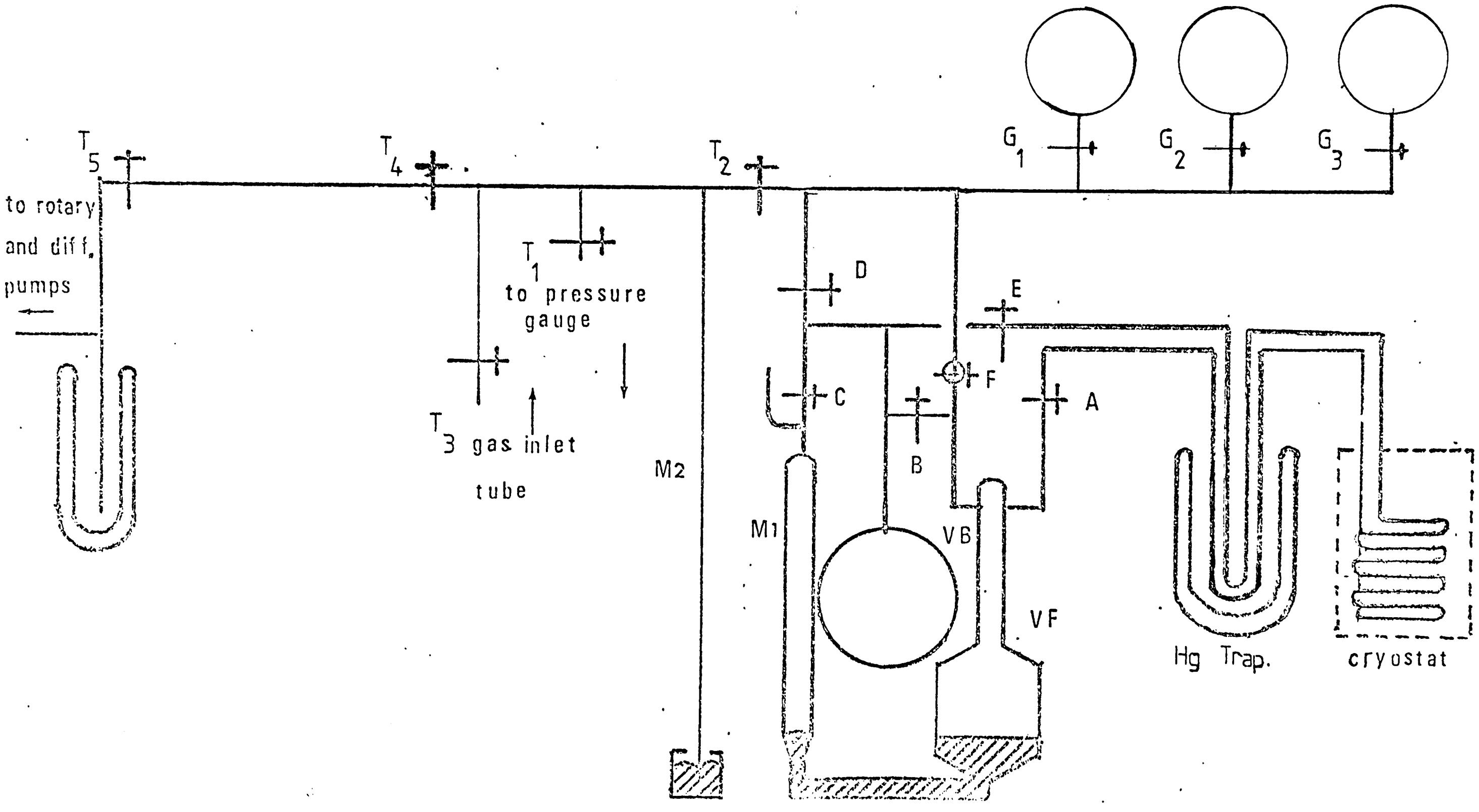
$$T/K = \theta/^oC + 273.16 \qquad (3.33)$$

The resistance R_θ was measured by connecting the thermometer in series with a standard resistor of value 10 kohm. The potential drops across the resistors when a constant current of 3 milliamp was passed were compared using a Tinsley type 4025 potentiometer.

(iv) The gas line

The gas line (Figure 3.6) was of wide bore tubing and served for the introduction of gas at the beginning of an experiment and for evacuation at the end of each run. It was separated from the pumps by means of tap T4 and a liquid nitrogen trap. The pumping system consisted of a single-stage rotary pump backing a water-cooled mercury diffusion pump, this combination evacuating the apparatus

FIGURE 3.6 : THE APPARATUS

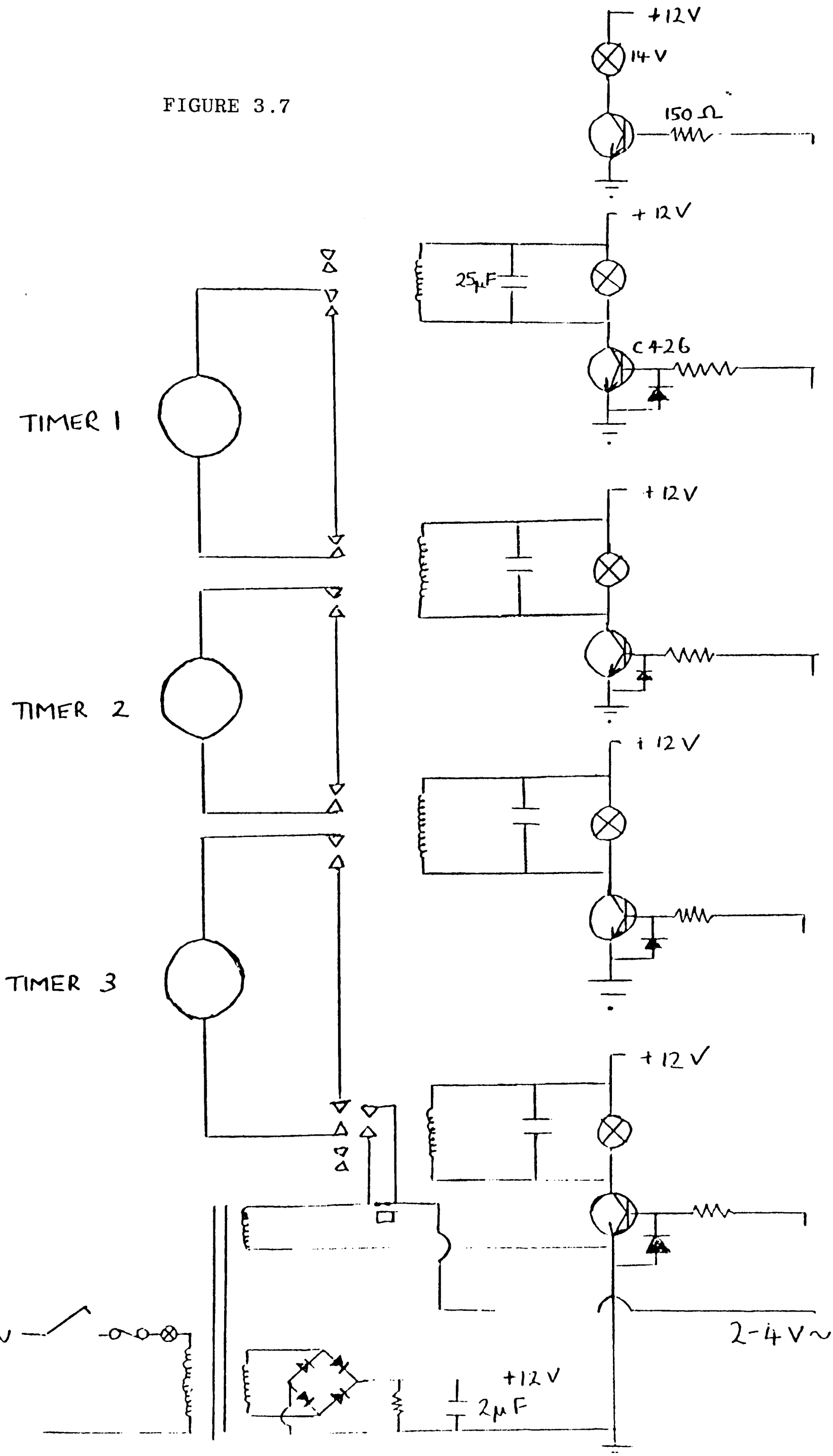


to a pressure of approximately 0.01 Torr in about 20 minutes. The pressure in the apparatus was indicated roughly by the capillary mercury manometer M2 which also acted as a blow-off. A thermocouple gauge connected to the gas line enabled the degree of vacuum to be ascertained. The pure gases were obtained from cylinders, passed through a drying tube containing phosphorous pentoxide and introduced into the apparatus through tap T3, the gas line and feed tube being first flushed with the gas, which was allowed to blow off at M2. The gases were then stored in the 5l globes G_1, G_2 and G_3. Gas mixtures were supplied pre-mixed by British Oxygen Co. Ltd. and were introduced into the apparatus as above.

(v) The measurement of time

Onto each of the pointers P_1-P_5 and the tungsten base rod PR on the manometer M1 (Figure 3.2) there was attached a metal collar which connected to a length of insulated wire leading out of the water bath. This enabled at 2-4V A.C. potential to be fed to each of the pointers which activated the timing system built in the Physical Chemistry Laboratory. The circuit diagram is shown in Figure 3.7. The run times could also be checked by the use of a stop watch as the pointers also activated a series of lights which were lit when the mercury was touching a particular pointer. This check was necessary as the times were subject to drift due to interference in the mains supply. They were subject to sudden jumps of a couple of seconds, consequently the manual stopwatch readings were used and the timers were

FIGURE 3.7


+12V
14V
150Ω
+12V
25μF
C426
+12V
+12V
TIMER 1
TIMER 2
TIMER 3
+12V
+12V
0V~
2-4V~
2μF

only used if verified or if a manual reading was missed. The overall accuracy of the timings was estimated by use of the GMT signals to be at least $\pm$ 0.2s in 1 hour.

C. The Procedure for Carrying Out a Run

(i) First filling

The viscometer and gas line were completely evacuated with all taps open. Taps T4, D and the needle-valve F were closed, and the appropriate gas was introduced into the gas line, the tap C was shut. Gas was then introduced into the viscometer via the needle valve F until the mercury in M1 had almost reached a pre-determined pointer. A few minutes were allowed for the gas to reach the temperature of the water bath (298K) and then the gas was allowed in very slowly until the appropriate bulb in the timing circuit was glowing brightly. The whole viscometer, excluding the space above the mercury in M1, had thus been filled to a certain known pressure. Tap C was then opened slowly and the mercury level fell as the space in M1 was filled with gas. In some runs the first filling was omitted by going straight to stage (ii), the initial pressure in the back vessel in these cases being zero.

(ii) Second filling

For the second filling, taps A and B were closed and the front vessel only was filled with gas, usually

to pointer 1, with the same precautions as before. A run was started by opening tap A, whereupon a sudden drop in the mercury level occurred as the pressures in the front vessel and the capillary leads were equalised. These fluctuations died away after about 10 seconds and timing commenced when the mercury level passed the next lower pointer. The time taken for the mercury level to pass between successive pairs of pointers was noted by means of a stop watch and timers. The breaking of the circuit at the pointers was usually very clearly defined except for very long runs when some flickering of the lights occurred. After the last reading had been noted tap B was opened to equalise the pressures and then the viscometer was evacuated by opening tap D to the vacuum line and the run ended.

By suitable choice of the pointer settings for the fillings a wide range of mean pressures in the capillary could be attained with a corresponding range of times of flow. In general at high temperatures, high pressure runs were done to obtain suitable times of flow and to reduce slip, at low temperatures, low pressure runs reduced curved pipe flow and gas imperfection corrections, as well as ensuring that the runs remained long enough to measure accurately. In general on the apparatus four of these different pressure runs are performed though in this work not all of them were used, however for convenience the conditions for each are shown below along with their abbreviations:

Type of Run	Pointer for: 1st filling	2nd filling
High Pressure (HP)	1	1
Medium Pressure (MP)	3	1
Low Pressure (LP)	-	1
P2	-	2

Each run was repeated at least once for a consistency check.

D.Dimensions of the Apparatus

Since before the present work was undertaken the manometer M1, front and back vessels were replaced the various volumes and pressures needed for the calculation of the correction terms were re-evaluated and are recorded here.

(i) Pressure differences at the pointers:

Pointer (i)	$[P_m(i) - P_f(i) - P_b(i)]$/cmHg
1	31.675
2	23.635
3	15.470
4	9.620
5	5.370

(ii) Area of cross-section of the manometer tube M1,

$A \simeq 1.767\ cm^2$.

(iii) Volume of the front vessel when mercury is at pointer 1 $V_1(1)$ = 995.0 cm^3 (bounded by taps A, B and F).

(iv) Volume of back vessel, from pointer 1 to the heat exchanger $V_2(1)$ = 1256 cm^3.

(v) Ratio of A to mean area of cross-section of front vessel, Z = 0.0254.

(vi) Volume of leads to capillary, V_{ci}:

V_{C1} = Volume of tubing between tap A and heat exchanger which is at room temperature (293K) = 21 cm^3

V_{C2} = Volume of tubing in the mercury trap, assumed at 200K = 8.5 cm^3.

V_{C3} = Volume of heat exchanger at cryostat temperature T_c = 5 cm^3.

V_{C4} = Volume of heat exchanger in the lagged area above the cryostat, taken to be the mean of room temperature and cryostat temperature = 5 cm^3.

V_{C5},V_{C6} = Volume of tubing leading to back vessel corresponding to V_{C3}, V_{C4} above = 2.5 cm^3, 5 cm^3 respectively.

CHAPTER 4

THE INVERSION OF TRANSPORT PROPERTY AND GAS IMPERFECTION DATA

(a) Introduction

It is possible, by using the expressions for transport properties obtained in Chapter 2, to calculate from experimental viscosity data the collision integral $\Omega^{(2,2)}_{exp}$ as a function of temperature. As was shown in Chapter 2, these collision integrals are a function of the intermolecular potential, but it is difficult to obtain the intermolecular potential from them. The reason for this is that the collision integrals arise from an average over the dynamics of all possible collisions at a particular temperature. Thus the collision integral is dependent, in principle, on the entire intermolecular potential at all separations. The technique of inverting these collision integrals in order to give the intermolecular potential was for many years thought to be impossible. Thus it was the common practice to fit the data to a potential of the Lennard-Jones (12-6) type (equation 4.1), with adjustable well depth (ε) and the collision diameter (σ).

$$U(r) = 4\varepsilon\left[\left(\frac{\sigma}{r}\right)^{12} - \left(\frac{\sigma}{r}\right)^{6}\right] \qquad (4.1)$$

The potential model which optimised the fit of the

data was then taken to be a good representation of the true potential function.

Unfortunately this procedure is severely limited and the results of such a fit are found to depend on which data are used. For example, low temperature viscosities give a well depth for argon based on a 12-6 function to be 124K whereas that for high temperature viscosities is 135K. The conclusion of results drawn from this procedure is that it can only give a rough estimate as to the values of ε and σ and that any potentials obtained by this technique should not be regarded as a true representation of the intermolecular potential function.

(b) Inversion of Viscosity Data

In the last decade it has become possible to extract the full potential from viscosity data by direct inversion of the collision integral $\Omega^{(2,2)}_{exp}(T)$. This technique was developed by Gough, Maitland and Smith (1) in 1972 and has since been extensively used by this group. The method will now be described in detail.

Experimental measurements of gas viscosities may be used to determine the experimental collision integrals as a function of temperature, by means of the expression (see Chapter 2)

$$\eta = \frac{\frac{5}{16}(m\pi kT)^{\frac{1}{2}}}{\Omega^{(2,2)}_{exp}(T)} \qquad f_\eta = \frac{\frac{5}{16}(m\pi kT)^{\frac{1}{2}}}{\pi\sigma^2\Omega^{(2,2)*}(T^*)} \quad f_\eta \qquad (4.2)$$

f_η being a factor close to unity (the correction to higher order - usually the Kihara second approximation in the present work (2)) which is almost independent of the detailed form of the intermolecular potential. A characteristic distance $\tilde{r}$ may be defined such that:

$$\tilde{r} = (\Omega^{(2,2)}_{exp})^{\frac{1}{2}} \qquad (4.3)$$

$\pi^{\frac{1}{2}}\tilde{r}$ is then the collision diameter of hard sphere molecules which have the same viscosity and hence the same collision integral at the temperature under consideration.

For molecules which have an intermolecular potential of an inverse power form such that $U(r) = A/r^m$ where the constant A can be both positive and negative, it can be shown that (3)

$$\tilde{r} = (kT/A)^{-1/m}F(m) \qquad (4.4)$$

Where the constant F(m) is a function of m only. Thus

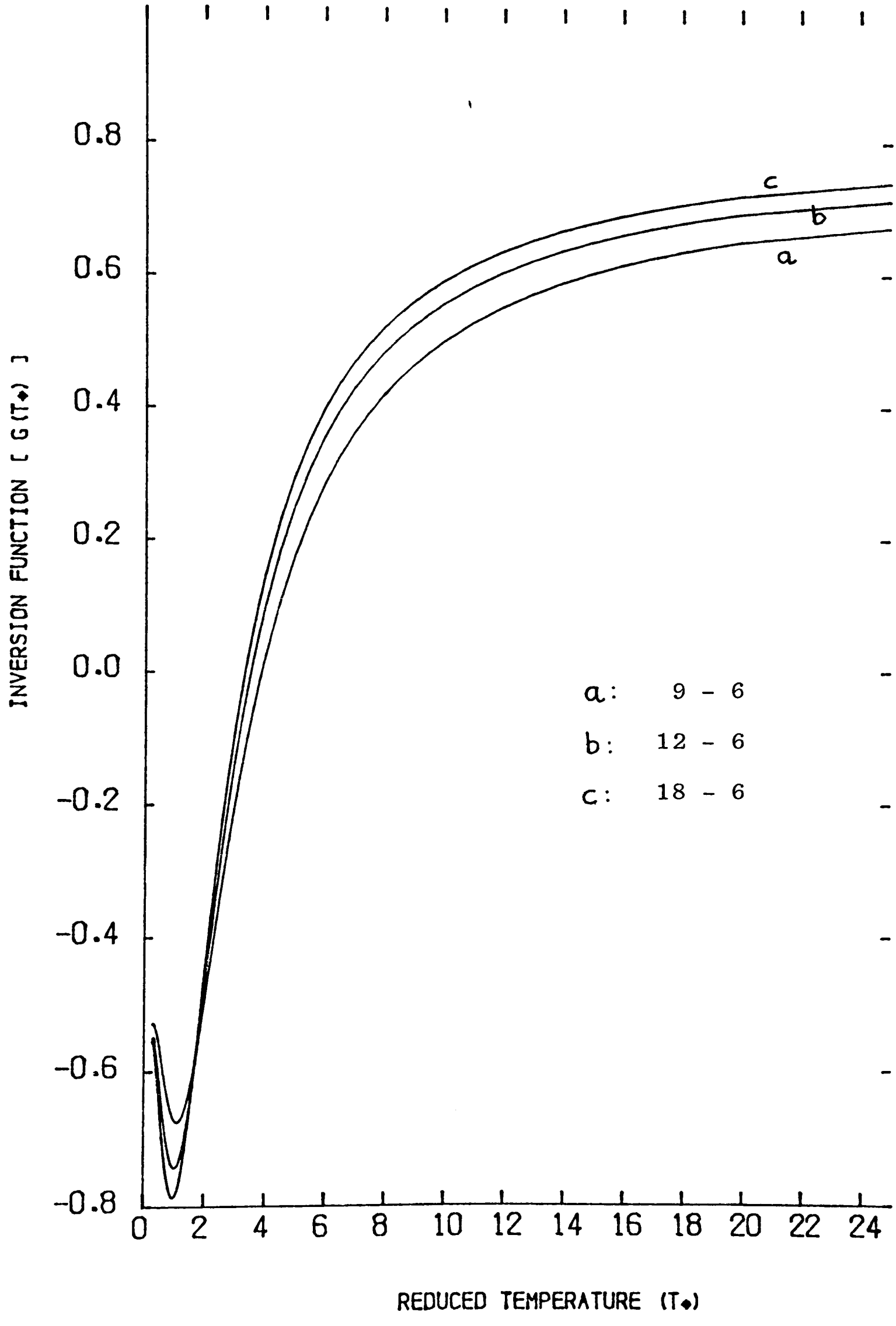
$$U(\tilde{r}) = kT.[F(m)]^{-m} = kT.G(m) \qquad (4.5)$$

and we can establish that at the separation $\tilde{r}$ given by equation (4.3), the potential energy is given by G(m).kT. This relationship was used by Hirschfelder and Eliason (4) as a convenient method of calculating the transport properties of molecules interacting with inverse power potentials. G(m) is a constant for a given inverse power law. As the exponent m of the repulsive forces varies, the value of G(m) changes slowly, and for m = 8 to 18 remains in the range 0.86 to 0.82 (5,6). For long range attractive forces where m = -6, G(m) = -0.58. Now realistic potentials obviously are both attractive and repulsive thus these may be considered to consist of an inverse power term (either attractive or repulsive) whose effective exponent m is a function of separation. Because of this G is a temperature dependent function changing from 0.8 at high temperatures where repulsive forces dominate to -0.58 at very low temperatures where the viscosity is determined by long range scattering and where the r^{-6} dispersion force is dominant.

The important feature of G(T) is, however, that it is, when expressed as a function of reduced temperature ($T^* = kT/\varepsilon$) very similar for a variety of potential functions. This is shown in Figure 4.1 where $G(T^*)$ is illustrated for a variety of n-6 potentials.

In order to invert viscosity data, an initial approximate function ("starting potential")must be utilised

FIGURE 4.1


INVERSION FUNCTION [G(T*)]
0.8
0.6
0.4
0.2
0.0
-0.2
-0.4
-0.6
-0.8
0
2
4
6
8
10
12
14
16
18
20
22
24
REDUCED TEMPERATURE (T*)
a
b
c
a: 9 - 6
b: 12 - 6
c: 18 - 6

to calculate $G(T^*)$ using the relationship

$$G_o(T^*) = \frac{U_o^*(\Omega^{(2,2)*}(T^*))^{\frac{1}{2}}}{T^*} = \frac{U_o(\Omega^{(2,2)\frac{1}{2}})}{kT} \qquad (4.6)$$

Now using a value of $\Omega_{exp}^{(2,2)}$ derived from viscosity data by equation (4.2) a new estimate (U_1) of the potential energy at a separation of $\tilde{r} = (\Omega_{exp})^{\frac{1}{2}}$ can be made assuming that

$$U_1(\tilde{r}) = G_o(T^*).kT \qquad (4.7)$$

where $T^* = kT/\varepsilon'$ and ε' is an estimate for the well depth of the substance under consideration. It is the basis of the inversion method that the series of points $(U_{n+1}, \tilde{r})$ are closer to the true potential function than the initial approximation $U_n(r)$ and that they constitute an improved potential function $U_{n+1}(r)$. If the collision integrals are now evaluated for this new function equation (4.6) may be used to obtain a new inversion function $G_{n+1}(T^*)$ which in turn will generate a better approximation to the true potential, and therefore we have the basis of an iterative procedure.

The above procedure has been extensively tested for simulated data (1). It was shown that in general three iterations gives a potential very close to the true potential energy function when starting from a wide variety of initial approximations.

Since experimental data cover a limited temperature range, inversion of such data defines the potential function over a limited range of separations. Extrapolations to this function are therefore necessary in order to iterate. The tests on simulated data showed that the nature of the extrapolation had little effect on the inversion.

Diffusion and thermal conductivity coefficients may also be inverted, the thermal conductivity inversion is almost identical for monatomic species since the same collision integral $\Omega^{(2,2)}(T)$ is involved. Diffusion coefficients involve a different collision integral, namely $\Omega^{(1,1)}(T)$ so the above inversion scheme would be repeated with $\Omega^{(2,2)}(T)$ replaced by $\Omega^{(1,1)}(T)$.

It is an important feature of these inversion methods that an estimate of the well depth ε' is required in order to invert the data. In the inversion of argon data (1) this is quite straightforward as the well depth of argon is known from analysis of the spectra of the argon dimer by Maitland and Smith (7), which is in close agreement to that obtained by other workers (8,9). When no independent value of ε' is available, however, the procedure is more complex. The procedure adopted in these cases will be described in detail later, in section c(iii), in the form in which it was applied in this work to the viscosities of Ar-Xe and Ar-N_2 mixtures.

(c) The Inversion of Second Virial Coefficients

(i) Previous Techniques

The classical second virial coefficient of a gas can be expressed (10)

$$\frac{B(T)}{\alpha} = \frac{2\pi N_A}{3T} \int_o^\infty \Delta \exp(-\phi/kT) d\phi \qquad (4.8)$$

where $\Delta = r_L^3 - r_R^3$, $\alpha = \exp(\varepsilon/kT)/k$ and $\phi = U + \varepsilon$. r_L and r_R are the inner and outer coordinates of the potential energy function at ϕ where ϕ is the energy expressed in K measured from the bottom of the well. In the repulsive region $\Delta = r_L^3$. In principle Δ may be obtained from B(T) by using the fact that $B(T)T/(^2/3\,\pi N_A\alpha)$ is the Laplace transform of Δ.(11,12). Thus inversion of B(T) should, in principle, be possible by this method to give uniquely the potential in the repulsive region and to give the well width as a function of depth in the attractive region. One possible method of performing the inversion is to fit $B(T)T/(2/3\pi N_A\alpha) = L$ to a function whose inverse Laplace transform is known. This was the basis of the first successful inversion procedure (13) but only proved useful in the case of helium, for which experimental results were available at sufficiently high (reduced) temperatures. The method gave the repulsive portion of the potential down to $U \approx 25\varepsilon$, but even here it was found necessary to correct for the influence of attractive forces.

Numerical inversion procedures based on quadrature transform equation (4.8) into a set of N linear equations

$$\underline{A}.\ \underline{\Delta} = \underline{L} \qquad (4.9)$$

where $\underline{A}$ is a N x N matrix and $\underline{\Delta}$ and $\underline{L}$ are N x 1 matrices. Inversion by $\underline{\Delta}^{-1} = \underline{A}^{-1}.\underline{L}$ gives N values of ϕ at the appropriate values of ϕ obtained from N values of B(T) (14). Unfortunately this formal inversion method is inherently unstable since matrix $\underline{A}$ is ill-conditioned, for although L (or B(T)) is relatively insensitive to small changes in ϕ, ϕ is unusually sensitive to small variations in L. This leads to the oscillation of solutions around the true one and although it is possible to invert B(T) data which is accurate to one part in 10^4 it is not practicable for experimental data which is rarely better than $\pm$ 1% and is usually worse (15).

Thus, although formal methods for the inversion of B(T) have not proved of value, less formal methods have been developed over the past few years which allow Δ to be extracted from second virial coefficient data with considerable accuracy (14). These less formal methods sought, in the repulsive region, to define a characteristic length from second virial coefficient data at a given temperature (analogous to equation (4.3) for the viscosity inversion) which could be related to a point on the potential energy function. The definition of this characteristic length $\tilde{r}$ was

$$\tilde{r} = \left[\frac{B + TdB/dT}{2/3\pi N_A}\right]^{1/3} \qquad (4.10)$$

and in the earliest work $\tilde{r}$ was related to the value of r at which U = kT, written r_T by a function $\alpha(T)$

$$\tilde{r} = \alpha(T)\ r_T \qquad (4.11)$$

It was the basis for the success of these methods that the function $\alpha(T)$ was insensitive to the detailed shape of the intermolecular potential function and could be calculated using an approximate potential function such as the Lennard-Jones 12-6 model. This allowed the repulsive branch at $U > 3\varepsilon$ to be extracted from second virial coefficient data with considerable accuracy (14). This was later improved (18) by use of an inversion function F(T) which is now a direct analogy to the G(T) function of equation (4.7) i.e.

$$U(\tilde{r}) = F(T).kT \qquad (4.12)$$

Again F(T) may be calculated from an approximate potential function. The inversion method in this case was not restricted to high repulsive energies. In the well region a similar inversion method was devised to extract $\Delta = r_L^3 - r_R^3$ from the attractive contribution to the virial coefficient approximated by $Battr = B - 2/3\pi N_A \sigma^3$. Again a function insensitive to the detailed shape of the potential energy function linked Δ and Battr.

The choice of definition of $\tilde{r}$ and other aspects of the method have been the subject of some investigation. It is not easy to justify the methods except in the special case of a very simple potential energy function such as $U(r) = A/r^n$. However despite this difficulty over formal justification the methods are found to be effective in recovering known potential energy functions from simulated experimental data. The new method now outlined, is more ambitious in that it seeks to obtain a complete potential energy function from B(T) despite the fact that such a procedure can in general be shown to be impossible (12).

(ii) A complete inversion method for B(T)

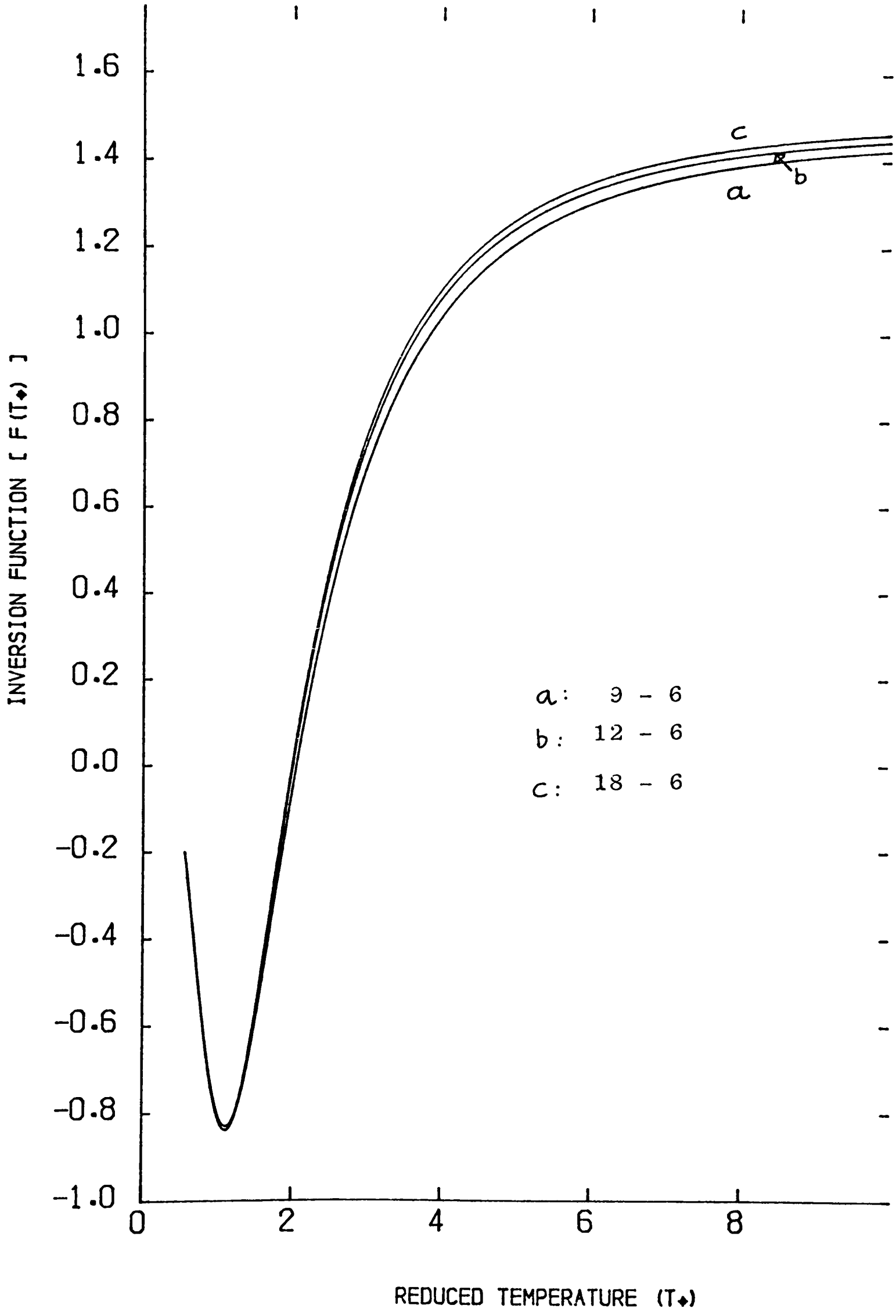
This new method (16) was under investigation at the end of the authors Part II and was further developed for application to real systems in the present work (17).

The method is based closely on those described above and in many respects is similar to the viscosity inversion procedure described previously. We write

$$U_1(\tilde{r}) = F_o(T).kT \qquad (4.13)$$

where $\tilde{r}$ is defined as before by equation (4.10). $F_o(T)$ is calculated from an initial approximate potential energy function, $U_o(r)$ by evaluating the values of B + T (dB/dT) predicted by the function. Values of $F(T^*)$ against T^* are shown in Figure 4.2 for a variety of n-6 potentials.

FIGURE 4.2


INVERSION FUNCTION [F(T*)]
1.6
1.4
1.2
1.0
0.8
0.6
0.4
0.2
0.0
-0.2
-0.4
-0.6
-0.8
-1.0
0
2
4
6
8
REDUCED TEMPERATURE (T*)
a
b
c
a: 9 - 6
b: 12 - 6
c: 18 - 6

The potential function $U_1(r)$ is found to be closer to the true potential than $U_o(r)$. This is then used to calculate $F_1(T)$ and so obtain a further improved potential function $U_2(r)$. Three iterations are used normally, it being found that further iteration produced only insignificant variations to the potential energy function.

As with the viscosity inversion procedure, in order to apply the method when data over only a limited temperature range are available, some method of extrapolating the function produced an inversion, at both large and small separations is required. In addition since $F_o(T)$ is calculated as a function of reduced temperature $(T^*) = kT/\varepsilon$ this means that some estimate of the well depth parameter ε is again required. This method of inversion is, within certain limits of uncertainty, able to give an estimate of ε. A number of criteria may be applied in order to assess the convergence of the method. In the case of simulated data this is fairly trivial in that the potential function resulting from inversion may be compared with that used to generate the data. This is obviously not possible when inverting real data and here we may use:

(i) the degree to which the potentials change on iteration

or

(ii) the degree to which B or B + T (dB/dT) calculated from the function agree with the experimental (or pseudo experimental data).

The method was fully tested on simulated data calculated for the Lennard-Jones 12-6 potential. Second virial coefficients were calculated in the experimentally accessible range of $T^* = 0.6$ to 10.0, although any upper limit from 4.0 would have served equally well. Data below 0.8 is however important as this data corresponds to the region of the potential at the bottom of the well. On inversion the data gave values of U(r) and r in the separation range of $r/\sigma = r^* = 1.60$ to 0.85. Extrapolation is important when calculating second virial coefficients from this potential in order to iterate since the contribution to the second virial coefficient from the potential where $r^* > 1.6$ can contribute 30% to B(T). Fortunately the long range behaviour of the potential energy functions of real substances is often known accurately. In inverting the data calculated from the 12-6 function, we assumed that the long range behaviour was $U = -C/r^6$. Four n-6 potential energy functions were employed in order to calculate $F_o(T)$. The results are shown in Tables 4.1 and 4.2 and the resulting functions are shown in Figure 4.3. In Table 4.1 the discrepancies between the 'experimental' values of $B + T(dB/dT)$ and those generated from the potential resulting from the inversion procedure are given as a percentage whereas deviations in B (ΔB) are given as a percentage of b^o ($b^o = 2/3\pi N_A \sigma^3$). The zeroth iteration gives the differences between the data and values calculated from the initial approximate potential. After three iterations the deviation in $B + T(dB/dT)$ is 0.03%, the mean deviation in B is 1.06%. The greater

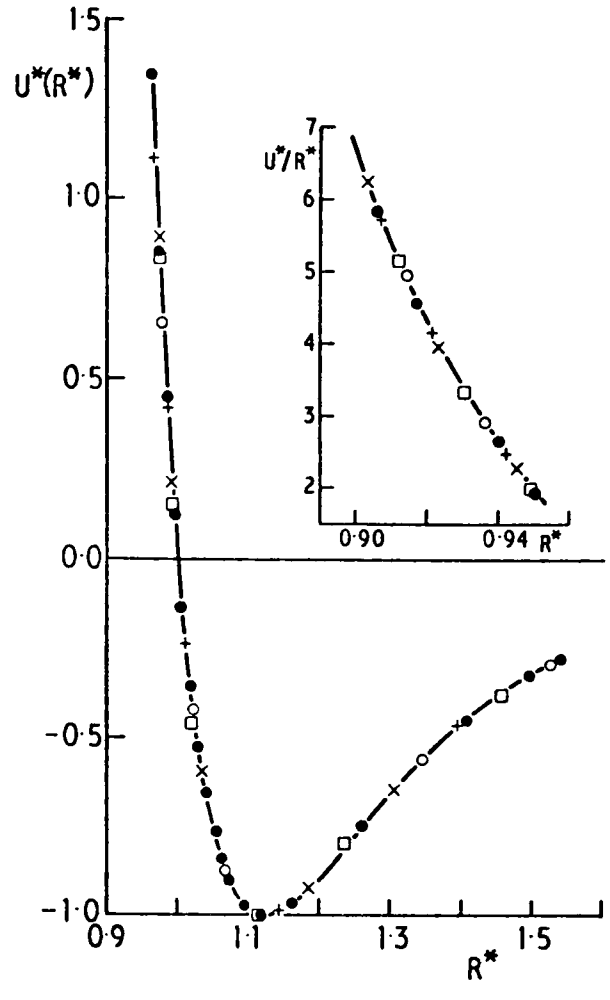


Figure 4.3 The inversion of pseudoexperimental second virial coefficient data calculated from the Lennard-Jones 12–6 potential energy function, ●. Results after the third iteration. Key: initial approximate potential ○ 18–6, +20–6, ×16–6, □ 9–6, $R^* = r/\sigma$.

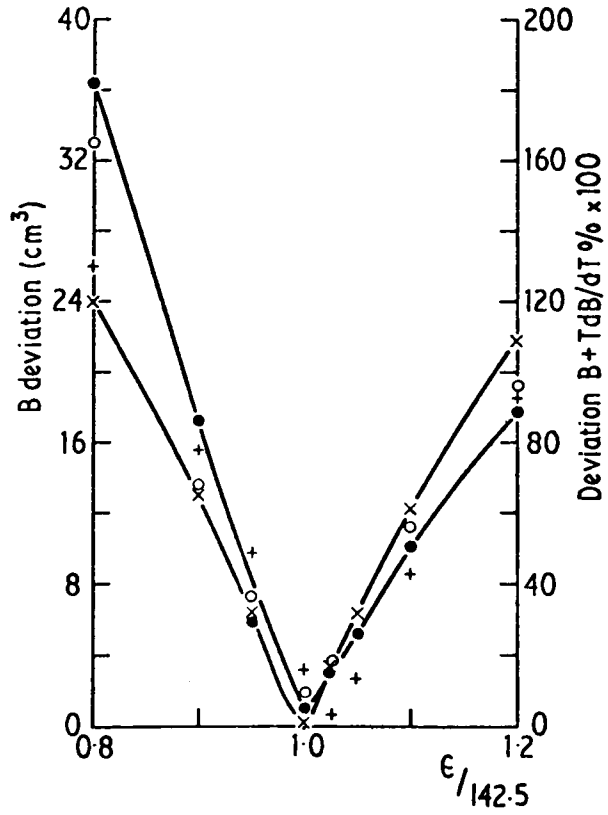


Figure 4.4 The effect of varying the well depth parameter ϵ on the mean deviation of the values of $B + T(dB/dT)$ and B obtained by inversion from the pseudoexperimental values. The simulated data were calculated using the BBMS potential function and the initial approximate potentials were the Lennard-Jones 12–6 function and the 11–6–8 function. The points represent values obtained after the third iteration. Key: 11–6–8 initial approximation: × deviation in B, ● deviation in $B + T(dB/dT)$. Solid lines link these data. 12–6 initial approximation: + deviation in B, ○ deviation in $B + T(dB/dT)$.

TABLE 4.1 : The inversion of data generated using the Lennard-Jones 12-6 function for the temperature range $T^* = 0.6$ to 10.0

		Initial Approximate Potential				
Iteration		20-6	18-6	16-6	9-6	Mean
0	$\Delta(B+T\ dB/dT)\%$	10.1	8.31	6.14	7.76	8.08
	$\frac{\Delta B \times 100}{b^o}$	65.2	54.9	41.7	62.8	56.2
1	$\Delta(B+T\ dB/dT)\%$	0.32	0.36	0.35	0.34	0.34
	$\frac{\Delta B \times 100}{b^o}$	0.64	1.68	2.4	2.6	1.8
2	$\Delta(B+T\ dB/dT)\%$	0.05	0.05	0.05	0.12	0.07
	$\frac{\Delta B \times 100}{b^o}$	0.08	1.14	2.0	1.5	1.2
3	$\Delta(B+T\ dB/dT)\%$	0.03	0.03	0.03	0.03	0.03
	$\frac{\Delta B \times 100}{b^o}$	0.10	1.15	2.1	0.9	1.1

TABLE 4.2 : The mean percentage deviation in r^* over 46 points in the range $r^* = 0.86 - 1.60$. The pseudo-experimental data were calculated from the Lennard-Jones 12-6 function. I.A.P. indicates initial approximate potential

	Iteration			
I.A.P.	0	1	2	3
20-6	2.649	0.098	0.053	0.058
18-6	2.315	0.103	0.036	0.041
16-6	1.741	0.090	0.034	0.037
9-6	1.758	0.258	0.139	0.108
Mean:	2.116	0.137	0.066	0.061

difference in B compared to B + T(dB/dT) is due to a greater contribution to B from the region of extrapolation than that for B + T(dB/dT). The percentage error in r over all the range of the potential covered by the inversion procedure is, averaged overall four initial approximations, and after the third iteration 0.06%.

The method was also tested on data simulated for argon (16) using the BBMS potential energy function which was first proposed for the gas on the basis of an analysis of the spectroscopic data for the argon dimer (7). Again the method reproduced the potential and virial coefficients to high accuracy. B + T(dB/dT) was reproduced to 0.09% on the third iteration, B to 3.1 cm^3 and the mean value of the deviation in r was found to be 0.38%.

(iii) Determination of the well depth parameter ε

In both tests described so far, we have assumed either implicitly, as in the first case, or explicitly a knowledge of the well depth parameter ε. A knowledge of the collision diameter (σ) is not required by the inversion method. We now examine the effects of an erroneous estimate of ε which might occur when inverting real experimental data for which ε is not known. In order to carry this out, ε was assigned values ranging from 20% greater to 20% less than its true value. For each value an inversion was performed on simulated argon data as already described.

In all cases the percentage deviation of B + T (dB/dT) and the mean deviation in B (expressed as a percentage of b^o) from the pseudo-experimental data was determined. The results are shown in Figure 4.4 for the two initial approximate potentials (12-6 and 11-6-8). It can be seen from the diagram that the deviations are minimized at values of ε very close to the true value for the BBMS potential of 142.5K. This procedure can be used to determine the value of ε, when, as for real data, the true value is unknown (19). The minima are quite sharp and would appear to define ε as 142 $\pm$ 2K. This method of minimization is similar to methods which have been shown to work in the inversion of gas transport property data (20,21).

(iv) Application of the virial inversion method to real data

When dealing with real data it is necessary, since the inversion method requires the derivative of the second virial coefficient with temperature for the evaluation of B + T(dB/dT), to fit the data to a smooth curve without either introducing spurious information or losing all the information implicit in B. Since B(T) varies so rapidly with temperature the choice of such a fitting procedure is difficult. Polynomial representations require so many parameters that instabilities arise when fitting a limited number of points. Hence the method

which we eventually chose, fits not the second virial coefficients themselves but a more slowly varying function. Essentially we fit the ratio of B to the value calculated using an approximate potential energy function and therefore we obtain

$$\frac{B(T)-b^o}{B_{12-6}(T)-b^o} = \frac{A}{T} + \frac{B}{T^2} + CT + DT^2 + E \qquad (4.14)$$

where $b^o = 2/3\pi N\sigma^3$. Accurate values of the collision diameter, σ and the well depth, ε, for the Lennard-Jones function are not required for this smoothing since a reasonable estimate of these parameters leads to an effective fit.

This method was applied to simulated data containing random errors. These were calculated from the BBMS potential function (7). Twenty-five second virial coefficients were accurately calculated in the temperature range 90-1400K. They were calculated by Simpson's rule from the following expression

$$B(T) = -2\pi N_A \int_o^\infty \{\exp(-U(r)/kT) - 1\}\, r^2 dr \qquad (4.15)$$

using 401 points in the integration for the range r/σ = 0.55 to 5.0 with long range and short range corrections. They were, therefore purely classical in nature. The values were then modified by adding to them random errors drawn from a gaussian distribution. These were calculated using variances which were based on the quoted experimental errors for argon (15). These were:

$$90 - 100K \pm 2\ cm^3\ ; \quad 100 - 250K \pm 1\ cm^3\ ;$$
$$250 - 700K \pm 0.5\ cm^3; \quad 700 - 1400K \pm 1\ cm^3:$$

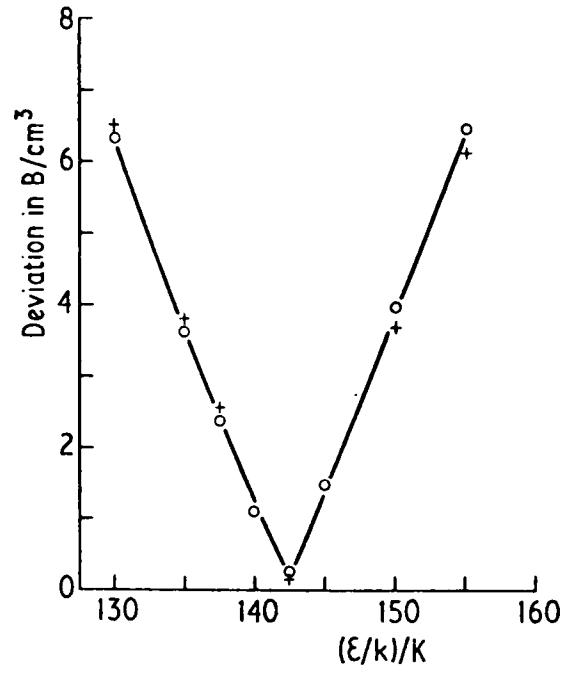
When incorporated into the pseudo-experimental data they led to an overall standard deviation of 0.92 cm^3 from the original exact data points. In addition a number of other data sets were constructed in which the errors were 0.5, 1.5 and 2.0 times the above values. These four sets along with the original exact points were then used to examine the effect of errors of different magnitude on the inversion method.

The data points, expressed as ratios of the second virial coefficients calculated from the Lennard-Jones funciton, were then fitted to the polynomial function equation (4.14). The effectiveness of this method of smoothing the data is illustrated clearly by a comparison of the deviations of the original and the smoothed data from the exactly calculated points. These values are given in the first half of Table 4.3.

The resulting smoothed data points were then inverted using a number of initial approximate potential energy functions (the 12-6, 9-6, 18-6 and 11-6-8 potentials). Three iterations were performed. Again short and long range extrapolations were necessary in order to iterate, and this was at long range based on the known values of the coefficients $C^{(6)}$, $C^{(8)}$ and $C^{(10)}$ in the dispersion force expression:

$$U(r) = - \frac{C^{(6)}}{r^6} - \frac{C^{(8)}}{r^8} - \frac{C^{(10)}}{r^{10}}$$

and consequently the BBMS function was used to extrapolate. At short range the form of the extrapolation was found not to be critical and so a scaled BBMS function was also used in this region. The inversion procedure was performed as described above using various estimates for the well depth parameter ε, and taking as the true ε, that value which minimised the deviations of the virial coefficients as calculated from the function produced on inversion from those used as data for the inversion. The minimisation procedure is illustrated for the error level corresponding to that expected for experiment (a level of 1.0 in Table 4.3) in Figure 4.5. The results of the minimisation procedure as applied to the other levels are shown in Table 4.3. In addition the deviations in r between the potential function produced by the minimisation procedure and the BBMS potential used to calculate the second virial coefficient points were calculated and are also shown in Table 4.3, expressed as absolute error in nanometers and also as a percentage. As can be seen from Figure 4.5 the best estimate for ε/k is 142 ± 5 which gives a corresponding value of $\sigma = 0.334$ nm in good agreement with the application of the inversion method to the exact data which results in estimates of $\varepsilon/k = 142.5 \pm 2K$ and $\sigma = 0.335$ nm which are essentially identical to their true values. The potential energy functions corresponding to these two minimisation procedures just described as applied to the exact data



F.gure 4.5 R.M.S. deviation of the calculated, from the pseudoexperimental second virial coefficients (with errors comparable to those of argon) as a function of the estimates of the well depth. Initial approximate potential function used 12–6, ○ ; 18–6, +.

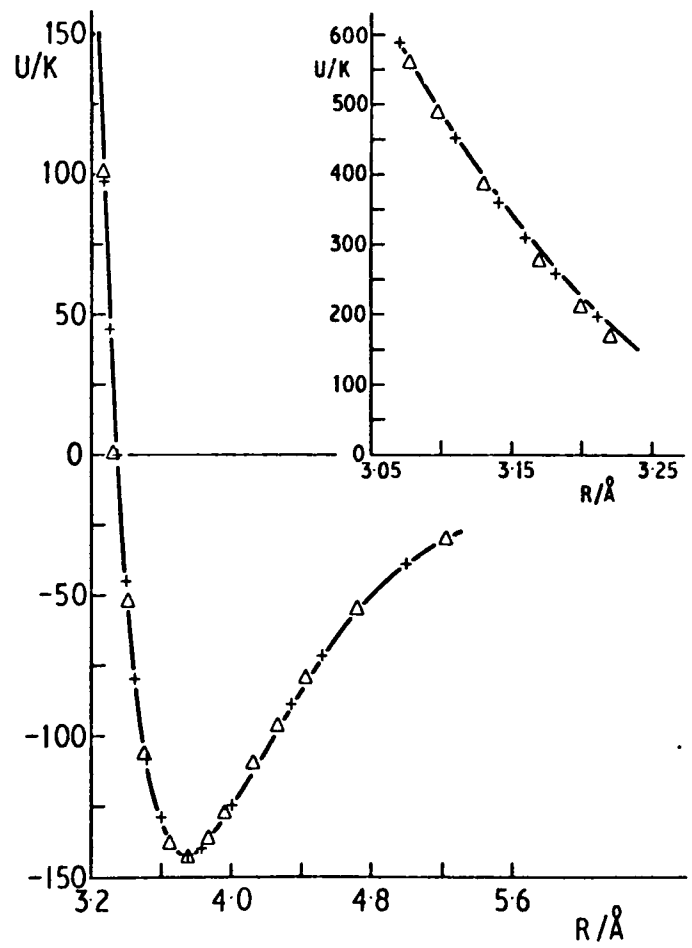


Figure 4.6 Potential energy functions obtained from the inversion of pseudoexperimental data. + exact, △ with random errors added (based on those for argon as described in text). The solid line is the potential energy function used to generate the data (BBMS).

and pseudo-experimental data with error level equal to 1.0 are shown in Figure 4.6 along with the BBMS potential. This confirms that where reasonably accurate data over an extended temperature range are available the method can be used first to define a value of ε and then to obtain the potential energy function to high accuracy.

In a recent publication (19) we reported the results of a blind test. In this test we were supplied with twelve second virial coefficients in the temperature range 65 -300K which were calculated from a potential function whose nature was unknown to the authors. This data was inverted in the manner described above and the minimisation procedure was performed to obtain the well depth. The results of this test were most satisfactory. The well depth parameter obtained by inversion was 87.2K whereas the exact value was 87.0K. The collision diameter, σ, was found to be 0.370 nm which was in complete agreement with the exact value of 0.370 nm. The potential function is shown in Figure 4.7 and it can be seen that the points obtained by inversion after three iterations are in excellent agreement with the true potential. The second virial coefficients calculated from the potential obtained on inversion agree with those supplied to an rms deviation of 0.46 cm^3.

Another aspect of the method is that it is possible, if low temperature virial coefficients are not available,

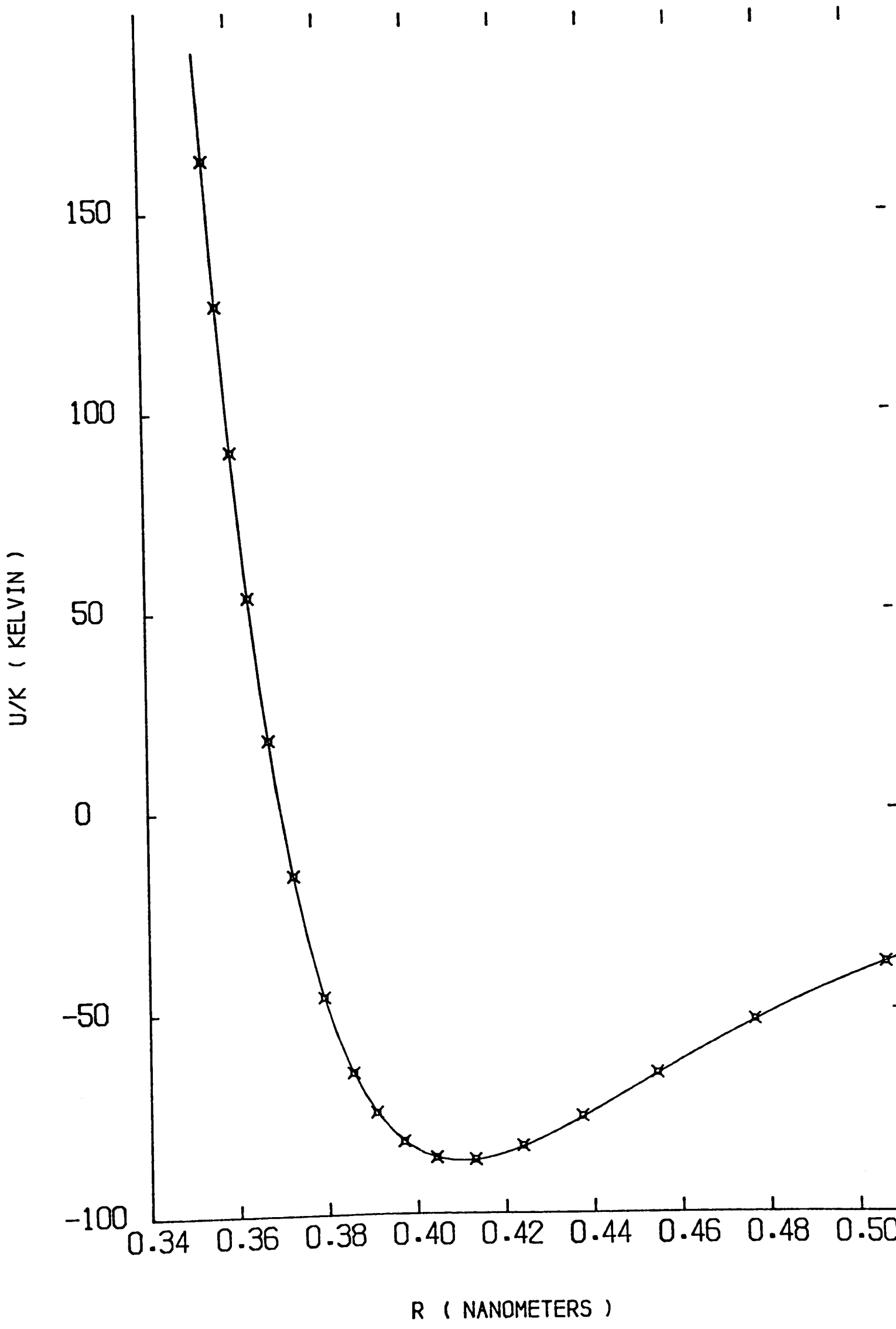
TABLE 4.3 : Results of inverting pseudo-experimental data with incorporated random errors

Error level*	0	0.5	1.0	1.5	2.0
Standard deviation of original data from exact values/cm^3	0	0.46	0.92	1.39	1.85
Standard deviation after fit to smoothing function/cm^3	0	0.09	0.17	0.25	0.31
Dev. in r x 100/ nm†	0.13	0.10	0.14	0.20	0.31
% dev in r†	0.36	0.32	0.48	0.68	1.00
Value of (ε/k) in K derived from the minimisation procedure	142.5±2	142.5±4	142±5	142±8	138±10

* Indicates relative to the estimated experimental errors for argon as described in the text.

† That is the deviation from the BBMS potential function used to calculate the data, after three iterations, initial approximate potential 12-6, BBMS extrapolation.

FIGURE 4.7 : The continuous line is the true form of the potential function ⋈ are the points derived from inversion.



to define the repulsive region to a high degree of accuracy from the inversion of high temperature second virial coefficients. This is possible with an estimate of ε which is in error by 10 percent since the repulsive region is largely insensitive to ε. This is illustrated by the percentage deviations in r obtained by inversion with an estimate of ε 10 percent in error. These are

U^* :	1	2	5
% dev in r :	0.5	0.2	0.1

(v) Application of the method to argon

Values of the second virial coefficients of argon in the temperature range 90-700K were taken from the values recommended in a recent compilation (15). Measurements below 90K were not included as their reliability had been questioned (15). The experimental data were first converted to the corresponding classical values by subtracting the quantum correction (22). This was calculated from a 12-6 potential as the magnitude of the quantum correction does not vary greatly with the form of the potential and in any case the corrections were at most 1.5% at low temperatures. These classical values were then fitted to the equation (4.14) and were inverted using the methods previously described. Again the value of ε was minimised and this is shown in Figure 4.8. This minimisation led to a value of ε/k of 150 $\pm$ 5K. The

value of sigma for this potential was 0.331 nm. These values, while being reasonably close to the best estimates for the intermolecular potential for argon of ε/k = 142.5 $\pm$ 1K and sigma = 0.335 nm are significantly removed from these values to suggest that the second virial coefficients for argon may contain systematic errors. The potential procedued by inversion; that is with a well depth of 150K does reproduce the transport properties and second virial coefficients reasonably well. The second virial coefficients in the temperature range 90-700K are reproduced to $\pm$ 2.2 cm^3 and the viscosity coefficients in the range 90-2000 K agree with the experimental values with a rms deviation of 0.9 percent. The error in the well depth is probably brought about by systematic errors in the low temperature second virial coefficients, this is because the virial coefficients above a value of T^* of approximately 2.5 correspond to the repulsive part of the potential which contributes very little to B(T). In addition it is at low temperatures where large experimental deviations are expected. This is one drawback of the virial inversion and it arises because the first derivative of the second virial coefficient data is required which puts a large demand on the precision of the experimental results.

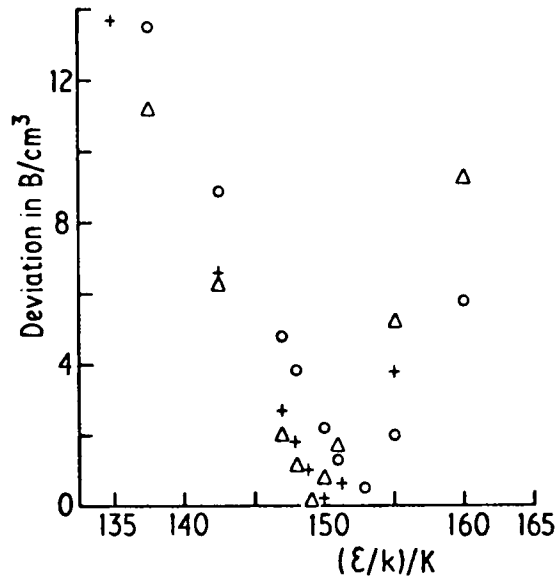


Figure 4.8 R.M.S. deviation of the calculated, from the experimental second virial coefficients of argon as a function of the estimate of the well depth. Initial approximate potential function used 11–6–8, △ ; 12–6, ○ ; BBMS, +.

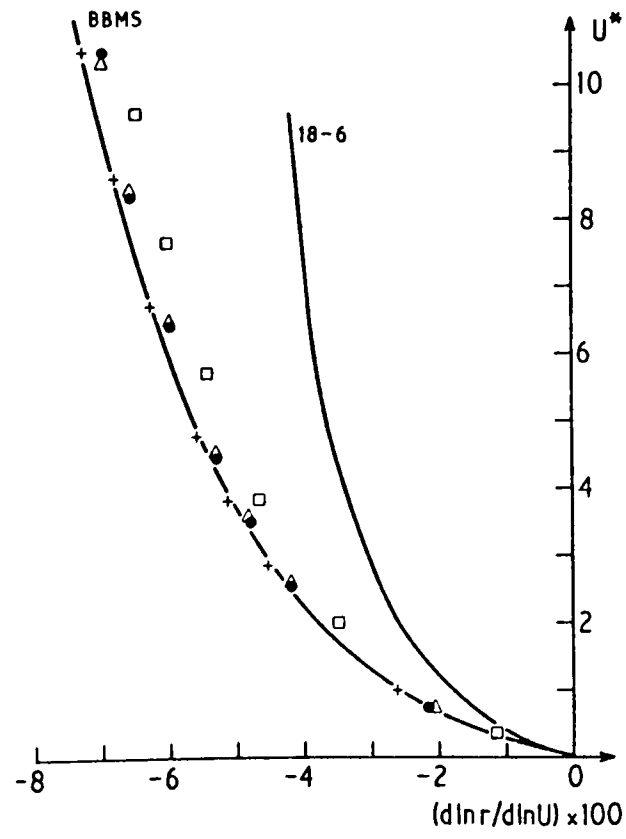


Fig. 4.9 The inversion of BBMS pseudo-experimental data. The derivatives appropriate to the BBMS [7] and the 18–6 functions are shown by solid lines. The data points refer to the results of inversion using differential initial approximate potentials: +: 9–6 potential; •: 12–6 potential; ▲: 11–6–8 potential; □: 18–6 potential.

(d) The Inversion of Isotopic Thermal Diffusion Data

(i) Introduction

Recently we have developed a direct inversion method for thermal diffusion data (23). The reduced thermal diffusion factor, α_o, has long been thought to be particularly sensitive to the nature of the potential function, and it has been suggested (24), that it could be used to distinguish between different model potentials when the experimental results are in error by as much as 20%.
In this new direct inversion method we inverted the thermal diffusion factor to give the slope of the potential energy function which is the only information implicitly contained in α_o. The previous inversion method (25) which gave the potential energy function itself did not do this directly as it required additional information in the form of viscosity or self-diffusion data.

The phenomenon of thermal diffusion is described rigorously by Chapman (26) and Enskog (27) who define the thermal diffusion factor by means of a mass flux equation for a binary mixture in a one-dimensional temperature gradient. Under steady state conditions this flux vanishes giving:

$$\frac{\partial x_1}{\partial z} = -k_T \frac{\partial \ell n T}{\partial z} \qquad (4.16)$$

Where x_1 is the mole fraction of species 1 and k_T is the thermal diffusion ratio. The thermal diffusion factor

α_T is obtained from k_T by removal of the composition dependence:

$$\alpha_T = k_T/x_1x_2 \qquad (4.17)$$

For a binary mixture of heavy isotopes, all the molecular force laws are the same and the expression for α_T may be expanded in powers of the small quantity $(M_1-M_2)/(M_2+M_2)$, conventionally only the first term is kept (28,29) and hence to this level of approximation we obtain:

$$\alpha_T = \alpha_o \frac{(M_1-M_2)}{(M_1+M_2)} \qquad (4.18)$$

this being sufficiently accurate for $(M_1-M_2)/(M_1+M_2) < 0.15$. α_o is then the dimensionless isotopic thermal diffusion factor and is independent of M_1 and M_2 as well as the composition of the mixture, it is a function of temperature and the potential energy function alone.

(ii) Inversion procedure

Thermal diffusion can be related to a ratio of collision integrals $C^* = \Omega^{(1,2)*}/\Omega^{(1,1)*}$. To first order Kihara has shown

$$(\alpha_o)_{K1} = 15(6C^*-5)/16A^* \qquad (4.19)$$

Where $A^* = \Omega^{(2,2)*}/\Omega^{(1,1)*}$ and is not particularly sensitive

to the nature of the potential energy function. The previous inversion method of Clancy and Smith (25) extracted $\Omega^{(1,2)}$ from the isotopic thermal diffusion factor $(\alpha_o)_{K1}$. From equation (4.19) it may be shown that

$$\Omega^{(1,2)*} = \left[\frac{8(\alpha_o)_{K1}A^*}{45} + 5/6\right]\Omega^{(1,1)*} \qquad (4.20)$$

The presence of $\Omega^{(1,1)*}$ requires that this be obtained either directly from self-diffusion data, or since this data is not in general very accurate the equation (4.20) may be rewritten

$$\Omega^{(1,2)*} = \left[\frac{8(\alpha_o)_{K1}}{45} + \frac{5}{6A^*}\right]\Omega^{(2,2)*} \qquad (4.21)$$

and now $\Omega^{(2,2)*}$ may be extracted as shown earlier from viscosity data. The inversion procedure now was exactly analogous to that for the transport properties with the appropriate characteristic distance being:

$$\tilde{r} = \Omega^{(1,2)*\,\frac{1}{2}} \qquad (4.22)$$

This method was applied to the experimental data of Taylor and Weissmann (30) for argon and krypton (25) and was found to give potentials in good agreement with those previously established for these substances, namely the BBMS function (7) for argon and the function of Gough, Maitland and Smith (31) for krypton.

(iii) The direct method

In this new method we develop a direct route to the logarithmic derivative of the potential in the repulsive region ($d\ell nr/d\ell nU$). The recursion formula for collision integrals

$$\frac{\Omega^{(\ell,s+1)}}{\Omega^{(\ell,s)}} = 1 + \frac{1}{s+2} \frac{\partial \ell n \Omega^{(\ell,s)}}{\partial \ell nT} \qquad (4.23)$$

enables us to write; since $C^* = \Omega^{*(1,2)}/\Omega^{*(1,1)}$

$$6C^* - 5 = 1 + 2\partial \ell n \Omega^{(1,1)}/\partial \ell nT \qquad (4.24)$$

By analogy with the transport property inversion methods already outlined, which relate each $(\Omega^{(\ell,s)},T)$ point to a point (r,U) on the potential we may expect $\partial \ell n \Omega^{(1,1)}/\partial \ell nT$ to be related to the logarithmic derivative of the potential $\partial \ell nr/\partial \ell nU$. We may therefore expect a relationship such as

$$\left(\frac{\partial \ell nr}{\partial \ell nU}\right)_{U=f(T^*)} = \frac{3(C^*-1)}{2} \qquad (4.25)$$

where $U = f(T^*)$ is the point on the potential curve at which the derivative is taken. Such an identity has been placed on a firmer theoretical basis by Mason and Monchick (32) who considered the specific case of potentials with hard repulsive cores and small well depth. This formal, though restricted analysis leads to the equation

$$C^* - 1 \approx \frac{2}{3}\left(\frac{\partial \ell n r}{\partial \ell n U}\right)_{U=V}\left(\frac{\partial \ell n V}{\partial \ell n T}\right) \qquad (4.26)$$

where V is the point at which the derivative is taken. In this case V is restricted to the repulsive part of the potential. For the case of simple inverse power potentials of the form $U = A/r^n$ this leads to an exact closed expression for C^*, however, for more realistic potentials this kind of expression for V cannot be obtained from this formal treatment.

In this new method we seek to develop a more flexible inversion procedure by analogy with previous inversion methods for viscosity and other transport properties. From this analysis therefore we consider each $(\partial \ell n \Omega^{(1,1)}/\partial \ell n T, T)$ point to correspond to a value of $(\partial \ell n r/\partial \ell n U, U)$; the correspondence $U = f(T^*)$ being effected by an inversion function. The value V at which the derivative is taken therefore becomes:

$$V = G_D(T^*)kT \qquad (4.27)$$

where the inversion function $G_D(T^*)$ is defined as

$$G_D(T^*) = U(\Omega^{*(1,1)^{\frac{1}{2}}})/kT \qquad (4.28)$$

This choice of V leads to an inversion procedure which, in principle, covers the entire range of the potential function.

Having identified the point at which the derivative is taken a further inversion function $H(T^*)$ is then required to complete the identity outlined in equation (4.25). Hence we obtain:

$$\left(\frac{\partial \ell n r}{\partial \ell n U}\right)_{U=G_D.kT} = \frac{3}{2}\,[C^*-1]H(T^*) \qquad (4.29)$$

Clearly from (4.26) we can identify V with $G_D.kT$ and therefore obtain a relationship between G_D and H of the form:

$$\frac{1}{H(T^*)} = \frac{\partial \ell n G_D(T^*)}{\partial \ell n T} + 1 \qquad (4.30)$$

and this relationship has been verified as accurate over a very wide range of T^* for simple potential functions.

In order to accomplish the inversion, then we obtain $C^*_{(exp)}$ from the Kihara analysis of our experimental data, hence using $G_D^{(o)}$ and $H^{(o)}$ calculated from some approximate potential, the first estimate of the logarithmic derivative becomes

$$\left(\frac{\partial \ell n r}{\partial \ell n U}\right)_{U=G_D^{(o)}\,kT} = \frac{3}{2}\,[C^*_{(exp)} - 1]H^{(o)} \qquad (4.31)$$

$G_D^{(o)}$ has the characteristic of a "good" inversion function in that it is relatively insensitive to the detailed form of the potential function. A discontinuity in $H^{(o)}$

occurs at the point corresponding to the potential minimum but due to the limited temperature range of experimental data for thermal diffusion this has little practical significance.

The inversion method was tested on pseudo-experimental data for argon and it was found that it closely reproduced the slope of the potential. However convergence is relatively slow as is shown in Figure 4.9 and since iteration is not possible this means that it is important to use as an initial approximate potential one which is not too far removed from the true potential for the system. This is shown in the figure where the results from the 18-6 potential which is considerably removed from the BBMS function (7) used to calculate the pseudo-experimental points are displaced from the slope expected from the BBMS function. Table 4.4 shows the mean % deviation in $\partial \ell nr/\partial \ell nU$ for the starting potential from the BBMS values and on inversion. It can be seen that with a reasonable starting potential inversion is satisfactory.

When dealing with real experimental data $(\alpha_o)_{exp}$ must be converted to those given by the first Kihara approximation by means of a correction function:

$$(\alpha_o)_{exp} = (\alpha_o)_{K1} \; f_\alpha \qquad (4.32)$$

Since the experimental value is very close to that given by the second Kihara approximation $(\alpha_o)_{K2}$; f_α may be calculated via

TABLE 4.4 : The results of inversion of BBMS pseudo-experimental data. Column A compares the derivatives for the initial approximate potential with the BBMS values, column B compares the values after inversion. The results only refer to the experimentally accessible repulsive region.

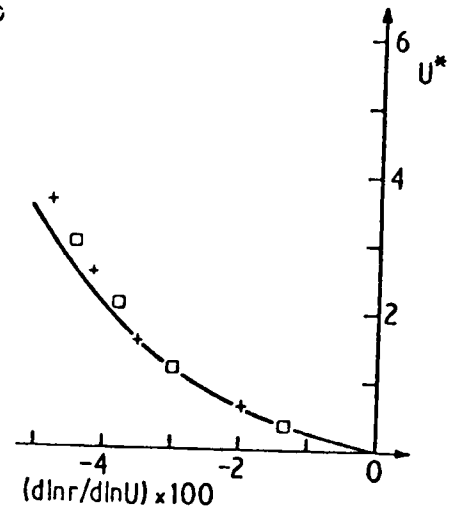
Starting Potential	Mean % deviation in $\partial \ell nr/\partial \ell nU$	
	A	B
9-6	7.1	1.7
12-6	13.4	2.3
11-6-8	14.2	2.9
18-6	29.8	8.3

$$f_\alpha = (\alpha_o)_{K2}/(\alpha_o)_{K1} \qquad (4.33)$$

Where $(\alpha_o)_{K2}$ is (23) a very complex function of collision integrals, however f_α has been found to be particularly insensitive to the potential used to calculate it (25) and therefore, in inverting argon and krypton data the BBMS potential (7) was used for f_α calculation. As with the other inversion methods a value of the well depth ε/k must be supplied. In this inversion of argon and krypton data the values derived from spectroscopic analysis (33,34) were used giving ε_{Ar} = 142.5K, ε_{Kr} = 199.2K. The method is particularly sensitive to the choice of well depth and a realistic value is required when inverting real data. The method was applied to the results of Taylor and Weissmann (30). The results for krypton were consistent with the GMS function (31) proposed for krypton (Figure 4.10) but the argon results suggested that the repulsive region of the argon potential was too "soft" in the BBMS function. The more recently proposed potential of Aziz and Chen (35) formulated on the basis of a wide range of thermophysical properties gives a closer representation of the potential gradient (Figure 4.11) but even this potential may, on the basis of these results, be too soft.

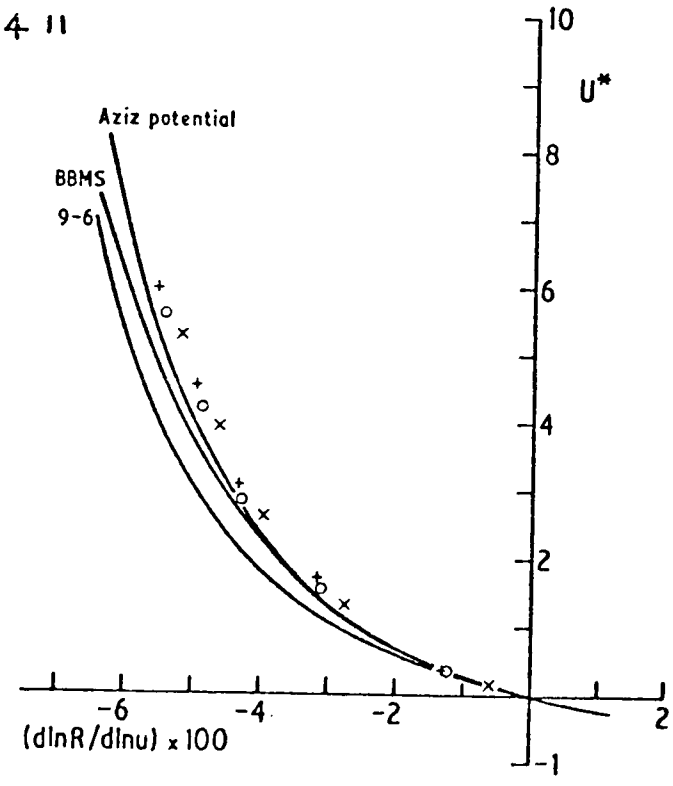
Having developed these inversion methods we will in the next two chapters look at their application to the gaseous viscosities for argon-xenon and argon-nitrogen to give intermolecular potentials for these interactions.

Fig 4 10



The inversion of real experimental data for krypton (30) The solid line shows the GMS function (31). The data points refer to the results of inversion using 12–6 (□) and BBMS (+) initial approximate potentials.

Fig 4 11



The inversion of real experimental data for argon (30) The solid lines refer to the BBMS (7) and Aziz (35) potentials. The data points refer to the results of inversion using different initial approximate potentials. X: 12–6 potential; +: BBMS potential; o: 9–6 potential.

CHAPTER 5

EXPERIMENTAL VISCOSITIES FOR Ar-Xe MIXTURES

a) Introduction

This chapter deals with the experimental results of the viscosity determinations of Ar-Xe mixtures. These mixture viscosities are then used to calculate the interaction viscosities for Ar-Xe which will be required in Chapter 6 in order to determine the intermolecular pair potential for the Ar-Xe interaction (1).

The viscosity of a mixture of Ar-Xe approximately 50 percent in argon was determined at seven temperatures from just above the boiling point of xenon 170K to 270K. The viscosities were measured relative to both nitrogen and argon at the same temperature.

Since the application of the correction terms described in Chapter 3 requires a knowledge of the pressures $\bar{P}_f$ and $\bar{P}_b$ and the ends of the capillary averaged over the period of a pointer drop it was necessary to calculate these. This is possible using the fact that at any instant the mercury height in the manometer M1 measures $P_m = P_f - P_b$, along with a knowledge of the total quantity of gas added during the filling of the apparatus.

b) Pressures at the Pointers

The effective volume of the apparatus depends on the capillary temperature T_c since this will control the quantity of gas contained in the heat exchanger and lead tubes to the capillary. The front volume consists of the front volume V_1 at temperature T_f and various small volumes V_{ci} at temperatures T_{ci}. There are corresponding volumes for the back part of the viscometer. These volumes are given in Chapter 3 B(d).

If we consider the gas before the capillary let there be n_1 moles at T_f and n_{ci} moles at T_{ci}. Using the ideal gas equation we obtain:

$$P_f V_1 = n_1 R T_f \tag{5.1}$$

and

$$P_f V_{ci} = n_{ci} R T_{ci} \qquad i = 1,2,3,4 \tag{5.2}$$

The total number of moles is

$$n = n_1 + \sum_i n_{ci}$$

$$= \frac{P_f}{RT_f} \left(V_1 + \sum_i V_{ci} \frac{T_f}{T_{ci}}\right) \tag{5.3}$$

Thus the "effective" front volume becomes

$$V_f = V_1 + \sum_i V_{ci} \, T_f/T_{ci} \tag{5.4}$$

with a similar expression for the back volume (V_b).

(i) First filling

For medium and high pressures there is a first filling to pointer N_1, the whole viscometer except the volume between the mercury surface and tap C (volume X) being filled to a pressure $P_m(N_1)$. Tap C is then opened and the pressure throughout the viscometer is given by the expression:

$$P = P_m(N_1)\frac{(V-X)}{V} \qquad (5.5)$$

where V is the total effective volume $V = V_f + V_b$. If there is no first filling P = 0.

(ii) Second filling

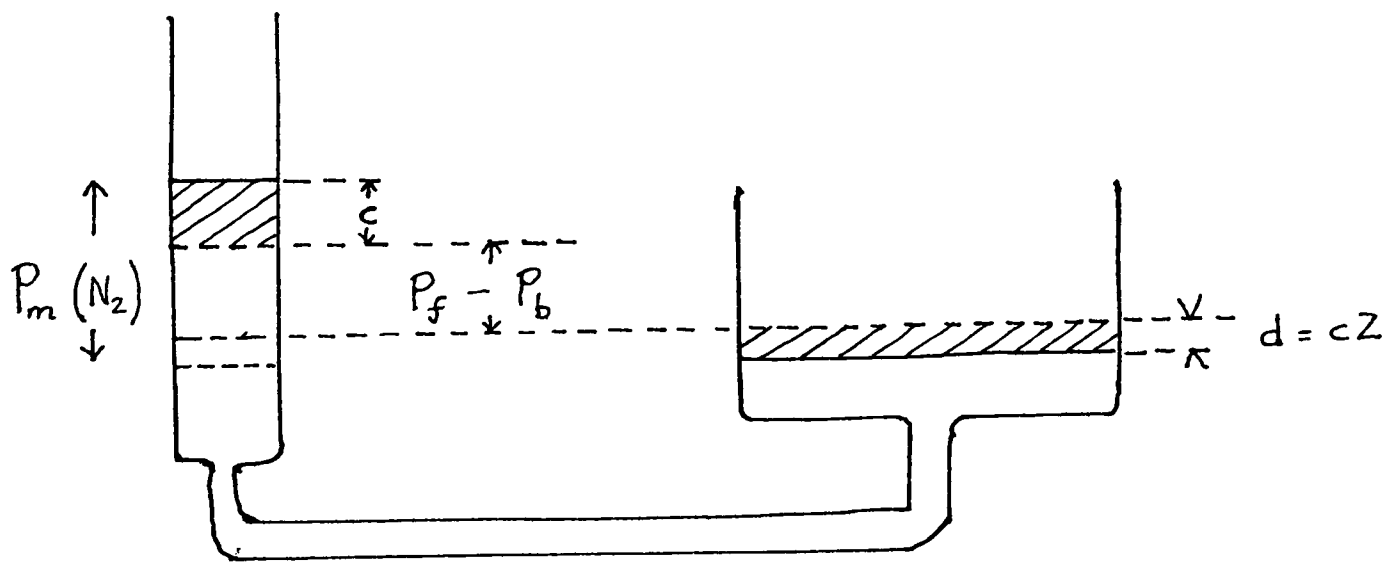
Gas is introduced at a pressure determined by pointer N_2. The back pressure also increases slightly due to the mercury surface rising to $P_b' = PV_b^o/V_b$, where V_b^o is the effective back volume, when the mercury surfaces are level. The small volumes in front of the capillary remain at pressure P and the pressure P_f in the front vessel is equal to $P_b' + P_m(N_2)$. It is now quite straightforward to calculate the total quantity of gas Q in the viscometer. The quantities before and after the capillary, Q_1 and Q_2 respectively in P-V units are

$$Q_1 = P_f{}'V_1 + P \sum_{i=1}^{4} V_{ci}\, T_f/T_{ci} \qquad (5.6)$$

$$Q_2 = P_b{}'V_b \qquad (5.7)$$

$$Q = Q_1 + Q_2 \qquad (5.8)$$

When the run begins with opening of tap A, there is an initial drop of the manometer level in M_1 due to the equalization of the pressures in the front vessel and in the lead tubes to the capillary. If we assume that this process is instantaneous then we can calculate P_f and P_b. This equalisation process is shown in the figure below.



Using the nomenclature introduced in Chapter 3 B(d) we obtain

$$Q_1 = P_f(V_f - cA) \tag{5.9}$$

$$Q_2 = P_b(V_b + cA) \tag{5.10}$$

and $P_f - P_b + c + d = P_f - P_b + c(1+Z) = P_m(N_2)$ as (5.11)

This produces a cubic equation in P_f writing $P_m(N_2)$ as P_m this is:

$$AVP_f^3 - [AQ + AVP_m - (1+z)V_fV]P_f^2 + [Q_1AP_m - (1+Z)Q_1(V+V_f)]P_f + (1+Z)Q_1^2 = 0 \tag{5.12}$$

This equation may be solved for P_f by Newton's method; $P_m(N_2)$ being used as a first approximation. This gives

$$P_b = P_f - P_m + (1+Z)(P_fV_f - Q_1)/P_fA \tag{5.13}$$

At any other pointer the pressures P_f and P_b are determined from

$$P_f = \frac{Q + P_mV_b}{V} \tag{5.14}$$

$$P_b = \frac{Q - P_mV_f}{V} \tag{5.15}$$

The relevant quantities were calculated for the pressures used in this work namely LP and P_2. They are shown in

TABLE 5:1 Pressure Corrections

A. Low Pressure (LP) Runs

Pointer	P_f	P_b	$\bar{P}_f$	$\bar{P}_b$	$\bar{P}$	$(\bar{P}_f^2-\bar{P}_b^2)$	$\frac{(\bar{P}_f^3-\bar{P}_b^3)}{(\bar{P}_f^2-\bar{P}_b^2)}$
1	30.366	0.0	28.573	1.572	15.072	813.917	28.654
2	26.779	3.144	24.572	5.020	14.796	578.588	25.423
3	22.365	6.895	20.750	8.205	14.478	363.240	23.075
4	19.135	9.515	17.947	10.452	14.199	212.843	21.793
5	16.758	11.388					

B. Very Low Pressure (P2) Runs

2	22.60	0.0	20.670	1.635	11.153	424.576	20.790
3	18.74	3.27	17.125	4.580	10.853	272.289	18.091
4	15.51	5.89	14.320	6.825	10.573	158.482	16.523
5	13.13	7.76					

Table 5.1. The temperature T_c is not critical and averages were used over the experimental temperature range. In addition it may be seen that the mean pressure $\bar{P}$ is only very slowly varying with pressure drop.

c) Times of Flow and Correction Terms

The 50/50 mixture of Ar-Xe which was used in these experiments was supplied pre-mixed by the British Oxygen Company. The composition of this was determined by BOC (Special Gases Division) and was also checked on arrival by using a mass-spectrometer in the Physical Chemistry Laboratory, Oxford.

The times of the runs are given in Table 5.2 for the seven temperatures determined. In each case at least two runs were made of both mixture and standard gas as a consistency check. The ratio of the times of the mixture and standard gas runs gives a rough ratio of the viscosities. This ratio was then corrected by multiplying by the ratio of the correction terms $\bar{k}_b$ $\bar{k}_s$ $\bar{k}_B$ and $\bar{k}_H$ for the mixture to that of the standard gas.

(i) Curved pipe flow

For each pointer drop the Dean number was calculated in experimental units equation (3.20) becomes

$$(\bar{D}_e) = 215.0 \frac{(\bar{P}_f^{\,2} - \bar{P}_b^{\,2})}{\eta^2 T_c} M \qquad (5.16)$$

Where pressures are in cmHg and the viscosity η is

TABLE 5.2 : Times of Run for Ar-Xe and Argon

Temp.	Type	Substance	Pointers 2-3	3-4	4-5
189.50	P_2	Ar	-	2386.0	3030.6
			-	2391.3	3021.7
189.50	P_2	Ar-Xe	-	2428.5	3079.1
			-	2445.6	3098.4
204.03	P_2	Ar	-	2734.4	3467.0
			-	2739.8	3469.0
204.03	P_2	Ar-Xe	-	2803.0	3552.8
			-	2803.2	3550.1
			-	2805.2	3552.6
211.75	P_2	Ar	-	2939.0	3726.8
			-	2939.3	3721.8
211.75	P_2	Ar-Xe	-	3015.9	3828.0
			-	3013.0	3821.6
220.81	P_2	Ar	-	3181.4	-
			-	3178.4	4029.5
			-	3178.8	4034.0
220.81	P_2	Ar-Xe		3266.5	4140.0
				3269.4	4134.5
232.81	P_2	Ar	-	3508.9	4447.9
			-	3512.0	4451.0
232.81	P_2	Ar-Xe	-	3622.0	4588.0
			-	3622.0	4591.5
259.30	LP	Ar	2831.2	3270.8	4111.0
			2831.4	3266.8	4113.6
259.30	LP	Ar-Xe	2948.9	3397.6	4286.9
			2946.4	3401.7	4274.7
268.6	LP	Ar	3017.7	3488.8	4386.0
			3025.0	3495.8	4397.5
			3016.0	3480.5	4393.1
268.6	LP	Ar-Xe	3140.8	3619.0	4557.5
			3143.5	3632.8	4563.2

in 10^{-7} kg m^{-1} s^{-1}. The value of η was either that of a standard gas or in the case of the mixture it was the standard gas viscosity multiplied by the rough ratio already obtained. No time flows had Dean numbers greater than 5 and indeed 1.2 is the highest. Therefore the runs should be almost completely unaffected by curved pipe flow.

(ii) Gas Imperfection

These terms $\bar{k}_b$ and $\bar{k}_B$ are given in experimental units as:

$$\bar{k}_b = 1 + \frac{2B_f P_f}{RT_f} = 1 + 1.072\ \bar{P}_f B_f \times 10^{-6} \qquad (5.17)$$

Here we require the second virial coefficient B_f at 298.2K, the temperature of the front vessel, whereas in the second

$$\bar{k}_B = 1 - \frac{2B_c}{3RT_c}\ \frac{(\bar{P}_f^{\,3}-\bar{P}_b^{\,3})}{(\bar{P}_f^{\,2}-\bar{P}_b^{\,2})} = 1-1.065\ \frac{(\bar{P}_f^{\,3}-\bar{P}_b^{\,3})}{(\bar{P}_f^{\,2}-\bar{P}_b^{\,2})}\ \frac{B_c}{T_c} \times 10^{-4} \qquad (5.18)$$

we require B_c at the capillary temperature. In both cases mean pressures are in cmHg and second virial coefficients are in cm^3 mol^{-1}. All virial coefficients were taken from the compilation of Dymond and Smith (2). These corrections were very small always being less than 0.3%. The mixture virial coefficients required were calculated from the expression:

$$B_{mix} = x_1^2 B_{11} + 2x_1 x_2 B_{12} + x_2^2 B_{22} \qquad (5.19)$$

where 11 and 22 refer to the pure components and 12 to the interaction virial coefficient.

(iii) Slip

The use of low pressure runs in order to reduce the effects of curved pipe flow and gas imperfection has the consequence that the corrections for slip are correspondingly larger. In the current work the slip correction was of the order of one percent at its maximum. The slip correction coefficient as described in Chapter 3 equations (3.10) and (3.11) was expressed in the present work in practical units as

$$\bar{k}_s = 1 + 0.162 \frac{K_s \eta}{\bar{p}} \left(\frac{T_c}{M}\right)^{\frac{1}{2}} \times 10^{-4} \qquad (5.20)$$

where

$$K_s / J^{\frac{1}{2}} K^{\frac{1}{2}} = 18.0 - 0.03 \ (T_c - 290) \qquad (5.21)$$

(iv) Kinetic energy

This is given by the equation (see (3.17))

$$\bar{k}_H = 1 - \frac{1.1 M \Delta (P_f V_f)}{8 \pi \eta L R T_f t} \qquad (5.22)$$

where $\Delta(P_f V_f)$ represents the change in this product from pointer 3 to pointer 4.

In experimental units this becomes:

$$k_M = 1-0.958 \frac{\Delta(P_f V_f)M}{\eta t} \times 10^{-4} \qquad (5.23)$$

with the time of flow t given in seconds and $\Delta(P_f V_f)$ in cmHg-cm^3 units. This correction was almost negligible in all cases being typically 0.01%.

When these corrections are applied to the rough ratio, the overall correction is usually very small due to the similarity of the terms for both mixture and standard gas being, typically, in the range 0.3 to 0.5%. The individual correction terms are shown in Table 5.3.

d) Final Accurate Ratios and Error Limits

The accurate ratio for argon-xenon/argon obtained by multiplying the rough ratios by the ratio of the correction terms are shown in Table 5.4. The accuracy of these can be assessed by considering the various possible sources of error as follows:

(i) Temperature and pressure fluctuations

The main source of error is the variation of the temperature of the run and the pressure of gas in the system for both mixture and standard gas determinations. The accuracy of filling to pointers was considered to introduce approximately $\pm$ 0.05% error into the times and therefore $\pm$ 0.1% into the ratios. The variation of temperature in the cryostat during the runs was low of

TABLE 5.3 : Correction Terms for Ar-Xe and Ar

A. Argon

T	Type	(D_e)	$\bar{k}_s$	$\bar{k}_b$	$\bar{k}_B$	$\bar{k}_H$	Pointer drop
189.50	P_2	0.5430	1.0103	0.9997	1.0006	0.99996	3-4
189.50	P_2	0.3160	1.0106	0.9998	1.0005	0.99996	4-5
204.03	P_2	0.4398	1.0112	0.9997	1.0004	0.99997	3-4
204.03	P_2	0.2560	1.0115	0.9998	1.0004	0.99997	4-5
211.75	P_2	0.3957	1.0117	0.9997	1.0004	0.99997	3-4
211.75	P_2	0.2303	1.0120	0.9998	1.0004	0.99997	4-5
220.81	P_2	0.3515	1.0122	0.9997	1.0003	0.99998	3-4
220.81	P_2	0.2046	1.0126	0.9998	1.0002	0.99998	4-5
232.81	P_2	0.3028	1.0129	0.9997	1.0003	0.99998	3-4
232.81	P_2	0.1762	1.0133	0.9998	1.0003	0.99998	4-5
259.3	LP	0.4758	1.0106	0.9996	1.0002	0.99998	2-3
259.3	LP	0.2987	1.0108	0.9996	1.0002	0.99998	3-4
259.3	LP	0.1750	1.0110	0.9997	1.0002	0.99998	4-5
268.6	LP	0.4314	1.0110	0.9996	1.0002	0.99998	2-3
268.6	LP	0.2708	1.0112	0.9996	1.0002	0.99998	3-4
268.6	LP	0.1587	1.0114	0.9997	1.0002	0.99998	4-5

TABLE 5.3 continued

B. Argon Xenon

T	Type	(D_e)	$\bar{k}_s$	$\bar{k}_b$	$\bar{k}_B$	$\bar{k}_H$	Pointer drop
189.50	P_2	1.1390	1.0071	0.9989	1.0016	0.99992	3-4
189.50	P_2	0.6624	1.0073	0.9991	1.0014	0.99992	4-5
204.03	P_2	0.9151	1.0078	0.9989	1.0013	0.99994	3-4
204.03	P_2	0.5328	1.0080	0.9991	1.0012	0.99994	4-5
211.75	P_2	0.8215	1.0081	0.9989	1.0011	0.99994	3-4
211.75	P_2	0.4769	1.0083	0.9991	1.0010	0.99994	4-5
220.81	P_2	0.7265	1.0085	0.9989	1.0010	0.99995	3-4
220.81	P_2	0.4242	1.0087	0.9991	1.0009	0.99995	4-5
232.81	P_2	0.6210	1.0090	0.9989	1.0008	0.99996	3-4
232.81	P_2	0.3616	1.0093	0.9991	1.0007	0.99996	4-5
259.3	LP	0.9585	1.0075	0.9984	1.0009	0.99996	2-3
259.3	LP	0.6030	1.0076	0.9987	1.0008	0.99996	3-4
259.3	LP	0.3527	1.0078	0.9988	1.0007	0.99996	4-5
268.6	LP	0.8708	1.0077	0.9984	1.0008	0.99996	2-3
268.6	LP	0.5485	1.0079	0.9987	1.0007	0.99996	3-4
268.6	LP	0.3213	1.0080	0.9988	1.0007	0.99996	4-5

TABLE 5.4 : Accurate Ratios and η_{mix} for Ar-Xe

Temp.	Pt	Ar-Xe/Ar Rough Ratio	Accurate	η_{mix}	Mean
189.50	3-4	1.02026	1.01744	154.32	154.3
	4-5	1.02069	1.01760	154.35	
204.03	3-4	1.02437	1.02085	165.74	165.7
	4-5	1.02417	1.02065	165.71	
211.75	3-4	1.02562	1.02185	171.61	171.7
	4-5	1.02698	1.02319	171.84	
220.81	3-4	1.02782	1.02382	178.57	178.4
	4-5	1.02617	1.02216	178.28	
232.81	3-4	1.03178	1.02748	187.89	187.9
	4-5	1.03153	1.02721	187.84	
259.30	2-3	1.04109	1.03725	208.49	
	3-4	1.04003	1.03623	208.29	208.4
	4-5	1.04097	1.03722	208.49	
268.60	2-3	1.04060	1.03658	214.80	
	3-4	1.03943	1.03547	214.57	214.6
	4-5	1.03828	1.03436	214.34	

order ± 0.03K. There was in addition to this short term drift a further long term drift in the mean temperature over the course of several runs which was more serious of the order ± 0.05 - 0.1% and hence introduced an error of ± 0.1 - ± 0.2% into the ratio. Hence the total error which might be expected from these sources is of the order ± 0.2 - 0.3%. In fact the biggest difference between the two ratios measured at the same temperature was 0.2% so this could be explained quite easily by the above sources of error.

(ii) Other sources of error

The absolute temperature determination is not likely to introduce any significant error as the platinum resistance thermometer was considered accurate to at least ± 0.05K which would at worst only introduce an error of ± 0.03% at the lowest temperature measured.

The correction terms would only introduce a small contribution to the error in the ratios due to uncertainty in the second virial coefficients of at worst ± 0.05%. The uncertainty in the slip coefficient would also introduce an error of ± 0.1%.

The total error level expected in the times of flow therefore is probably of the order of ± 0.5%.

(iii) Consistency check of Ar-N_2 ratios

As a consistency check, at each temperature the ratio of the Ar/N_2 viscosities was determined. From the low temperature N_2 standard of Dawe and Smith (3) and the accurate Ar/N_2 ratios a viscosity for argon was calculated and this was compared with that from the argon standard which was used in this work (1) and which was largely based on the work of of Gough et al (4) for the temperature range 120-300K and Maitland and Smith (5) for the range 300-1600K.

The viscosities of the argon standard were expressed in the form of a smooth curve of the form:

$$\ell n(S) = A\ \ell n\ T + B/T + C/T^2 + D \qquad (5.24)$$

where $S = \eta/10^{-7}$ kgm^{-1} s^{-1}, T is the temperature in Kelvin and the coefficients are

$A_1 = 0.583152$	$A_2 = 0.599369$
$B_1 = -96.1924$	$B_2 = -57.50409$
$C_1 = 2923.99$	$C_2 = -3118.53$
$D_1 = 2.38966$	$D_2 = 2.236$

subscripts 1 referring to the temperature range 120-300K and subscripts 2 referring to 300-1700K. The results are shown in Table 5.5 and it may be seen that the results are excellent with the largest error being 0.14% and a root mean square deviation of 0.10%.

TABLE 5.5 : Comparison of Ar_{calc} with $Ar_{standard}$

T	Accurate Ratio	$\eta_{Ar_{calc}}$	$\eta_{Ar_{stand}}$	% error
189.5	1.23269	151.803	151.676	-0.084
204.03	1.23911	162.581	162.357	-0.138
211.75	1.24077	167.988	167.941	-0.028
220.81	1.24419	174.450	174.416	-0.019
232.81	1.25066	183.173	182.863	-0.170
259.30	1.25744	200.863	201.005	0.071
268.60	1.26150	207.194	207.216	0.011

root mean square error 0.10%

e) Final Viscosities of the Binary Mixtures

The final viscosities of the Ar-Xe mixtures were obtained by multiplying the accurate ratios shown in Table 5.4 with the viscosity of the smooth curve of the argon standard shown above. The resulting mixture viscosities are also shown in Table 5.4. These are estimated to be accurate to at least 1%.

(i) Comparison with other workers

The Ar-Xe viscosity results from this work have been compared with those of Barr (6) and Harris (7) who measured mixture viscosities at the same mole fraction of xenon namely 0.5183 as was used in the present measurements. The points from this work have, therefore, been fitted to a smooth curve of the form of equation (5.24) in order to facilitate the comparison with the previous work of Barr and Harris.

The coefficients of this curve were:

$$A = -0.555943 \ ;$$

$$B = -656.304 \ ;$$

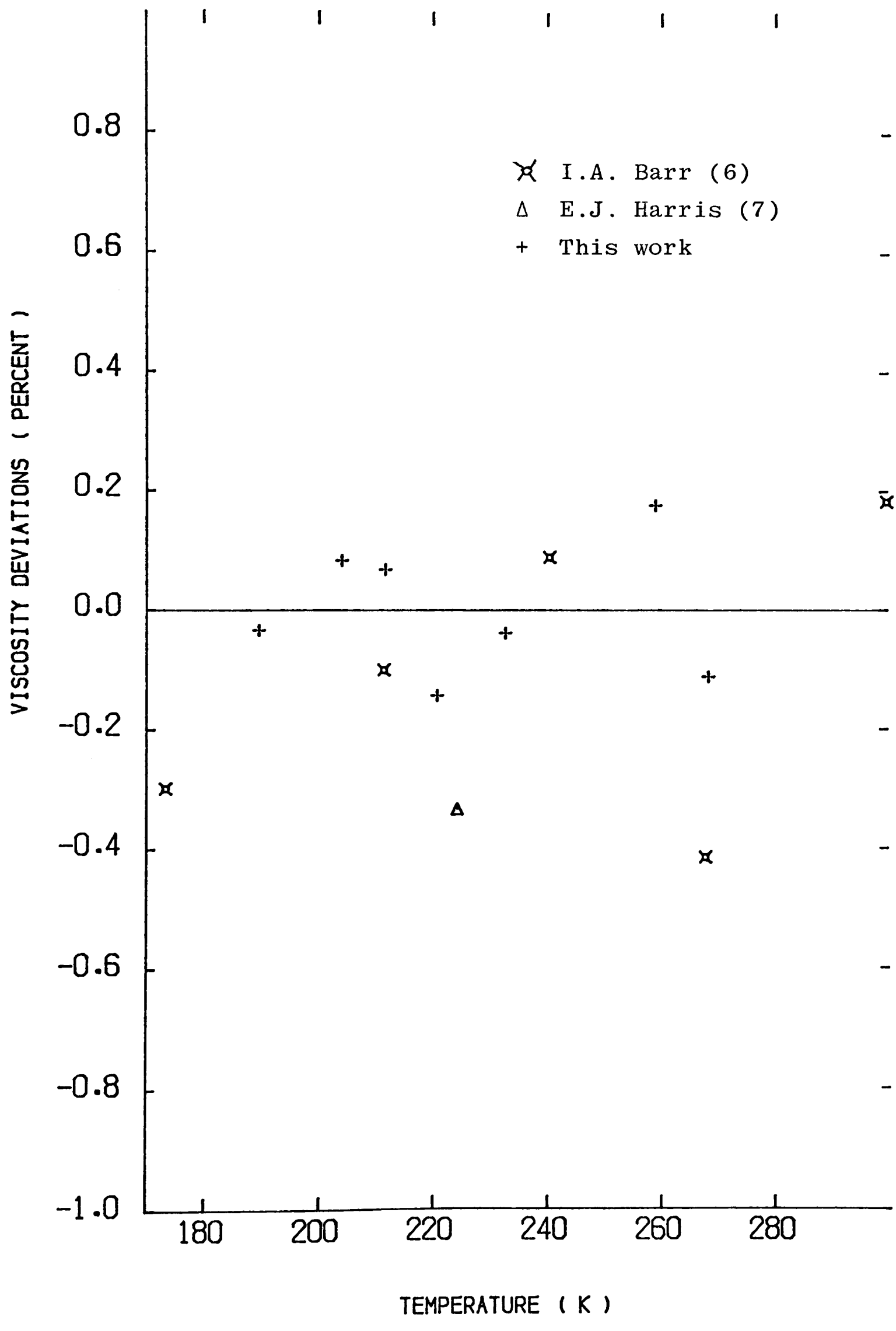
$$C = 35414.8 \ ;$$

$$D = 10.4320 \ :$$

over the temperature range 189 to 270K.

The percentage deviations of the available mixture viscosities from this smooth curve are plotted in Figure 5.1.

FIGURE 5.1


I.A. Barr (6)
E.J. Harris (7)
This work
VISCOSITY DEVIATIONS (PERCENT)
0.8
0.6
0.4
0.2
0.0
-0.2
-0.4
-0.6
-0.8
-1.0
180
200
220
240
260
280
TEMPERATURE (K)

As can be seen from this deviation plot the largest deviation is -0.4% which is certainly within the largest expected experimental error of one percent, and the largest deviation of the present work is 0.2%, again well within the expected limits.

f) Interaction Viscosities

As described in Chapter 2, theChapman-Enskog theory gives an expression for the coefficient of viscosity of a binary mixture, η_{mix}, in terms of the viscosities of the pure components, η_1 and η_2 and the interaction viscosity η_{12}. This interaction viscosity may be thought to be analogous to the expressions for a single component with the intermolecular potential as that between the unlike species. The molecular weight in this case is interpreted as twice the reduced mass:

$$M_{12} = \frac{2M_1M_2}{M_1+M_2} \qquad (5.25)$$

The interaction viscosity η_{12} does therefore contain the information which on inversion gives the potential describing the interactions between unlike molecules. We gave in Chapter 2 the expression for η_{mix} in terms of the pure component viscosities, the interaction viscosity and the ratio of the collision integrals for viscosity and diffusion (A_{12}^*) of the unlike potential energy function at the reduced temperature of the viscosity determination

$$A_{12}^{*} = \Omega_{12}^{(2,2)*}/\Omega_{12}^{(1,1)*} \qquad (5.26)$$

Although it is not possible to determine both A_{12}^{*} and η_{12} from measurements of η_{mix} as a function of composition, we can by assuming a form for A_{12}^{*} extract η_{12} easily as the solution to a quadratic equation (8).

In order to obtain A_{12}^{*} we must assume a form for the potential of the unlike interactions. Fortunately A_{12}^{*} is fairly insensitive to the detailed form of the potential function and therefore we used the BBMS potential which is a good representation of the pure components and used a value of the well depth as derived from the Fender-Halsey Rule (9)

$$\varepsilon_{12} = \frac{2\varepsilon_1 \cdot \varepsilon_2}{(\varepsilon_1 + \varepsilon_2)} \qquad (5.27)$$

The interaction viscosities were calculated and are shown in Table (5.6). All available values of η_{12} including this work, the results of Barr, Harris and Matthews (6,7) and also η_{12} extracted from the mixture viscosities measured by Kestin et al (11) (six measurements in the temperature range 298-773K) were fitted to the function (5.24). This fit was made over two temperature regions joined at 300K and the coefficients for the fit are:

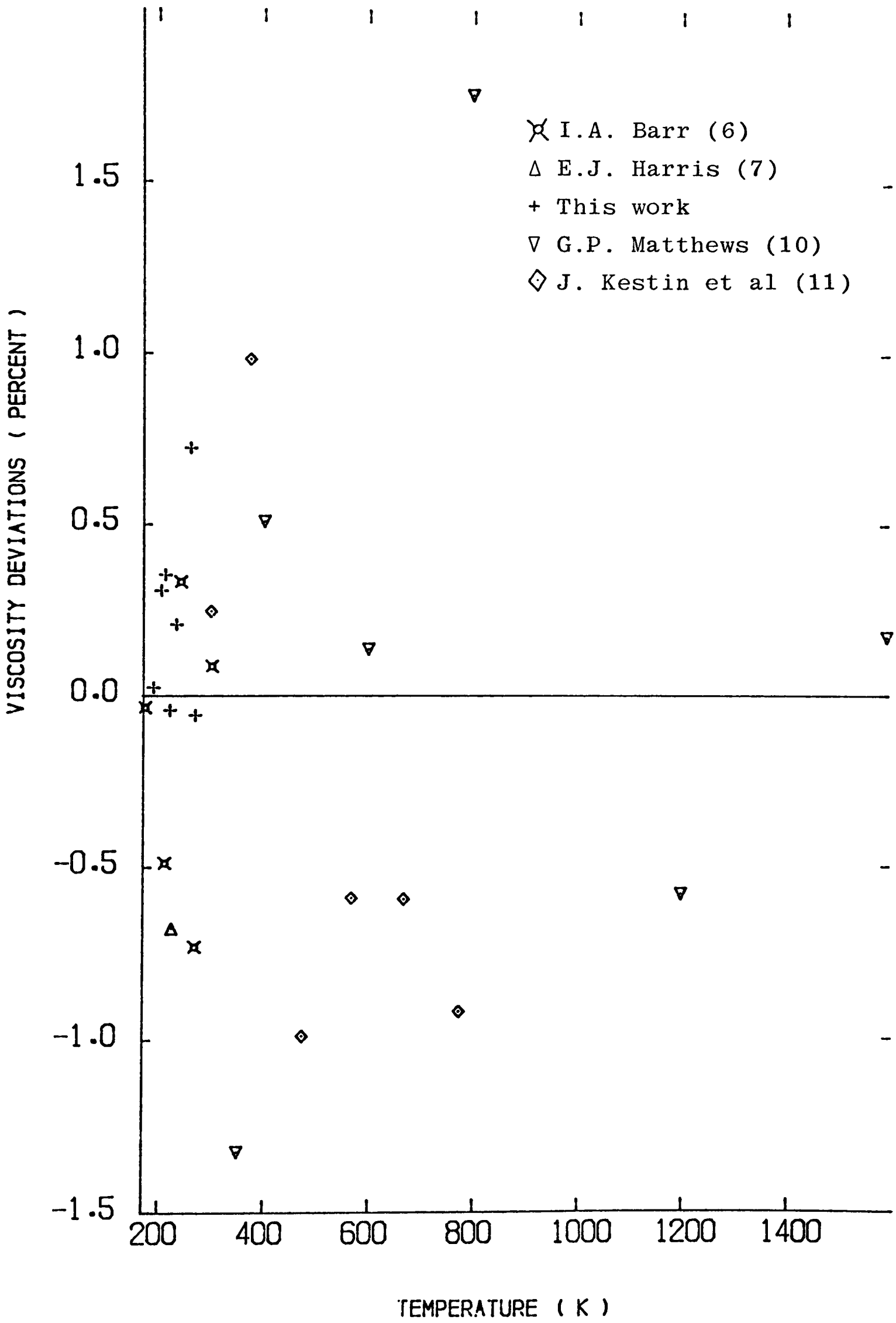
170 - 300K	300 - 1700K
A = -0.406517;	A = 0.673668 ;
B = -560.561 ;	B = 44.7584 ;
C = 28958.7 ;	C = -24101.38 ;
D = 9.229297 :	D = 1.64000 :

The deviations of all this data from the smooth curve are shown in Figure 5.2. The overall root mean square percentage deviation of all data points from the smooth curve is 0.67%. The maximum expected error in the interaction viscosity is about $\pm$ 1.5% for results determined on the low temperature viscometer used in the present work. On the high temperature viscometer due to the greater difficulty in temperature stabilisation as well as greater slip corrections the error is estimated to be $\pm$ 2%. All deviations are less than 2% and there are only two points with deviations of more than one percent which were measured on the high temperature viscometer. We can say therefore that the results obtained in this laboratory are consistent with those of Kestin et al. This data will, therefore,using the methods of inversion described in Chapter 4 be used to obtain the potential for the argon-xenon interaction in the next chapter.

TABLE 5.6 : Interaction viscosities for argon-xenon.

T	A^*	η_{Ar}	η_{Xe}	χ_{Xe}	η_{mix}	η_{12}
189.50	1.1098	151.7	148.0	0.5183	154.3	140.6
204.03	1.1101	162.4	158.8	0.5183	165.7	151.2
211.75	1.1095	167.9	164.7	0.5183	171.7	156.7
220.81	1.1088	174.4	171.6	0.5183	178.4	162.4
232.81	1.1079	182.9	180.8	0.5183	187.9	171.1
259.30	1.1061	201.0	201.2	0.5183	208.4	189.8
268.60	1.1056	207.2	208.4	0.5183	214.6	194.3

FIGURE 5.2


I.A. Barr (6)
E.J. Harris (7)
This work
G.P. Matthews (10)
J. Kestin et al (11)
VISCOSITY DEVIATIONS (PERCENT)
1.5
1.0
0.5
0.0
-0.5
-1.0
-1.5
200
400
600
800
1000
1200
1400
TEMPERATURE (K)

CHAPTER 6

THE APPLICATION OF THE INVERSION TECHNIQUES TO THE GASEOUS VISCOSITIES OF Ar-Xe AND Ar-N_2

A. An Intermolecular Potential for Ar-Xe

(i) Introduction

In the previous Chapter we described the determination of viscosities for argon-xenon mixtures. We obtained values for the interaction viscosity η_{12}, (which contains the information about the argon-xenon interaction alone) from the measured mixture viscosity which has the form:

$$[\eta_{mix}]_1 = \frac{1 + Z_\eta}{X_\eta + Y_\eta} \qquad (6.1)$$

where X_η, Y_η, and Z_η are complex functions of η_1, η_2 and η_{12} where the subscripts 1,2 refer to pure components and 12 refers to the mixed interaction. The full expressions for X_η, Y_η and Z_η have been given in Chapter 2 (see equation (2.92)).

The interaction viscosity η_{12} may be inverted by the viscosity inversion technique described in Chapter 4 to give the potential function for the argon-xenon interaction. The results of this inversion are described in the next section.

(ii) The inversion of Ar-Xe interaction viscosities

All available viscosity data for argon-xenon were analysed and values of the interaction viscosity η_{12} determined. These data were then fitted to the smooth curve

$$\ell n\eta = A\ \ell n\ T + B/T + C/T^2 + D \qquad (6.2)$$

over two temperature ranges 173-300K and 300K to 1600K. The coefficients for this curve were given in Chapter 5.

The inversion procedure was carried out as described in Chapter 4 for a number of estimates of the well depth parameter, ε, and the resulting potentials used to calculate the viscosity and second virial coefficients of argon-xenon which were then compared with experimental data. The value of ε which led to the best agreement with the experimental data was taken to be the best estimate of ε.

If experimental data are available over a wide temperature range and so only a short extrapolation is required at large separations, then it is possible to perform several iterations. In other cases, where the temperature range is more limited a single interation is desirable. The extrapolation used was a scaled BBMS (1) potential which was obtained for the argon-argon interaction and has a realistic shape. The initial approximate potentials used in order to calculate the

first approximation $G_o(T)$ to initiate the inversion procedure were the BBMS function and also the Lennard-Jones 12-6 function. The range of ε/k used as estimates for the well depth were in the region 160 to 210K which covered the spread of well depths suggested by previous workers.

The results of these inversions are shown in Table 6.1 for the BBMS initial approximate potential and in Table 6.2 for the 12-6 initial potential. Also in the tables are given the percentage deviations in the viscosity ($\%\Delta\eta$) as calculated from the function produced on inversion and ΔB the deviation (in $cm^3\ mol^{-1}$) of the second virial coefficients calculated from those given in the compilation of Dymond and Smith (2). Comparing our calculated second virial coefficients with experimental values caused considerable problems because there is large disagreement between the second virial coefficients of different workers. In addition the estimated maximum error in the data is quoted to be $\pm$ 6 cm^3 (2) which suggests that not too much reliance should be placed on the minimisations of their deviations. From Tables 6.1 and 6.2 it can be seen that the minimisation in the viscosity suggests a well depth of 185 $\pm$ 5K which corresponds in the cases of both starting potentials to deviations in the second virial coefficients of approximately 3 cm^3 which seems acceptable given the large experimental uncertainties.

TABLE 6.1 : Results for argon xenon using the BBMS potential as the initial approximate potential

ε/k(K)	σ(nm x 10)	$\%\Delta\eta$	$\Delta B(cm^3 mol^{-1})$
160	3.688	2.21	7.86
170	3.661	1.48	3.97
180	3.636	1.01	1.84
185	3.625	0.95	2.64
190	3.614	1.04	4.15
200	3.594	1.45	7.12
210	3.576	2.01	9.90

TABLE 6.2 : Results for argon xenon using the 12-6 potential as the initial approximate potential

ε/k(K)	σ(nm x 10)	$\%\Delta\eta$	$\Delta B(cm^3 mol^{-1})$
160	3.677	2.41	7.07
170	3.650	1.58	3.21
180	3.626	0.98	2.18
185	3.615	0.82	3.43
190	3.605	0.83	5.06
200	3.585	1.19	8.12
210	3.568	1.74	10.94

(iii) Discussion

(a) Binary diffusion coefficients

The interaction viscosities, η_{12}, may, to a first order approximation be directly related to the binary diffusion coefficient without direct reference to the potential function by means of the expression

$$[D_{12}]_1 = 6/5[\eta_{12}]_1 \frac{A_{12}^* RT}{\mu} \qquad (6.3)$$

where μ is the reduced mass, and A_{12}^* is the ratio of collision integrals $\Omega^{*(2,2)}/\Omega^{*(1,1)}$ and is only weakly dependent on the shape of the potential energy function. Equation (6.3) may be used either to calculate the diffusion coefficients when no experimental values are available, or, when such data exist, to provide a consistency check on the viscosity and diffusion measurements. However its value as a consistency check is somewhat limited by the accuracy of measured diffusion coefficients. These are difficult to measure to an accuracy of better than $\pm$ 5%. Furthermore the application of equation (6.3) does not give the true diffusion coefficients directly since equation (6.3) is only valid to first approximation. The analysis of the mixture viscosity to give the interaction viscosity was also not strictly valid since equation (6.1) is also a first order approximation. Mason and Marrero (3) have shown

that the second approximation to D can be represented by:

$$[D_{12}]_2 = [D_{12}]_1 (1 + \Delta_{12}) \qquad (6.4)$$

where Δ_{12} is a correction that involves the concentration dependence of D_{12}. This correction term has been described by Mason and Marrero in the form of a semi-empirical expression:

$$\Delta_{12} = \xi(6C_{12}^* - 5)^2 [ax_1/(1+cx_1)] \qquad (6.5)$$

ξ, a and c are constants, x_1 is the mole fraction of the heavier species and C_{12}^* is the ratio of two collision integrals

$$C_{12}^* = \Omega_{12}^{(1,2)*}/\Omega_{12}^{(1,1)*} \qquad (6.6)$$

which is insensitive to the form of the potential. Mason and Marrero (3) and Storvick and Mason (4) made a careful analysis of D_{12} and they concluded that for approximately equal masses $[D_{12}]_1$ is probably accurate to at least 2%. For all practical cases where the masses are unequal it is probably safe to regard $[D_{12}]_1$ as accurate to 5% and the second approximation $[D_{12}]_2$ as within 2%. It would be expected that in most cases they would be considerably better than this. Since the η_{12} values of this work obviously have implicit random errors

of an estimated 1% the composition dependence of the diffusion coefficient is lost and therefore it is acceptable to use the average η_{12} at each temperature, C_{12}^* and A_{12}^* were calculated from the BBMS potential function. We used the comparison equation (6.3) in order to calculate $[D_{12}]_1$ from the interaction viscosities, these were then corrected to $[D_{12}]_2$ using equations 6.4 and 6.5. The deviations of $[D_{12}]_2$ from the experimental values of Mason and Marrero (3), after taking into account all the approximations made in their evaluation, were within the expected uncertainty limits. In general, in view of the complications involved in this traditional form of analysis it seemed more reasonable to calculate $[D_{12}]_2$ directly from the potential function obtained on inversion of the interaction viscosities. The results of all these calculations are shown in Table 6.3, where it may be seen that in the region where the experimental errors are expected to be smallest i.e. below 500K $[D_{12}]_2$ calculated from the potential are much closer to the experimental values than are those calculated by equation 6.3. The rms deviation of the experimental measurements from the values calculated from the potential in the temperature range 170-1600K at 2.6% is well within the quoted experimental errors of Mason and Marrero which are for example over 5% above 1000K.

TABLE 6.3 : The binary diffusion coefficients for argon-xenon $[D_{12}]_{potl}$ are the values calculated from the potential fucntion proposed in this work. The units of D_{12} are 10^{-6} m^2 s^{-1}.

T	D_{12}exptl(3)	$[D_{12}]_1$	$[D_{12}]_2$	$[D_{12}]_{potl}$
173.29	3.9243	4.060	4.129	3.9702
189.50	4.6981	4.812	4.894	4.7323
204.03	5.4409	5.574	5.668	5.4667
211.48	5.8395	5.927	6.027	5.8618
211.75	5.8542	5.992	6.093	5.8763
220.81	6.3553	6.472	6.582	6.3736
224.34	6.5551	6.630	6.742	6.5721
232.81	7.0452	7.183	7.305	7.0593
240.56	7.5065	7.657	7.787	7.5184
259.30	8.6721	8.886	9.036	8.6797
267.98	9.2356	9.288	9.445	9.2415
268.60	9.2764	9.393	9.551	9.2822
299.95	11.436	11.520	11.715	11.437
350.00	15.264	15.439	15.700	15.254
400.00	19.536	20.265	20.608	19.502
600.00	40.737	41.838	42.546	40.375
797.9	67.643	69.675	70.854	66.464
1200.7	138.681	136.68	138.99	134.20
1597.4	228.004	223.6	227.4	218.30
Rms% dev.		2.2%	3.7%	1.4%

(b) Comparison of Potential Function

A number of potential energy functions have been proposed over recent years for the argon-xenon interaction. Parson et al (5), on the basis of molecular beam differential cross-section scattering data propose a function of the form

$$U(r)=\varepsilon[f(r^*) - (1+f(r^*))(\Gamma_o \exp\{-[(r^*-1)/\gamma_o]^2\} + \Gamma_1 \exp\{-[(r^*-r_1)/\gamma_1]^2\})] \quad (6.7)$$

where $r^* = r/r_m$, f(r) is the Lennard-Jones (30-6) function, $\gamma_o = 0.5$, $\gamma_1 = 0.25$, $r_1 = 1.45$, $\Gamma_o = 0.13$ and $\Gamma_1 = -0.06$. The remaining parameters are given in Table 6.4. Bobetic and Barker (6) using the same experimental data fitted the Barker and Pompe function (7)

$$U(r) = \varepsilon[U_o(r) + U_1(r)] \quad (6.8)$$

where

$$U_o(r) = \sum_{i=o}^{5} A_i(r-1)^i e^{\alpha(1-r)} - \sum_{i=o}^{2} \frac{C_{6+2i}}{r^{6+2i_{+\delta}}} \quad (6.9)$$

and

$$U_1(r) = [P(r-1)^4 + Q(r-1)^5]e^{\alpha'(1-r)} \text{ if } r > 1 \quad (6.10)$$

or $U_1(r) = 0$ if $r < 1$

P = 40, Q = 80, α' = 12.5. All other parameters apart from ε/k were arithmetical means of values proposed for the Ar-Ar and Xe-Xe interactions (8).

Schneider (9) on the basis of the electron gas model has proposed a numerical function. Maitland and Wakeham (10) inverted the limited transport coefficient data that were available in 1976 and fitted their resulting numerical potential to the $n(r^*)$-6 functional form described in Chapter 1 (equations 1.34 and 1.35). Another $n(r^*)$-6 potential was suggested by Van der Biesen et al. (11) who based their potential on their measurements of total cross-section data for argon-xenon collisions. A different functional form, namely a (12-6-8) potential function (Hanley-Klein (12)):

$$U^*(r^*) = [1/(12-6)][6+2\gamma](1/r^*) - [1/(12-6)]$$

$$x\ [12-\gamma(12-8)](1/r^*)^6 - \gamma/(r^*)^8 \qquad (6.11)$$

where $U^* = U/\varepsilon$, $r^* = r/r_m$, for this potential γ = 2.5. was proposed by Asora et al (13) who obtained the potential parameters by a fit to viscosity and second virial coefficient data.

The deviations of the properties calculated using these six potential functions from the recommended experimental values are given in Table 6.4 along with the corresponding values from the present work. Second

virial coefficent deviations are based on the data given in the compilation of Dymond and Smith (2), and viscosity deviations are from the smooth curves of the present work. Total cross-section data also given in Table 6.4 are based on data calculated from the potential of van den Biesen (11), which was designed specifically to accurately reproduce them. It was not possible to calculate reliable total cross-sections for the Schneider function due to its numerical form. Of the most recent potential functions in Table 6.4, those of Bobetic and Barker and van den Biesen et al are very similar in form and characteristic parameters to each other as well as to the potential function from this work. The Asora potential, on the other hand, has a much deeper well. This potential seems to display the dangers of force fitting experimental data to an unrealistic form of the potential function. Although it fits well the data from which it was derived, namely viscosity and second virial coefficients, it does not adequately reproduce the total cross-sections. Furthermore, since the well depth of the Asora potential (212.5K) is 7% deeper than the prediction of the geometric mean rule, a rule which usually gives well depths which are too deep, we feel that this potential is not realistic for Ar-Xe. The fact that the potentials of Bobetic and Barker, van den Biesen et al. and that from this work are all of extremely similar shape leads us to believe that a function close to the true potential

of the system has been achieved; the potential from this work seems to be marginally superior in predicting the whole range of properties. The potential from this work is tabulated in Table 6.5. The figure 6.1 shows several of the most recent potentials for argon-xenon along with deviation plots. It is clearly seen from this that the potential in the present work is in very good agreement with those of Bobetic and Barker and van den Biesen et al.

(c) Combining Rules

Many rules have been suggested by which the characteristic parameters of potentials corresponding to mixed interactions may be calculated from those of the like interactions. The most straightforward of these are Berthelot's geometric mean rule (13) for ε_{12}

$$\varepsilon_{12} = (\varepsilon_{11} \cdot \varepsilon_{22})^{\frac{1}{2}} \qquad (6.12)$$

and the Lorentz arithmetic rules for σ_{12},

$$\sigma_{12} = \frac{\sigma_{11} + \sigma_{22}}{2} \qquad (6.13)$$

The geometric mean rule is now generally regarded as inadequate for most purposes (14,15). Another set of rules have been proposed by Hudson and McCoubrey (14) which are based on the London dispersion formula

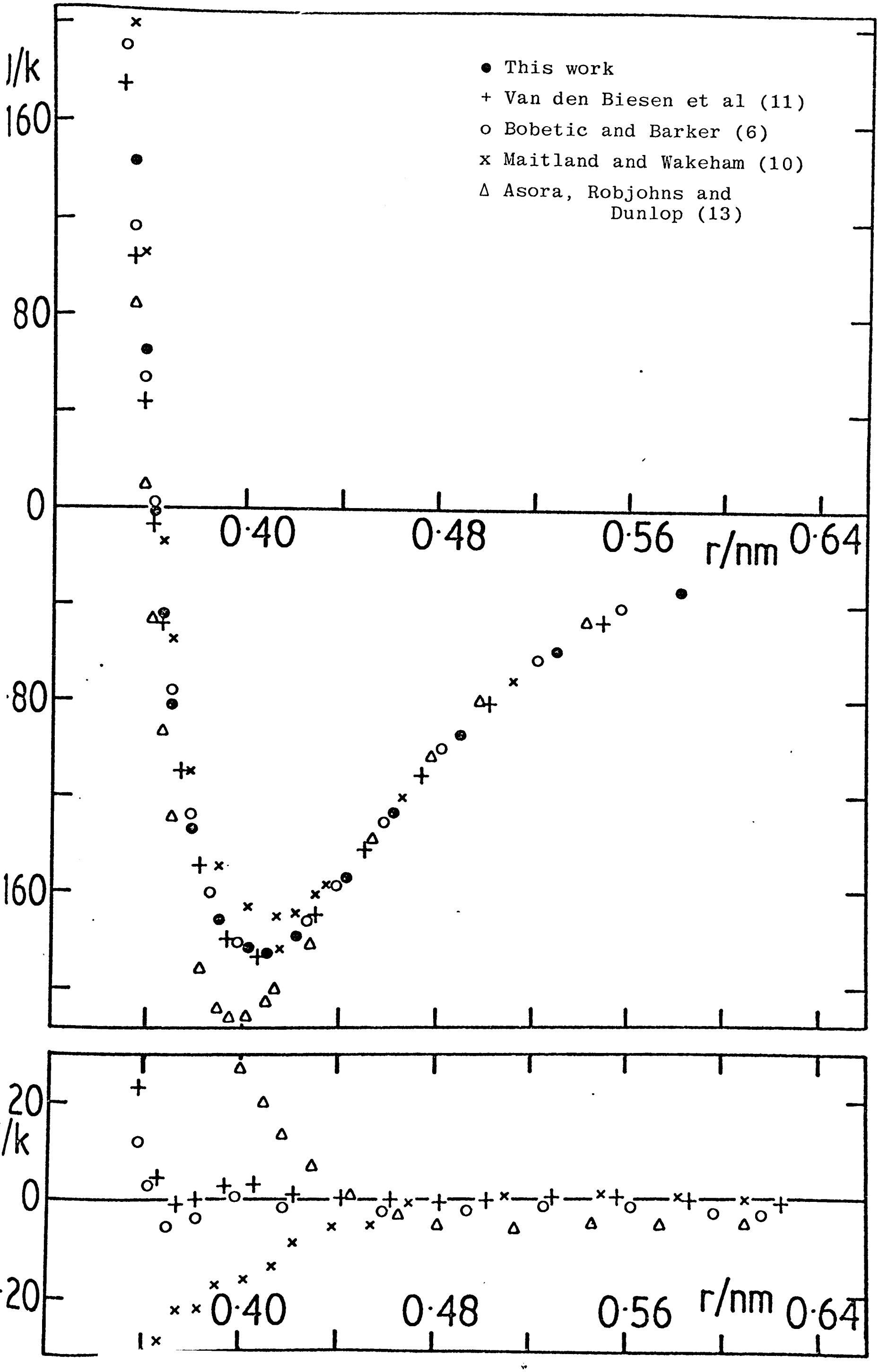

I/k
160
80
0
0·40
0·48
0·56
r/nm
0·64
● This work
+ Van den Biesen et al (11)
o Bobetic and Barker (6)
x Maitland and Wakeham (10)
Δ Asora, Robjohns and Dunlop (13)
80
160
20
I/k
0
-20
0·40
0·48
0·56
r/nm
0·64

TABLE 6.4 Comparison of potential energy functions

Potential	Type	Principal Source	ε/k K	σ nm	r_m nm	ΔB cm^3	%$\Delta\eta$	% dev in extrema of total cross sections	rms total deviation
This work	Numerical	Viscosity inversion	185.0	0.3625	0.409	2.6	0.8	2.3	5.32
Bobetic & Barker (6)	Barker-Pompe (7)	Molecular Beam Scattering	185.0	0.3619	0.40634	2.468	1.637	2.5	10.5
van den Biesen et al (11)	$n(r^*)$-6	Total cross section	187.4	0.3625	0.406	3.984	1.721	-	-
Asora et al (13)	n-m-6(12)	Fitted properties	212.5	0.3558	0.3945	1.750	0.728	13.0	53.8
Parson et al (5)	Morse-van der Waals	Differential cross sections	189.8	-	0.410	20.00	14.502	15.0	14.74
Maitland & Wakeham (10)	$n(r^*)$-6	Viscosity Diffusion	170.0	0.3651	0.4134	3.577	1.940	13.0	15.5
Schneider (9)	Numerical	Electron Gas Model	177.5	0.355	0.392	23.75	8.45	-	-

TABLE 6.5 : The potential function for argon-xenon interactions obtained by the inversion of viscosity data. Extrapolations were used for r < 0.334 and r > 0.455 nm.

r/nm	U/k/K
0.3263	1276.0
0.3302	1032.3
0.3422	481.8
0.3502	236.4
0.3542	143.1
0.3582	66.6
0.3621	4.9
0.3661	-43.9
0.3701	-82.0
0.3741	-111.4
0.3781	-133.6
0.3861	-162.4
0.3940	-177.3
0.4020	-183.6
0.4100	-185.0
0.4180	-181.7
0.4300	-169.8
0.4459	-149.3
0.4658	-122.5
0.4858	-98.9
0.5097	-75.1
0.5500	-47.1
0.6014	-28.0
0.6692	-14.1
0.7210	-8.3

$$\varepsilon_{12} = \frac{\sigma_1^3 \sigma_2^3}{\sigma_{12}^6} (\varepsilon_1 \cdot \varepsilon_2)^{\frac{1}{2}} \qquad (6.14)$$

$$\varepsilon_{12} = \frac{2(I_1 \cdot I_2)^{\frac{1}{2}}}{(I_1 + I_2)} \cdot \frac{\sigma_1^3 \sigma_2^3}{\sigma_{12}^6} (\varepsilon_1 \cdot \varepsilon_2)^{\frac{1}{2}} \qquad (6.15)$$

Equation (6.15) where I_1 and I_2 are ionization potentials is the complete form of equation (6.14). Two further combining rules have been proposed by Fender and Halsey (16) which are based on the Kirkwood-Muller expression for C_6 (17,18)

$$\varepsilon_{12} = \frac{2\varepsilon_1 \cdot \varepsilon_2}{(\varepsilon_1 + \varepsilon_2)} \qquad (6.16)$$

$$\varepsilon_{12} = \frac{2\varepsilon_1 \varepsilon_2}{\chi_1 \chi_2} \left[\frac{\varepsilon_1 \sigma_1^6}{\chi_2^2} + \frac{\varepsilon_2 \sigma_2^6}{\chi_2^2} \right]^{-1} \frac{2\sigma_1 \sigma_2}{\sigma_1 + \sigma_2}^6 \qquad (6.17)$$

where χ = magnetic susceptibility.

Equation (6.17) is the complete form of equation (6.16). It has been found previously that the best predictions tend to come from the Fender-Halsey equation (6.16) (19) the other rules tending to give values close to that of the unsatisfactory geometric mean. None of the above rules, however, was found to give an adequate description of the interaction of He with the

other noble gases. In predicting the well depth ε_{12} using the various rules we used the BBMS well depth for argon - 145.5K. The well depth for xenon is not as well defined as that of argon and in this work we used the value of 281K which is due to Barker et al (20). The predictions of the various rules are shown in Table 6.6. In general they all appear to be too high compared with the most recent potentials, however the Fender-Halsey rule equation (6.16) does reasonably well coming within 2½% of the value for this work.

(iv) Conclusion

In conclusion therefore we have obtained a potential function for argon-xenon on inversion of viscosity data over a wide temperature range which is capable of reproducing a wide range of properties and which is also in good agreement with the work of other workers who derived their potentials from molecular beam scattering data. We had hoped that the results would provide a good test of the combining rules, however, in this respect the results do not show any rule to be completely satisfactory, although the simple Fender-Halsey rule gives an acceptable prediction.

TABLE 6.6 Values of the well depth predicted by various combining rules

Combining Rule	Equation	Prediction for well depth ε/k (K)
Hudson and McCoubrey	(6.14)	196.9
Hudson and McCoubrey	(6.15)	192.5
Fender and Halsey	(6.16)	189.1
Fender and Halsey	(6.17)	196.8
Geometric Mean	(6.12)	200.1

B. A Potential Function for Argon Nitrogen Interactions

(i) Introduction

The inversion methods developed in Chapter 4 have been applied with considerable success to the transport properties and second virial coefficients of monatomic species. This was shown in the first half of this Chapter in their application to the interaction viscosities of argon-xenon mixtures. The next logical step in the development of these inversion methods is their application to anisotropic interactions which has been of considerable interest in the present work (21) and which will be described in Chapter 7. In order to provide data suitable for these studies we have recently (22) measured the viscosities for argon-nitrogen over a wide temperature range 119-1600K. In the second half of this Chapter therefore we will describe the calculation of interaction viscosities for argon-nitrogen from the mixture viscosities and the application of the inversion methods to these η_{12} values in order to obtain an effective isotropic potential for the argon-nitrogen interaction.

(ii) The interaction viscosities

The mixture viscosities for argon-nitrogen mixtures of mole fraction ranging from 25-75% argon have been determined by Matthews (23) at high temperature and recently by Schofield (24) at low temperatures from

120K to 298K. It was proposed therefore to calculate the interaction viscosities from their work and compare their values with those determined from mixture viscosity determinations recorded by other workers.

The only measurements recorded in the literature are by Kestin and co-workers (25,26). They recorded mixture viscosities for four compositions over the temperature range 293-767K. Their data were analysed to give the interaction viscosities in the same way as for the Ar-Xe data already described. The resulting interaction viscosities from the work of Kestin along with the results of Matthews and Schofield were fitted to a smooth curve of the form of equation 6.2 over the two temperature ranges 119-300K and 300-1600K. The coefficients for this curve are shown in Table 6.7 and the interaction viscosities calculated from the various sources are shown in Table 6.8. The percentage deviations of the viscosities calculated from the smooth curve from the data of Table 6.8 were calculated and the deviation plot is shown in Figure 6.2. The rms percentage deviation of all the points from the curve is 0.5% with the largest deviation of any single point being around 1%. These deviations are well within the expected error limits given the uncertainties involved in the calculation of the interaction viscosities. The results then constitute a consistent set of results over the temperature range 120-1600K.

TABLE 6.7 Coefficients of the curve

$$\ell n\eta = A\ \ell n\ T + B/T + C/T^2 + D$$

for Argon-Nitrogen interaction viscosities

	A	B	C	D
120-300K	1.380227	237.3904	- 12696.7	- 3.21158
300-1600K	0.707301	101.2348	- 23859.5	1.201747

TABLE 6.8 Interaction Viscosities for argon-nitrogen

Temperature	Source	η_{12} (10^{-7} kgm^{-1} s^{-1})
118.9	(1)	88.40
151.14	(1)	113.30
203.94	(1)	146.30
240.18	(1)	167.90
293.00	(4)	197.73
293.18	(1)	199.70
298.00	(3)	200.52
298.18	(1)	202.00
303.00	(4)	203.40
367.00	(3)	237.39
400.00	(2)	257.20
467.00	(3)	285.21
571.00	(3)	327.32
600.00	(2)	343.20
673.00	(3)	366.15
767.00	(3)	400.69
797.9	(2)	411.30
1200.7	(2)	531.90
1597.4	(2)	650.10

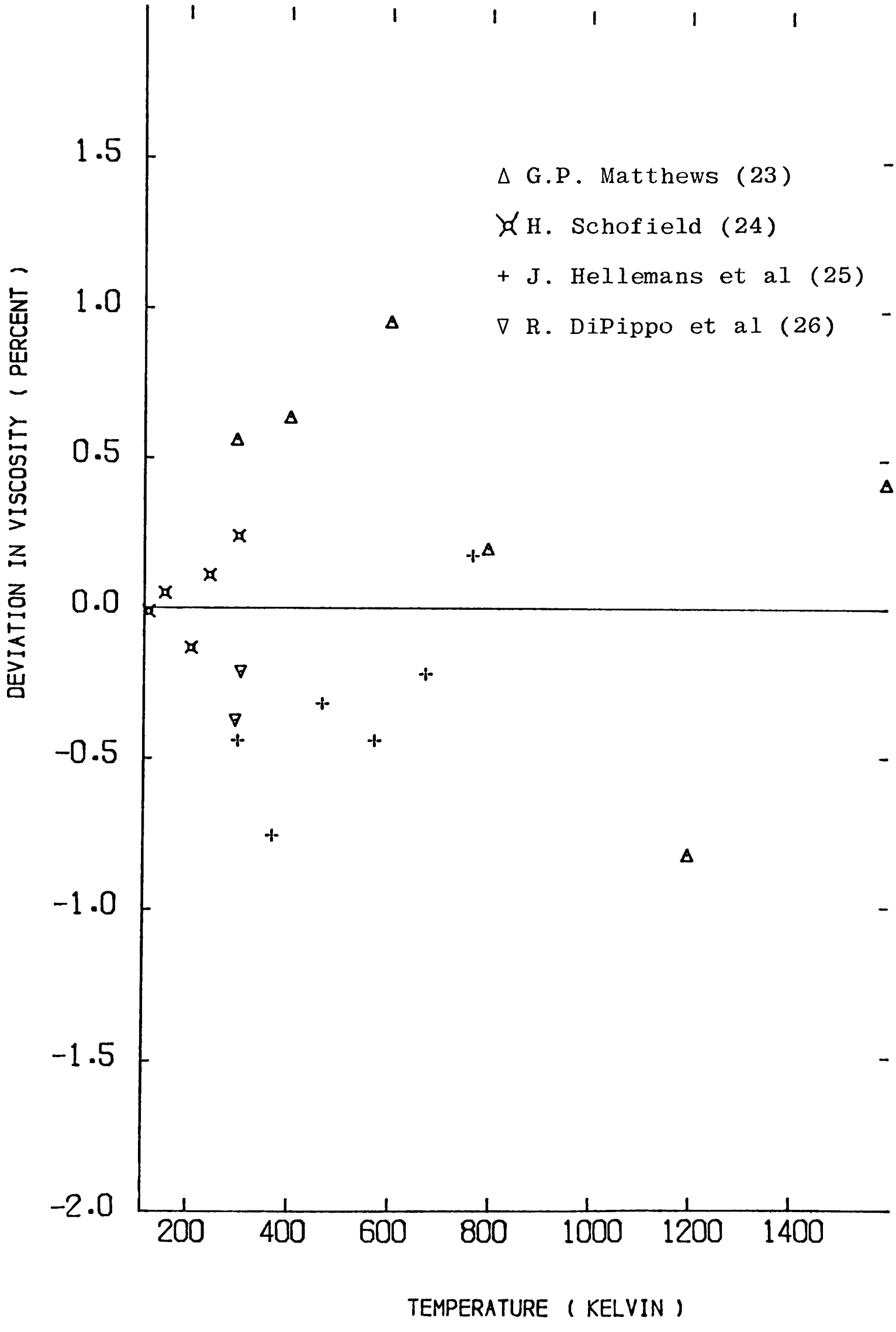
(1) H. Schofield (24)

(2) G.P. Matthews (23)

(3) J.H. Hellemans et al. (25)

(4) R. DiPippo et al. (26)

FIGURE 6.2 : Deviations in interactive viscosities (η_{12}) for argon-nitrogen.



(iii) Results of inversion

The interaction viscosities derived from the smooth curve described above were inverted using two starting potentials (used to calculate the initial approximate $G_o(T)$). These two potentials were the BBMS function (1) and the Lennard-Jones 12-6 function. In the case of argon-nitrogen the form of the extrapolation was found to be very important. This is because the lowest temperature (119K) is relatively high compared to the well depth and so the extrapolation begins relatively close to the bottom of the potential well, where $r/\sigma \approx 1.25$. Two forms of extrapolation were used initially, namely scaled BBMS and 12-6 functions. The results of these inversions, as will be seen later, suggested a more suitable form which was adopted for the final series of inversion.

The basic procedure adopted for the inversions was the same as that used previously for argon-xenon. A series of estimates for the well depth parameter ε were tried. After each inversion the deviations of the viscosities and second virial coefficients from the experimental values were calculated. The results of these inversions are shown in Tables 6.9 and 6.10.

As can be seen from Tables 6.9 and 6.10 the minimisation of the deviation in the viscosities suggest a fairly consistent value for the well depth of 122.5 $\pm$ 5K.

TABLE 6.9 Results for the inversion of argon-nitrogen data (I)

ε/k(K)	σ(x10nm)	%Δη	ΔB	I.A.P.*	Extrap
115.0	3.466	0.860	2.50	12-6	12-6
117.5	3.457	0.780	3.54	12-6	12-6
120.0	3.449	0.721	5.13	12-6	12-6
122.5	3.440	0.729	5.33	12-6	12-6
125.0	3.432	0.812	7.64	12-6	12-6
130.0	3.418	1.098	10.29	12-6	12-6
140.0	3.391	1.787	15.23	12-6	12-6
115.0	3.477	0.779	1.84	BBMS	12-6
117.5	3.468	0.738	2.75	BBMS	12-6
120.0	3.458	0.740	4.18	BBMS	12-6
122.5	3.450	0.806	5.37	BBMS	12-6
125.0	3.442	0.942	6.68	BBMS	12-6
130.0	3.427	1.251	9.23	BBMS	12-6
140.0	3.400	1.908	14.05	BBMS	12-6

*I.A.P. refers to the initial approximate potential used to calculate $G_o(T)$.

TABLE 6.10 Results for the inversion of argon-nitrogen data (II)

ε/k(K)	σ (x10nm)	$\%\Delta\eta$	$\Delta B(cm^3mol^{-1})$	I.A.P.*	Extrap.
115.0	3.466	1.115	11.56	12-6	BBMS
120.0	3.449	0.826	8.53	12-6	BBMS
122.5	3.440	0.740	7.43	12-6	BBMS
125.0	3.432	0.718	6.27	12-6	BBMS
127.5	3.425	0.762	4.62	12-6	BBMS
130.0	3.418	0.873	3.58	12-6	BBMS
140.0	3.391	1.563	2.99	12-6	BBMS
115.0	3.477	1.036	12.41	BBMS	BBMS
120.0	3.458	0.829	9.46	BBMS	BBMS
122.5	3.450	0.796	8.36	BBMS	BBMS
125.0	3.442	0.832	7.19	BBMS	BBMS
127.5	3.434	0.929	5.61	BBMS	BBMS
130.0	3.427	1.065	4.53	BBMS	BBMS
140.0	3.400	1.717	2.26	BBMS	BBMS

*I.A.P. refers to the initial approximate potential used to calculate $G_o(T)$.

TABLE 6.11 Results for the inversion of argon-nitrogen data using a linear combination of 12-6 and BBMS extrapolations

ε/k(K)	σ(x10nm)	$\Delta\eta$(%)	$\Delta B(cm^3mol^{-1})$	I.A.P.
117.5	3.457	0.875	3.93	12-6
120.0	3.449	0.770	2.27	12-6
122.5	3.440	0.735	1.45	12-6
125.0	3.432	0.775	1.42	12-6
127.5	3.425	0.864	2.52	12-6
117.5	3.468	0.858	4.72	BBMS
120.0	3.458	0.812	3.08	BBMS
122.5	3.450	0.832	2.05	BBMS
125.0	3.442	0.919	1.28	BBMS
127.5	3.434	1.039	1.67	BBMS

The deviations of the second virial coefficients however can be seen quite easily to depend on the extrapolation used. Although the large experimental uncertainties in the second virial coefficient data of $\pm$ 3-5 cm^3 $mole^{-1}$ make evaluation of these results difficult it nevertheless seems as though the true form for the long range extrapolation lies between those resulting from the BBMS and 12-6 functions. It should be noted that the short-range extrapolation has little effect on the second virial coefficients. A second series of inversions were therefore performed using this linear combination of BBMS and 12-6 extrapolations. The results for these are shown in Table 6.11.

As can be seen from Table 6.11 the deviations in the second virial coefficients are minimised very close to the minimisation in the viscosity data. All the data seem to be consistent with the values for the well depth parameter given above i.e. 122.5 $\pm$ 5K, this corresponds to a value σ as 0.344 $\pm$ 0.001 nm.

(iv) Discussion

(a) The diffusion coefficients

The diffusion coefficients to a first and second approximation $[D_{12}]_1$ and $[D_{12}]_2$ as defined by equations (6.3) and (6.4) were calculated and were compared with the experimental values of Marrero and Mason (27) for the

temperature range 244-1600K. In addition the self diffusion coefficients were also calculated directly from the potential function derived on inversion. The results for all these calculations are shown in Table 6.12. The experimental uncertainties in D_{12} are quite large; they are given by Marrero and Mason as:

$\pm$ 2% at 300K

$\pm$ 3% at 500K

$\pm$ 7% at 1000K.

The results of the calculation from the potential over the temperature range 244-2600K give a rms percentage deviation in D_{12} as 2.62% with deviations of around 1.5% for the temperature range 250-850K and up to 5% for the range 850-1600K. These are then entirely consistent with the experimental results given the experimental uncertainties.

(b) Comparison with other workers

The potentials which have been proposed for the argon-nitrogen differ widely in their parameters for well depth and collision diameter. Both isotropic and anisotropic potentials have been proposed although the latter appear, in general to be of a rather crude form at the present time. In our investigation we have of course assumed that the properties for the argon-nitrogen system may be represented by an isotropic potential, however, we have obtained this potential by inversion

TABLE 6.12 Results for argon-nitrogen self diffusion coefficients

T(K)	A_{12}^*	C_{12}^*	$[D_{12}]_1$	$[D_{12}]_2$	$[D_{12}]_{POTL}$	$[D_{12}]_{EXPT}$ (27)
293.2	1.1035	0.8947	0.201	0.202	0.191	0.190
298.18	1.1026	0.8957	0.207	0.207	0.197	0.196
400.0	1.1078	0.9100	0.355	0.365	0.331	0.327
600.0	1.1178	0.9231	0.718	0.721	0.669	0.666
797.9	1.1268	0.9279	1.153	1.158	1.088	1.097
1200.7	1.1411	0.9300	2.272	2.283	2.174	2.246
1597.4	1.1519	0.9290	3.729	3.746	3.526	3.703
rms % deviation :			5.32	5.60	2.36	

methods alone whereas the potentials proposed in the literature do unfortunately follow the unsatisfactory approach of curve fitting to a non realistic potential form such as the Lennard Jones 12-6 function. Our potential would therefore be expected to perform much more satisfactorily for a wide range of properties than potentials obtained by curve fitting. The potential we obtain here also has important consequences after taking into account the recent results obtained by inverting the properties calculated from an anisotropic potential (21). These results which are discussed in Chapter 7 suggest that the transport properties and second virial coefficients for an anisotropic system may be represented by a single isotropic potential function.

Most of the previous functions proposed for the argon-nitrogen system have been derived from molecular beam scattering data. There are also calculations available based on the electron gas model by Kim and co-workers (28,29). These electron gas model calculations propose anisotropic potential functions, however, their functional form make it difficult to calculate transport properties in order to compare the results of their potential with experiment.

The isotropic potentials proposed for argon-nitrogen based on molecular beam scattering data depend rather unfortunately on the analysis of scattering data in terms of a Lennard Jones n-6 type analytical form. Such an analysis although leading in some cases to

potentials with well depths very close to that obtained in the present work nevertheless leads to transport properties and second virial coefficients which differ considerably from the latest experimental values. A good example of this is provided by the potentials proposed on the basis of differential cross section data by Tully and Lee (30). They suggested three potentials which fitted their differential cross-section data all with a value for r_m of 0.390 $\pm$ 0.02 nm. The results are shown in Table 6.13 for the deviation of viscosity coefficients and second virial coefficients.

Similar deviations result from calculations based on the analysis of Anlauf, Bickes and Bernstein (31) of scattering data in the rainbow region. They tried LJ(n-6) potentials where ($8 < n < 24$) and in fact could not fit their data very successfully. The best fit with a 20-6 potential and a well depth of 119.5K produces the deviations shown in Table 6.13 which are very large. Other workers (32,33) using differential cross-section scattering data obtained well depths from the analysis of their results close to those of the present work. Cavallini et al obtained a value of 124 $\pm$ 11 and Grosser et al. obtained a value of 118 $\pm$ 11, however Cavallini do not give a value for σ or r_m so it was not possible to calculate any properties from their potential and the value of r_m proposed by Grosser and Kalas is obviously very inaccurate since they give a value of 6 $\mathring{A}$.

Anistropic potentials have been proposed by several workers. These are in general, however, a little crude in nature. Pattengill et al (33) has suggested a model of the following form:

$$V(r,\theta) = (C_{12}/r^{12})[1 + b_2P_2(\cos\theta)] -$$

$$(C_6/r^6)\ [1 + a_2P_2(\cos\theta)] \qquad (6.18)$$

where r is the Ar-N_2 centre of mass separation, θ is the angle between the line joining centre of mass and N_2 axis. $P_2(x)$ is the second Legendre polynomial. $C_{12} = 4\varepsilon\sigma^{12}$ and $C_6 = 4\varepsilon\sigma^6$. The well depth is given as 119.5K which is based on the work of Anlauf et al. (31) and the value for the collision diameter 0.35 nm is also from the molecular beam scattering data of Aulauf et al. as well as from transport properties. a_2 which is the attractive anisotropy parameter was based on the polarizability parameter of N_2 (34). The repulsive anisotropy parameter, however, was not known with any certainty and an estimate was made using a dumb bell model (35). The values of a_2 and b_2 were:

$$a_2 = 0.13 \text{ and } b_2 = 0.5\ (^{+0.2}_{-0.1})$$

This potential of Pattengill et al was used to calculate the second virial coefficients and the viscosities were also calculated by means of the Mason, Monchick

approximation. These methods for calculating the properties from an anisotropic potential are discussed in detail in Chapter 7.

The deviations in the viscosity coefficient are found to be only weakly dependent on the value of b_2. The two extreme values where b_2 = 0.4 and 0.7 are given in Table 6.12. The second virial coefficients do depend to a larger extent on b_2 as shown in the Table. This potential performs better than the isotropic potentials already considered with the exception of that from the present work, however it still has a non-realistic form as shown by the large deviations in the second virial coefficient which range from 15-21 cm^3 $mole^{-1}$.

Another anistropic potential based on a modification of the electron gas model has been suggested recently by Lee and Kim (29). Theyexpressed their calculations in the form of a Legendre series:

$$V(R,\cos\theta) = V_o(R)[1 + A_2(R)P_2(\cos\theta) + A_4(R)P_4(\cos\theta)] \qquad (6.19)$$

where the coefficients of the Legendre polynomials $A_2(R)$ and $A_4(R)$ are functions of separation. The form of the potential makes calculation of the transport properties difficult and so only the deviations of the second virial coefficients are shown in Table 6.13. The overall rms deviation was 11.9 cm^3 although this potential was particularly good in reproducing the second

virial coefficients for the temperatures above 150K where the average deviation was only 2 cm^3. The low temperature deviations were, however, quite high being up to 37 cm^3 at 90K.

Lee and Kim compared the spherical average of their potential with the potentials devised from differential cross-section scattering data and found that this spherical average has a similar well depth to that of Tully and Lee (30) for example. This however is not a true comparison as the Tully and Lee parameter is an effective spherical potential and not the true spherical potential. We obtain this result ourselves in the inversion of properties calculated from an anisotropic potential. The potential we obtained on inversion (discussed in Chapter 7) was <u>not</u> the spherical average of the anisotropic potential. This makes it difficult to compare any spherical potential proposed for argon-nitrogen with any anistropic model other than by calculation of the properties from each potential.

In principle, the most detailed information on the argon-nitrogen system is contained in the results of the observation of the infra-red spectrum of the bound dimer as measured by Henderson and Ewing (36). The spectrum is illustrated in Figure 6.3. The $Q_1(J)$ and $S_1(J)$ marks on the spectrum indicate vibration-rotation transitions frequencies of the free N_2 molecule. Vibrational transitions involving the bending mode of the $Ar-N_2$

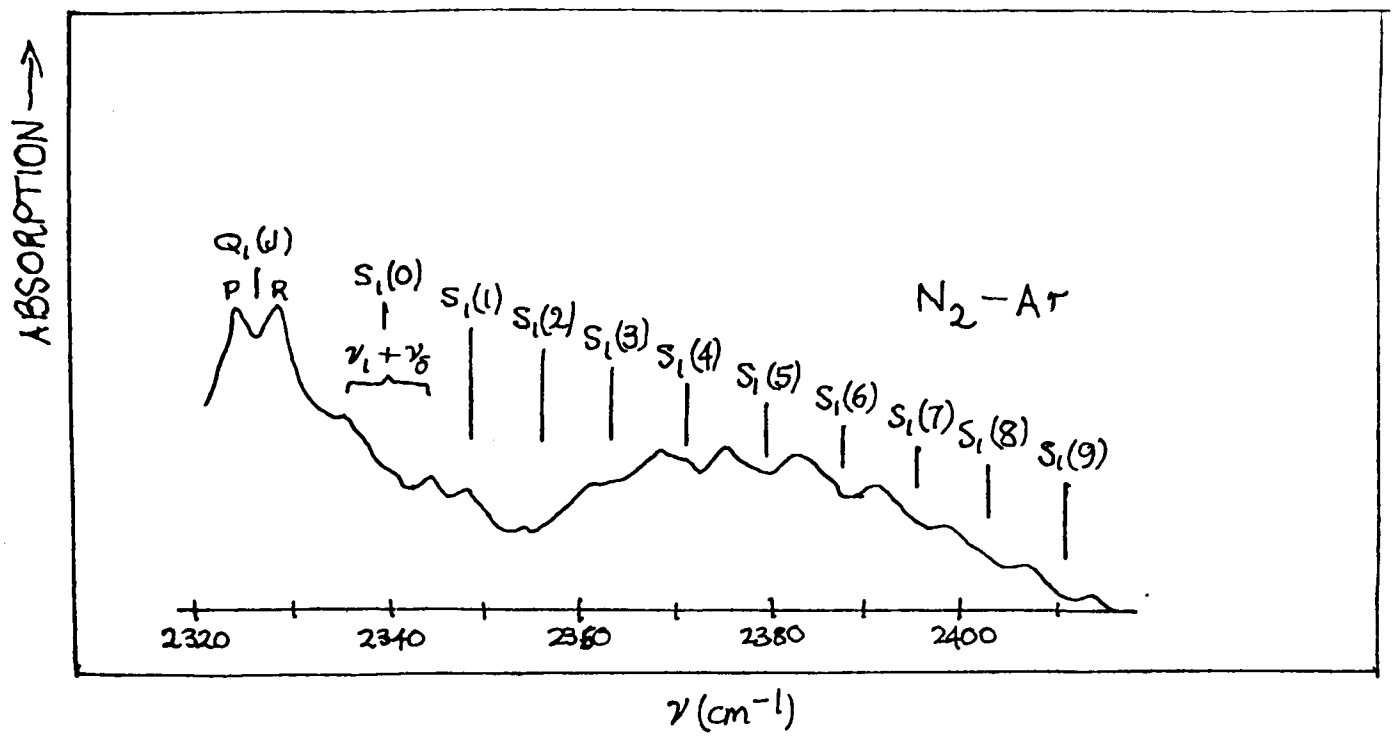


FIGURE 6.3 : Infra-red spectrum of N_2-Ar in nitrogen and argon at a pressure near 100k Nm^{-2} at 87K.

dimer are indicated by $\nu_1 + \nu_\delta$. Since these features of the Ar-N_2 dimer and the freely rotating N_2 molecule do not match up this suggests that the rotation of the N_2 molecule in the Ar-N_2 dimer is hindered. Ewing (37) has analysed the spectrum, the rotational envelope of the P and R branches being consistent with a value of r_m = 0.39 $\pm$ 0.02 nm which is in good agreement with that from this work. The analysis of the spectrum is extremely complex and Ewing used a trial analytical potential which has the rather simple form:

$$U(r,\theta) = \varepsilon \left[\left(\frac{r_m}{r}\right)^{12} - 2\left(\frac{r_m}{r}\right)^{6} \right] + \frac{V_o}{2}(\cos 2\theta) \qquad (6.20)$$

He obtained ε/k = 112K from the geometric mean of Hrischfelder, Curtiss and Bird's well depth for $(N_2)_2$ (38) and Tonaka and Yoshino's spectroscopic well depth for Ar_2 (39). With this value of ε/k and r_m = 0.39 nm, the spectrum may be interpreted by using a value of V_o = 29K with a "T" shaped equilibrium position at = 90^o. This "T" shape is the same result as that obtained by Lee and Kim with the extended electron gas model. Unfortunately the long range behaviour of this function which goes positive at various angles means that the evaluation of properties from it is impossible to any degree of certainty. The second virial coefficients will be fairly unaffected by this long range behaviour but the transport property collision integrals cannot be calculated and consequently only the second virial coefficient deviation being quite large at about 21 cm^3

TABLE 6.13 Comparison of various potentials proposed for argon-nitrogen

Potential Type	Author	ε/k(K)	σ(x10nm)	r_m(x10nm)	$\Delta\eta$(%)	ΔB $cm^3 mole^{-1}$
20-6 (30)	Tully & Lee	139	3.5±0.1	3.9±0.3	8.00	4.28
12-6 (30)	" "	136	3.5±0.1	3.9±0.3	7.39	40.71
8-6 (30)	" "	138	3.5±0.1	3.9±0.3	9.19	115.6
20-6 (31)	Anlauf et al	119.5±4	3.58	3.9	8.33	21.45
This work*		125.5	3.44±0.01		0.74	1.45
12-6 anisotropic (33)	Pattengill et al	See Text	b_2 = 0.4		2.15	15.6
			b_2 = 0.7		2.48	21.7
Numerical (29)	Kim & Lee	See Text			-	11.9
12-6 anistropic (37)	Ewing	See Text		3.9±0.3	-	21.2

*The potential from this work is tabulated in Table 6.14

TABLE 6.14 : The potential function for argon-nitrogen interactions obtained by inversion of viscosity data. Extrapolations were used for r < 0.309 and r > 0.424 rm

r(nm)	U/k (K)
0.2701	5249.3
0.2804	3559.2
0.2908	2329.6
0.3012	1456.2
0.3115	851.83
0.3240	368.63
0.3344	124.79
0.3406	36.013
0.3427	13.439
0.3447	-5.8980
0.3468	-21.804
0.3510	-48.587
0.3572	-75.472
0.3655	-99.508
0.3759	-116.80
0.3842	-122.18
0.3862	-122.48
0.3883	-122.26
0.4008	-115.55
0.4194	-99.454
0.4443	-78.480
0.4817	-52.027
0.5211	-33.206
0.6020	-14.477

$mole^{-1}$ is shown in Table 6.13.

(v) Conclusion

There are considerable variations among the potentials proposed for the argon-nitrogen interaction. However, the potential from this work seems to be one of the first which does not follow a predetermined form such as that of Lennard Jones (n-6) as well as calculating to high accuracy the transport properties and second virial coefficients. It is also hoped that it will be of use in more sophisticated analyses of the experimental results from this system. In addition, although the potential is isotropic in form, it is possible particularly in the light of some of the results discussed in the next Chapter, that it could be used for example in the calculation of further properties of the system such as the differential scattering and total cross-section scattering.

CHAPTER 7

THE INVERSION OF THERMOPHYSICAL PROPERTIES FROM ANISOTROPIC POTENTIAL FUNCTIONS

(a) Introduction

The technique of inversion of thermophysical properties to obtain pair potential energy functions has been described in theory in Chapter 4 and as applied to the gaseous viscosities of argon-xenon and argon-nitrogen in Chapter 6. In this chapter we look at the effects of applying such techniques to the properties of anisotropic molecules. Only recently have such investigations been undertaken. Maitland et al (1) have investigated inversion of gas viscosity data calculated using the infinite order sudden (IOS) approximation (2). They found that the potential which they obtained on inversion was not similar to the unweighted spherical average of the anisotropic potential they used and nor was it closely related to the potential function for any particular angular orientation. In this work we applied the latest inversion methods developed for second virial coefficient inversion (3) and the transport property inversion method used in the previous Chapter to the second virial coefficients and transport properties for a model anisotropic system - the di-Lennard-Jones potential.

(b) Application to a Model Anisotropic System

The di-Lennard-Jones potential which we used in this work consists of two Lennard-Jones centres each interacting with parameters ε/k = 33.46K and σ = 0.3266 nm. The anisotropy of the system is defined by l/σ where l is the separation of the two centres (see Figure 7.1). In this work we took this ratio of l/σ to be 0.3292.

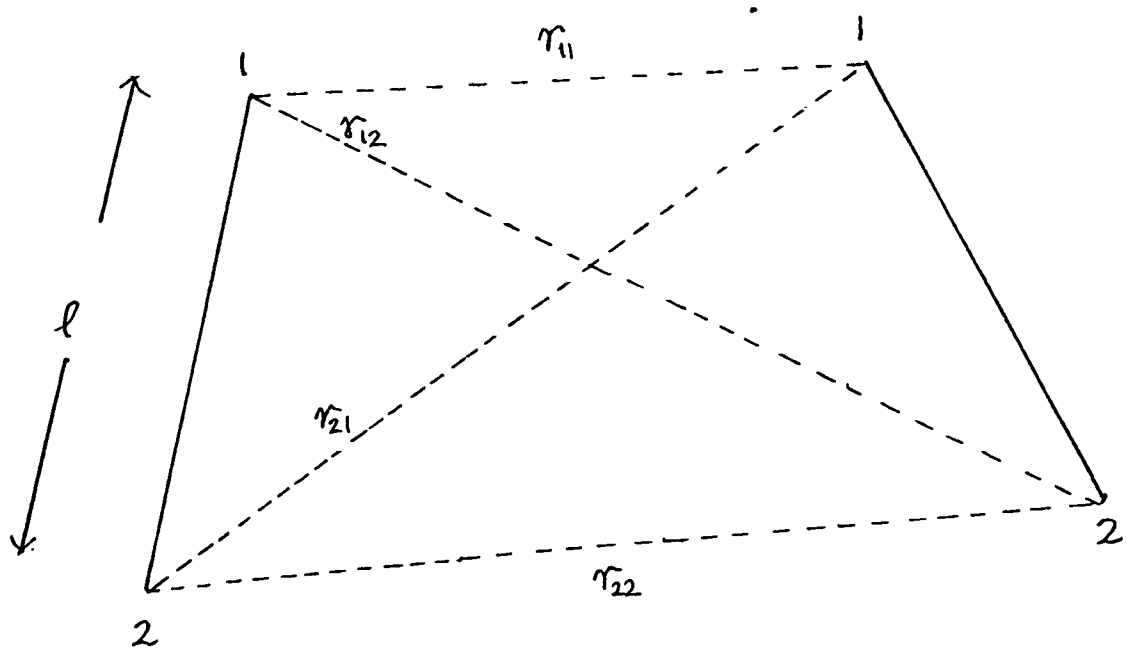


FIGURE 7.1

This is a degree of anisotropy which is consistent with modern suggestions for the N_2-N_2 system (e.g. (4)). The two centre di-Lennard-Jones potential therefore becomes:

$$U_{ij} = 4\varepsilon \sum_{l=1}^{2} \sum_{m=1}^{2} \left[\left(\frac{\sigma}{r_{lm}} \right)^{12} - \left(\frac{\sigma}{r_{lm}} \right)^{6} \right] \qquad (7.1)$$

The classical second virial coefficients were calculated from the anisotropic potential by means of the expression

$$B(T) = -\frac{N_A}{4} \int_0^{\infty} r_{12}^2 dr_{12} \int_0^{\pi} \sin\theta_1 \, d\theta_1 \int_0^{\pi} \sin\theta_2 d\theta_2 \int_0^{2\pi} f_{12}(r_{12}\theta_1, \theta_2, \theta_{12}) d\phi_{12} \qquad (7.2)$$

which is valid for linear molecules. Where $\phi_{12} = \phi_1 - \phi_2$ and $f_{12} = \exp(-U_{12}/kT) - 1$ is the Mayer f function (5). This integration was performed using a non-product algorithm method (6) which required a total of 16128 function evaluations to give the second virial coefficient accurate to about 0.02 $cm^3\ mol^{-1}$.

The transport properties were calculated using the Mason Monchick approximation (7). Mason and Monchick proposed a simple scheme whereby the collision integrals (see Chapter 2) may be calculated. The principal assumptions made in their approach are that first, the energy transfer between translation and internal modes does not affect the transport properties, and second the relative angular orientation of the molecules remains unchanged throughout the collisional process. They suggested therefore that the calculation should be performed by computing the fixed angle collsion

integrals $\Omega^{(n,s)}(T,\omega)$ for the collision of two molecules at the fixed relative orientation ω. This is then the calculation of the collisional integrals for the potential at fixed orientation $U(r,\omega)$. The collision integral for the non-spherical potential is then obtained quite simply by averaging the fixed orientation collision integrals with equal weight over all space. Thus

$$<\Omega^{(n,s)}(T)> = \frac{1}{8\pi}\int_{-1}^{1}\int_{-1}^{1}\int_{o}^{2\pi}\Omega^{(n,s)}(T,\omega)d\phi d(\cos\theta_1) d(\cos\theta_2) \qquad (7.3)$$

This integration was carried out using a program based on that of Price (8) which utilizes a 5 point Gaussian-Legendre Integration in $d(\cos\theta_1)$ and $d(\cos\theta_2)$ and a 5 point Gaussian-Chebyshev Integration in ϕ. This calculation took about 120 seconds to calculate the collision integrals for 40 temperatures on the CDC 7600 computer of London University.

Since in general, inversion of data over a limited temperature range only defines the potential function over a limited range of r, some form of extrapolation is required and in this work we used two types of extrapolation which are very different in form. These were the Lennard-Jones 18-6 function and the BBMS function (9) proposed for argon on the basis of the analysis of the u.v. spectra of the argon dimer.

Two different transport properties were calculated from the collisional integrals. These were viscosity depending on $\Omega^{(2,2)}(T)$ and self diffusion which depends on a different collisional integral $\Omega^{(1,1)}(T)$. These were calculated for temperatures over the range 50-2000K. The second virial coefficients were calculated in the temperature range 70-700K.

The inversion procedures as described in Chapter 4 were then applied to the properties. Each inversion as applied to the viscosity, self-diffusion and second virial coefficient data produced a potential which was capable of reproducing the appropriate property to high accuracy. Typically the viscosity and self diffusion data were reproduced to $\pm$ 0.2% and the second virial coefficients to $\pm$ 0.5 cm^3. However the most striking feature of these inversions is that *the potentials produced on inversion of the three properties are all extremely similar* to each other as shown in Figure 7.2. It should also be noted that these potentials are very different except at long range where the anisotropy is no longer manifest, from the unweighted spherical average also shown in Figure 7.2. In particular the potentials from inversion are deeper by 15% than the spherical average which has characteristic parameters of σ = 0.370 nm and ε/k = 87K. The potentials from inversion, on the other hand, have characteristic parameters of $\varepsilon/k \approx$ 100K and $\sigma \approx$ 0.360 nm. The results of the inversion of the second virial coefficients and

viscosities are shown in Tables 7.1 and 7.2. These Tables show the results of the minimisation procedure which has been described previously to obtain the well depth parameter ε. In the tables the results are shown for the two extrapolation functions used as well as the four different potentials used to calculate the initial approximate inversion function $G_o(T)$. The results for the self-diffusion inversion are not shown as they give results which are essentially identical to those in Table 7.2 for the viscosity inversion.

It was found, within the uncertainties involved in the inversion procedure, that all three properties were consistent with a *single* potential function which had a well depth of $\varepsilon/k = 100 \pm 3K$ and a collision diameter $\sigma = 0.360 \pm 0.02$ nm. This function, which is shown in Figure 7.2 as the continuous line, reproduced the virial coefficient data to a standard deviation of 1.6 cm^3, the viscosity coefficients to 1.6% and self-diffusion coefficient data to 1.1%. These errors, though greater than when the properties are calculated from the potential produced by inverting that property alone, would be found acceptable if the method were being applied to real experimental data.

(c) Conclusions

From these results we can conclude that:

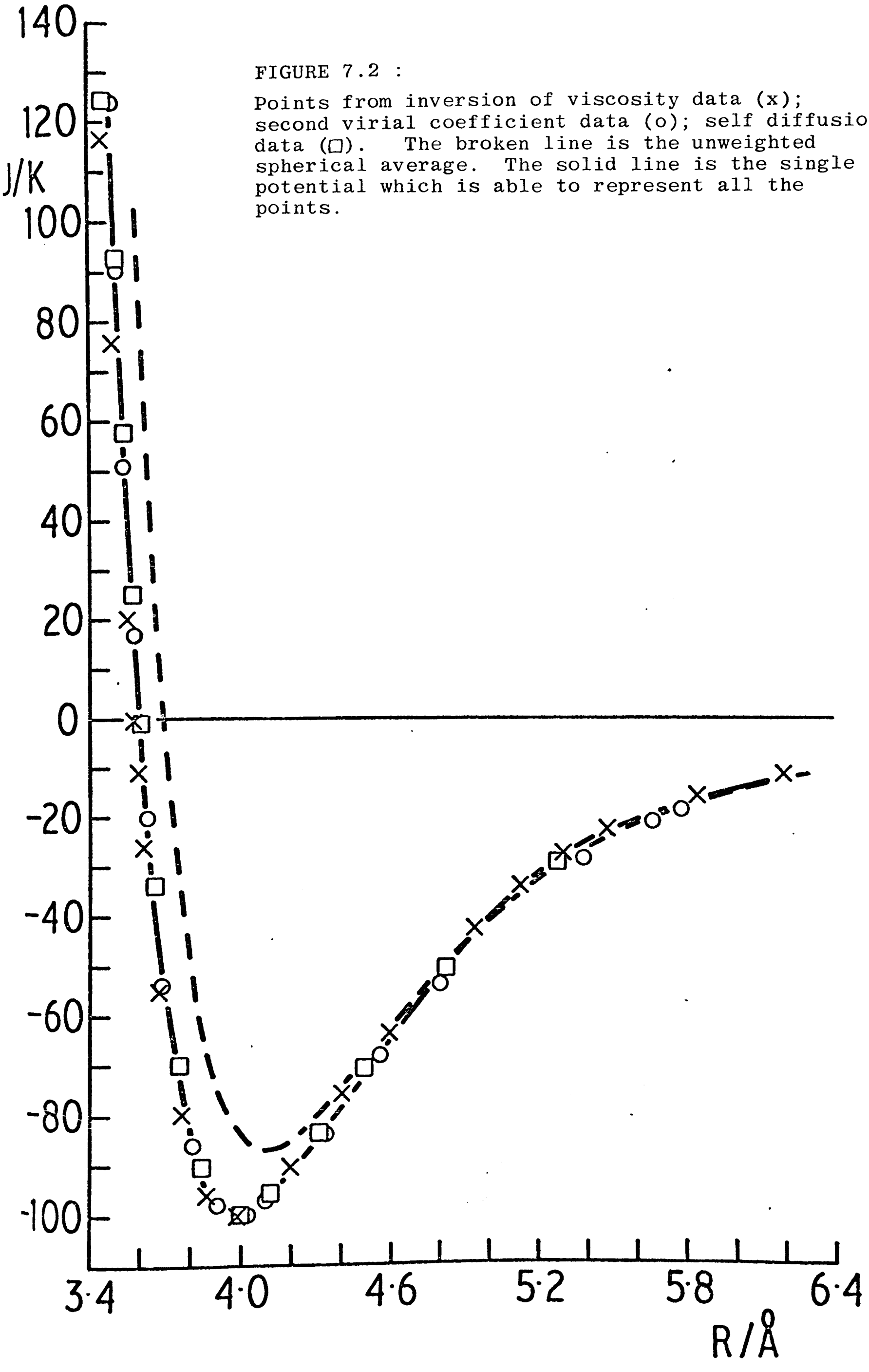


FIGURE 7.2 :

Points from inversion of viscosity data (x); second virial coefficient data (o); self diffusion data (□). The broken line is the unweighted spherical average. The solid line is the single potential which is able to represent all the points.

TABLE 7.1 Virial Inversion Results

I.A.P.*	BBMS extrapolation		18-6 extrapolation	
	ε/k(K)	σ(x10nm)	ε/k(K)	σ(x10nm)
12-6	100 ± 3	3.59 ± 0.01	103 ± 1	3.585 ± 0.005
18-6	100 ± 3	3.59 ± 0.01	103 ± 2	3.58 ± 0.01
9-6	100 ± 3	3.58 ± 0.01	103 ± 3	3.58 ± 0.01
BBMS	100 ± 3	3.60 ± 0.01	103 ± 2	3.60 ± 0.01

*I.A.P. refers to the initial approximate potential used for calculating $G_o(T)$

TABLE 7.2 Viscosity Inversion Results

I.A.P.*	BBMS extrapolation		18-6 extrapolation	
	ε/k(K)	σ(x10nm)	ε/k(K)	σ(x10nm)
12-6	97 ± 3	3.60 ± 0.01	97 ± 3	3.59 ± 0.01
18-6	105 ± 5	3.55 ± 0.02	103 ± 3	3.56 ± 0.02
9-6	97 ± 4	3.60 ± 0.02	97 ± 2	3.59 ± 0.01
BBMS	103 ± 3	3.57 ± 0.02	99 ± 2	3.58 ± 0.01

*I.A.P. refers to the initial approximate potential used for calculating $G_o(T)$

(i) For molecules with the degree of anistropy assumed in this work an effective spherical potential function can predict the second virial coefficients to high accuracy.

(ii) This function can be obtained directly by the application of established inversion techniques.

Other conclusions are subject to the validity of the Mason Monchick approximation which we used to calculate the collision integrals. However if this model is employed we can obtain, by inversion procedures, effective spherical potential functions which can accurately reproduce the viscosity and self diffusion data. The most striking observation must be, however, that the potential functions for the three properties are very similar and yet completely different from the unweighted spherical average.

The generality of these conclusions was tested by the application of the method to potentials of various anisotropy.

(d) Investigation of the Effect of Anisotropy

In the previous section we discussed the results of our inversion of properties calculated from anisotropic potentials, and described the discovery that a wide range of properties of the anisotropic system could be represented by a single isotropic potential. In this

section we used the same kind of anisotropic two centre di-Lennard-Jones potential. The values of ε/k = 33.46 and the collision diameter parameter σ = 0.3266 nm were the same for the site-site interaction. The anisotropy parameter $1/\sigma$ was varied the lowest level of aniso - tropy considered being half that of the pseudo nitrogen potential considered previously and the highest level being twice it.

In each case we calculated the second virial coefficients and collision integrals and hence the viscosity coefficients. The virial coefficients were inverted, in the traditional manner already described, for a selection of well depths and the potential with a value of ε/k which minimised the deviation of the virial coefficients was accepted as the effective spherical potential for the virial coefficients. The results for the inversions at the different levels of anisotropy are shown in Table 7.3.

The potentials obtained on inversion as indicated in the Table 7.3 were then used to calculate viscosity coefficients which were then compared with those obtained from a Mason Monchick type calculation of the collision integrals for the anisotropic potential. The deviations of the viscosities calculated from the potential obtained on inversion of the virial coefficients and those calculated from the anisotropic potential are shown below:

$1/\sigma$	0.1646	0.3292	0.4938	0.6584
$\%\eta$	0.444	0.872	1.262	1.8036

As can be readily seen from the results above when the anisotropy is low then the potential from the virial inversion performs extremely well in predicting the viscosity coefficients for the system. In addition the viscosity coefficients calculated from the anisotropic potentials were also inverted and the results of these inversions in terms of the values of ε/k and σ for the potentials at various levels of anisotropy are also shown in Table 7.3. This shows that the potentials resulting from the inversion of virial coefficients and viscosity coefficients have very similar parameters for well depth and collision diameter when the level of anisotropy is less than 0.4938. It seems, therefore, that the phenomenon of there being one effective isotropic potential which can reproduce a wide range of thermophysical properties is a function of anisotropy as might have been expected.

(e) Discussion

Now we want to try to propose an explanation of the observations described above. The first point which is very obvious is that the isotropic "effective" potential which we will call $U_{inv}(r)$ is not the same potential as the unweighted spherical average produced by

TABLE 7.3 Results of Inversion of Viscosities and Second Virial Coefficients

Property				
Virial		Viscosity		Anisotropy($1/\sigma$)
ε/k(K)	σ(nm)	ε/k(K)	σ(nm)	
120 ± 2	0.337 ± 0.001	120 ± 3	0.337 ± 0.001	0.1646
100 ± 3	0.360 ± 0.002	100 ± 3	0.360 ± 0.001	0.3292
90 ± 5	0.377 ± 0.002	90 ± 5	0.375 ± 0.003	0.4938
80 ± 6	0.398 ± 0.003	75 ± 7	0.398 ± 0.004	0.6584

$$U_{spherical}(r) = \left\langle U(r, \omega_1, \omega_2) \right\rangle \qquad (7.4)$$

This result is not at all unexpected and was shown by Parker and Pack (2) who calculated viscosities from the spherical average of an anisotropic function and showed them to be considerably different from those calculated directly from the anisotropic potential.

The question which we need to try to answer is what kind of average needs to be performed on the anisotropic potential in order to give the "effective" isotropic potential $U_{inv}(r)$.

There are several kinds of average which may be performed on the di-Lennard-Jones system. The first type of averaging which is performed at fixed separation, r, between the centre of masses of the system may be divided into two classes one a Boltzmann type of averaging and the other a so-called "free energy" averaging method. The relevant equations for these two methods are shown in Figure 7.3 along with a diagramatic representation of a fixed r method of averaging.

In this type of averaging the problem of relating the anisotropic potential to that produced on inversion becomes a problem of evaluating the weighting temperature T_θ. If we consider the inversion method then we know that

FIGURE 7.3 Fixed Separation Averaging Methods

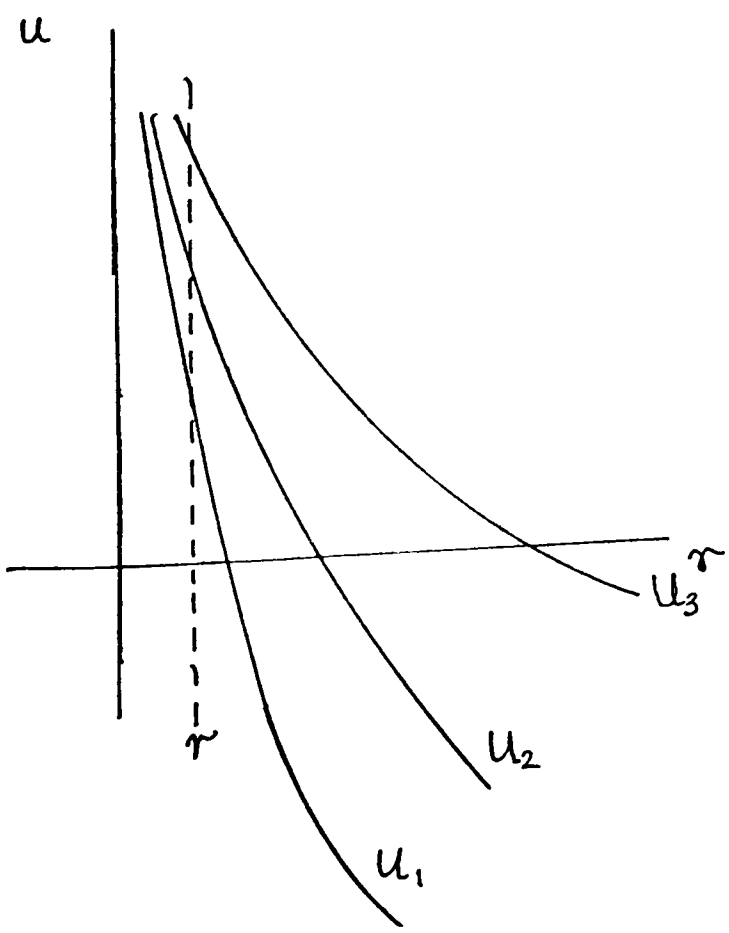
(i) Boltzmann Averaging

$$U(r)_{\text{averaged}} = \frac{\int \ldots \int \phi \times e^{-\phi/kT_\theta} d\omega_1 d\omega_2}{\int \ldots \int e^{-\phi/kT_\theta} d\omega_1 d\omega_2} \qquad (7.5)$$

(ii) Free Energy Averaging

$$U(r)_{\text{averaged}} = -kT_\theta \ln \int \ldots \int e^{-\phi/kT_\theta} d\omega_1 d\omega_2 \qquad (7.6)$$

where ϕ is the angle dependent potential and T_θ is a weighting temperature.



In this fixed r method of averaging a section is taken through the different potentials as a function of orientation (U_1, U_2, U_3 ....) with a weighting which may for example be of Boltzmann type. The point (U_{averaged}, r) on the averaged potential will lie at the same value of r as that at which the section was taken.

(1) The property gives rise to a characteristic length $\tilde{r}$.

(2) The value of U at this value of $\tilde{r}$ comes from the inversion function $U(\tilde{r}) = G_o(T).kT$.

Therefore we might expect $T_\theta = \frac{U(r)}{kG_o(T)}$ if the averaging method behaved ideally. This is identical to saying that for a particular property P(T) at temperature T, we would expect T_θ to be T for the separation given by the property (in terms of its characteristic length). This was in fact found not to be the case in practice. T_θ varied far more rapidly than $U(\tilde{r})/kG_o(T)$.

In order to try to understand the functional variation of T_θ with separation we calculated its value by an iterative procedure in which we averaged the anisotropic function by the method of free energy averaging and in a trial and error type algorithm evaluated the value of T_θ necessary at a particular value of r to produce a value of U corresponding to the point (r,U) on the potential produced on inversion. Initially we performed this procedure for the di-Lennard-Jones potential with $1/\sigma = 0.3292$. This function is shown in Figure 7.4. It may be seen to be a steep function which falls rapidly with increasing r and which becomes undefined at values of r much greater than r_m. This inability to define T_θ at these separations is an indication that anisotropy of the potential function has become unimportant and this

is shown quite obviously in the form of the inverted potential at long range which tends towards that of the simple unweighted spherical average of equation (7.4).

We also calculated the weighting temperature T_θ for potentials with differing anisotropy and also shown in Figure 7.4 are the values of T_θ as a function of separation for the levels of anisotropy equal to $1/\sigma = 0.1646$ and $1/\sigma = 0.4938$. These may quite easily be seen to be dissimilar in absolute terms but all with the same functional form and falling off at a value of r which corresponds to the bottom of the potential well (i.e. r_m). It was hoped that this effective temperature as a function of separation r would be very similar for di-Lennard-Jones and di-BBMS potentials, with the same parameters for the individual site-site potentials ($\varepsilon/k = 33.46K$ and $\sigma = 0.3266$ nm) and the same level of anisotropy. To test this, we calculated virial coefficients for a di-BBMS potential with anisotropy $1/\sigma = 0.3292$. These virial coefficients were inverted in the usual way and an effective spherical potential was obtained. The value of T_θ as a function of separation which produced this effective potential by a free energy average of the di-BBMS potential was calculated. The two T_θ functions for the di-BBMS and di-Lennard-Jones potential are shown in Figure 7.5. Although the curves have the same shape they are apparently displaced from one another by some distance which remains remarkably

FIGURE 7.4 :

⨳ points for $\ell/\sigma = 0.1646$

∇ points for $\ell/\sigma = 0.3292$

Δ points for $\ell/\sigma = 0.4938$

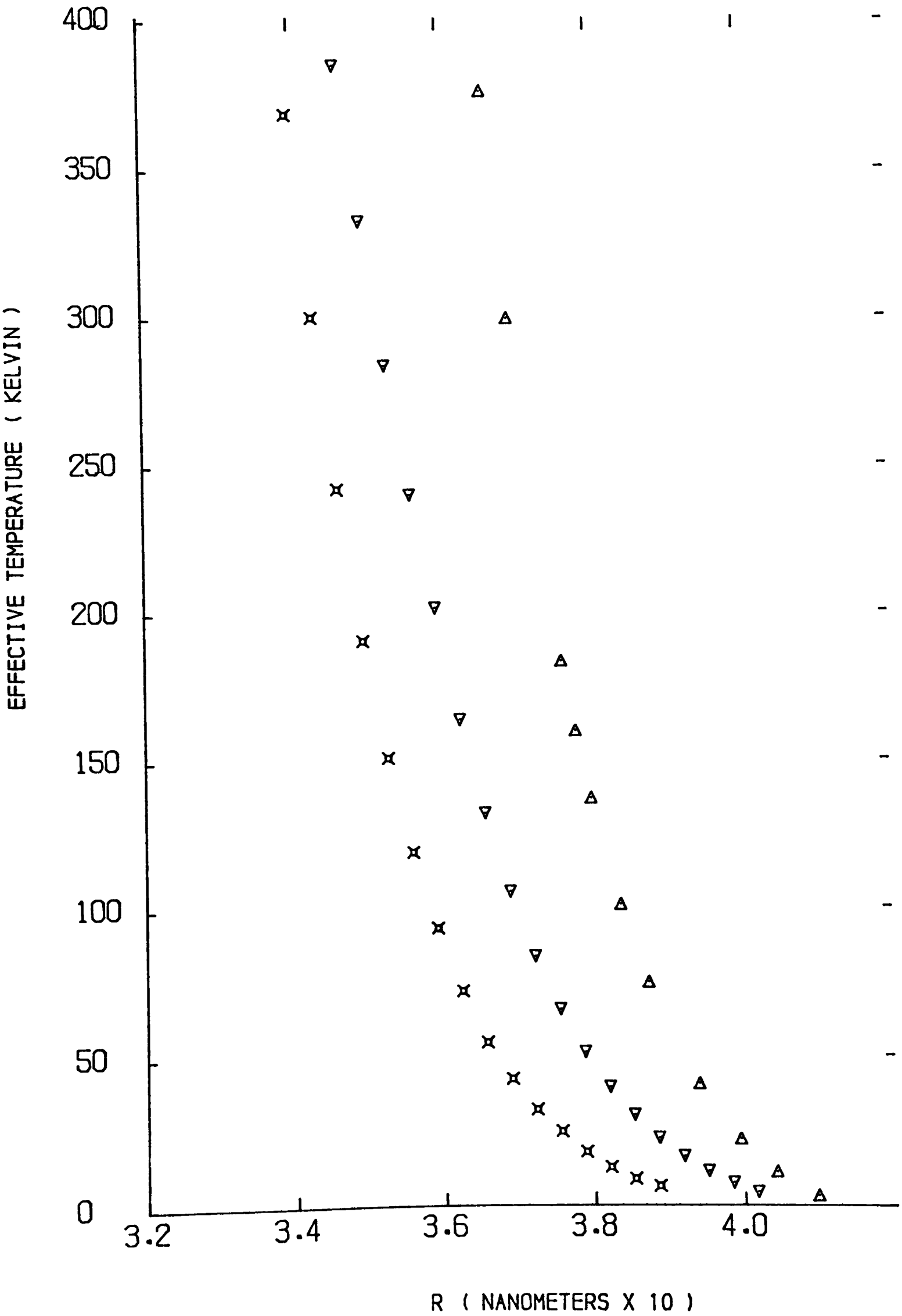
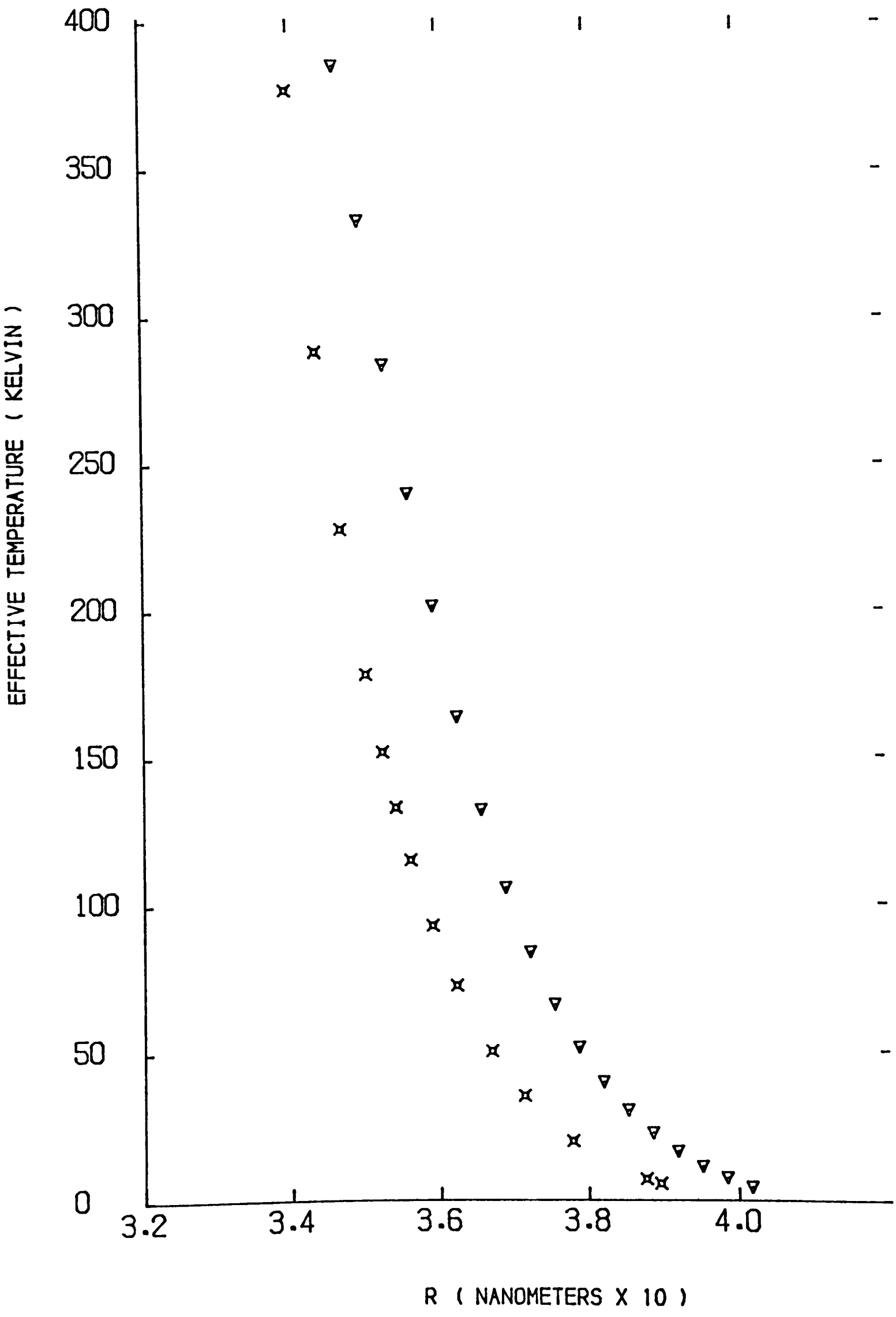


FIGURE 7.5

⨳ points for $\ell/\sigma = 0.3292$ di-BBMS anisotropic function

▽ points for $\ell/\sigma = 0.3292$ di-Lennard-Jones anisotropic function.



consistent over the range of r considered. Unfortunately upon further investigation with other degrees of anisotropy this appears to be fortuitous. The effective temperature averaging method is of value in providing an insight into where anisotropy is important and how it varies with separation, but unfortunately it proves to be unsuccessful in a predictive capacity for calculating the effective spherical potential from the anistropic potential since it varies considerably with the level of anisotropy and the form of the anisotropic function. The results of the Boltzmann averaging technique will not be included here since it was found that T_θ for this method behaved in an exactly analogous form to that described above for the free energy averaging method.

Another way of looking at the averaging performed in obtaining the effective spherical potential may be studied by considering the anisotropic potential to be made up of many fixed orientation potentials. It is possible to perform averages at fixed orientation as follows.

In obtaining the potential U(r) by inversion we use the inversion function $G_o(T)$ to define a value of $U(\tilde{r})$ from the relationship

$$U(\tilde{r}) = G_o(T).\ kT. \qquad (7.7)$$

This procedure is repeated for a series of temperatures.

The value of $\tilde{r}$ at these temperatures is given by either:

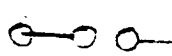
$$\tilde{r} = \left[\frac{B + TdB/dT}{2/3\,\pi\,N_A}\right]^{1/3} \qquad (7.8)$$

or $$\tilde{r} = (\Omega^{(2,2)})^{\frac{1}{2}} \qquad (7.9)$$

depending on which property is being inverted. Now we seek to find an averaging method which operates in an analogous fashion to that of the inversion methods. Since in the inversion methods the property, be it a second virial coefficient or a viscosity coefficient, maps on to a distance and the temperature at which the property is determined maps on to energy (via the inversion function), then it seems possible that the averaging we are seeking should operate at a fixed temperature.

The procedure for carrying out the averaging is outlined schematically in Figure 7.6. Consider the anisotropic potential to be made up of the individual angle dependent potentials V_a, V_b, V_c etc. On the diagram possible orientations are shown. We will call these potentials at the angles ω_a, ω_b, ω_c (only considering the orientation in one plane for simplicity) V_a, V_b and V_c. Now if we consider the hypothetical step 1. In this step for each of the cases illustrated a, b and c, we calculate a property (second virial coefficient or transport property) P at fixed temperature T_F. This

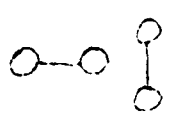
FIGURE 7.6



V_a P_{ω_a} inversion at fixed orientation ω_a $\tilde{r}_{\omega_a}$ gives point $V_a(\tilde{r}_{\omega_a})$

a)

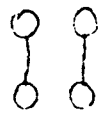
All operations at fixed temperature T_F



V_b P_{ω_b} inversion at fixed orientation ω_b $\tilde{r}_{\omega_b}$ gives point $V_b(\tilde{r}_{\omega_b})$ $U_{av}(r)$

b)

All operations at fixed temperature T_F



V_c P_{ω_c} inversion at fixed orientation ω_c $\tilde{r}_{\omega_c}$ gives point $V_c(\tilde{r}_{\omega_c})$

c)

All operations at fixed temperature T_F

property will have a different value according to the angle of orientation ω. We have, therefore three properties P_{ω_a}, P_{ω_b} and P_{ω_c}. Now we can in step 2, invert these properties to give characteristic lengths $\tilde{r}$ according to equations (7.8) and (7.9). We will have then three different lengths $\tilde{r}_{\omega_a}$, $\tilde{r}_{\omega_b}$ and $\tilde{r}_{\omega_c}$. For each of these separations $\tilde{r}$ there will be a corresponding energy, step 2; which will be given by $V_a(\tilde{r}_{\omega_a})$, $V_b(\tilde{r}_{\omega_b})$ and $V_c(\tilde{r}_{\omega_c})$. Thus, what we have done in steps 1 to 3 is to map the temperature T_F on to a corresponding energy $V_a(\tilde{r}_{\omega_a})$ etc. at a distance given by the property. The final step of this procedure is to take all these individual points $V_a(\tilde{r}_{\omega_a})$ etc. and perform a simple unweighted averaging over all space to give on the final isotropic potential an energy $\langle V \rangle$ at an average separation which is given by the value of $\langle P_\omega \rangle$ using (7.8) or (7.9). Thus we have averaged the anisotropic function at fixed temperature. In one sense the above procedure is very similar to what happens in the Mason Monchick approach to evaluate transport properties. In the Mason-Monchick technique the collision integrals are evaluated at fixed orientation and the final anisotropic collision integral is the simple unweighted spherical average of all the individual fixed orientation collision integrals.

$$\text{Thus} \quad \langle\Omega^{l,s}(T)\rangle = \int \Omega^{l,s}(T,\omega)d\omega \qquad (7.10)$$

See also equation (7.3). This is identical to the procedure in Figure 7.6 for defining <r> when the substitution of equation (7.9) is made as now this equation becomes, ignoring constant factors,

$$\langle\tilde{r}^2(T)\rangle = \int \tilde{r}^2(T,\omega)d\omega \qquad (7.11)$$

In the case of the second virial coefficient there is no approximation involved, the analogous form of equation (7.10) being:

$$\langle B + TdB/dT\rangle = \int [B(T,\omega) + TdB(T,\omega)/dT]d\omega \qquad (7.12)$$

and hence

$$\langle\tilde{r}^3(T)\rangle = \int \tilde{r}^3(T,\omega)d\omega \qquad (7.13)$$

In the inversion method it is apparent that the value of r obtained as the characteristic length at any temperature T will be given by the application of equations (7.8) or (7.9) to the anisotropic potential. This will of course either be the left hand side of equation (7.10) or (7.12) and therefore, the method outlined in Figure 7.6 will at any temperature T give a value of r on the effective spherical potential which is identical to that produced on inversion.

It now becomes possible to understand why the potentials from the inversion of viscosities and second virial coefficients are almost identical. This is because the evaluation of the property calculated from the anisotropic potential is performed in an identical manner for both second virial coefficients and transport properties. Each evaluation involves exactly the same averaging over the space, i.e. evaluation of the property at fixed orientation and then unweighted spherical averaging over all these orientations. This is of course subject to the restriction of the Mason Monchick approximation as applied to the transport coefficients.

We carried out this type of averaging in order to test the above hypothesis initially for two levels of anisotropy, $1/\sigma = 0.1646$ and 0.3292. The procedure followed was at a particular temperature to calculate the expression $B + TdB/dT$ at a fixed angle of orientation and then evaluate r_{ω_a} etc as outlined in Figure 7.6. The potential obtained by this method of averaging was for an anisotropy of 0.1646 very similar to that obtained by inversion and on using it to calculate the second virial coefficients and viscosity coefficients performed very well indeed reproducing the virial coefficients to within 0.89 cm^3 and the viscosities to better than 0.37%.

For a level of anistropy equal to 0.3292 the potential obtained by this averaging method performed satisfactorily, reproducing the virial coefficients to better than 2 cm^3 and the viscosity coefficients to 1%. Comparing these potentials to those produced on inversion is less satisfactory. With an anisotropy parameter of 0.1646 the potentials compare very well as can be seen from Figure 7.7. However when $1/\sigma = 0.3292$ there is a considerable difference in the well depth parameters of $\approx$100K $\pm$ 3 for the potential from inversion whereas that from the averaging method is 90K. The potentials agree very well in the repulsive region, but deviate appreciably in the attractive region as shown in Figure 7.8. The agreement in the repulsive region is somewhat surprising since it is in this region where one would expect the effect of anisotropy to be most pronounced. This observation also applies to the repulsive region of the potential for a level of anisotropy equal to 0.1646 as can be seen from Figure 7.7 in which extremely good agreement between the potential resulting from inversion and that by this method of averaging is apparent in the repulsive region. One problem is that the extrapolation chosen, particularly for long range, can cause considerable variation in the values of the second virial coefficient calculated from the potentials produced both by inversion and by averaging.

FIGURE 7.7 : Continuous line is the potential which results from the inversion of second virial coefficients calculated from a di-Lennard-Jones potential with $\ell/\sigma = 0.1646$. ⨳ indicates points from the averaging method at fixed orientation (Figure 7.6)

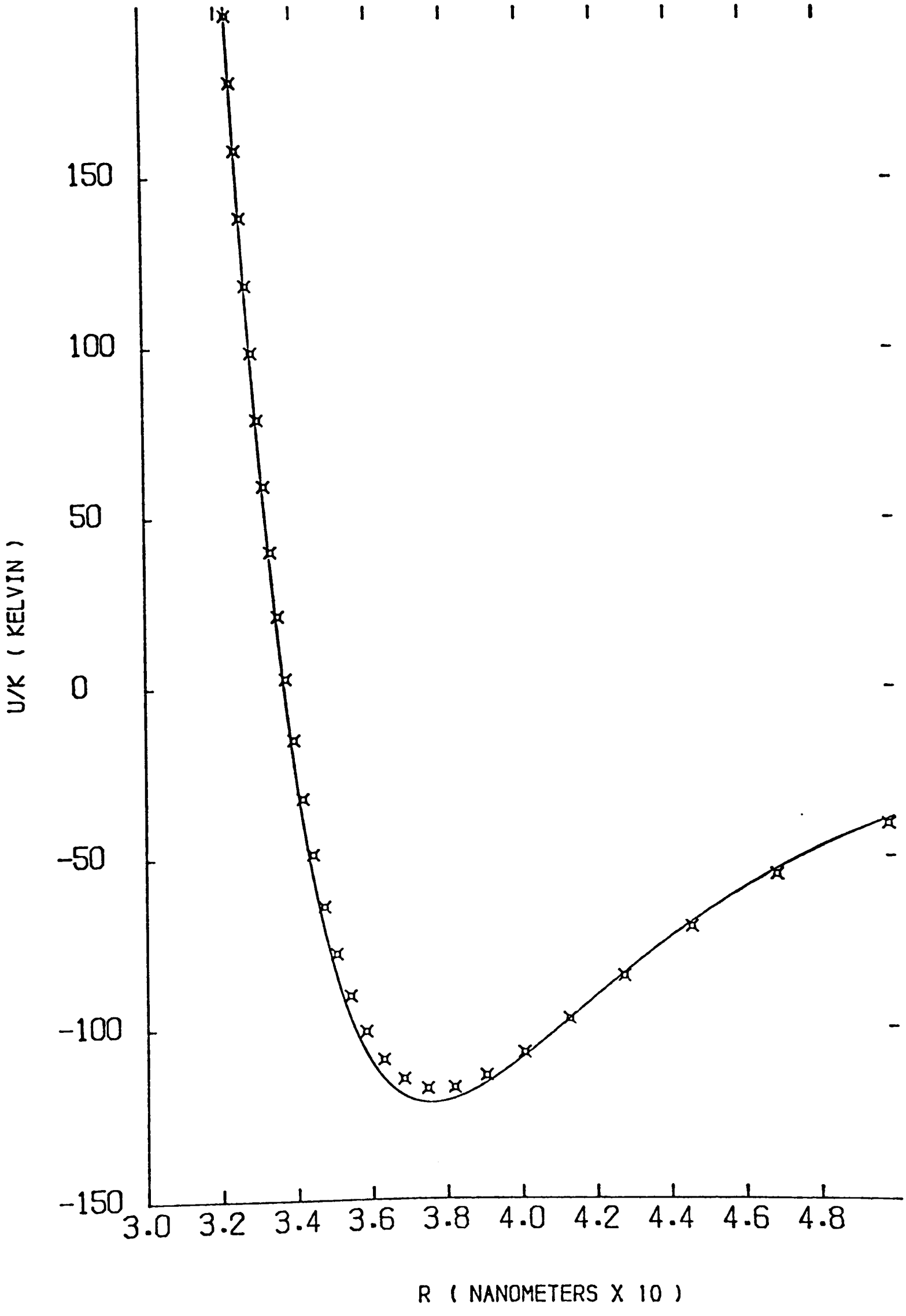
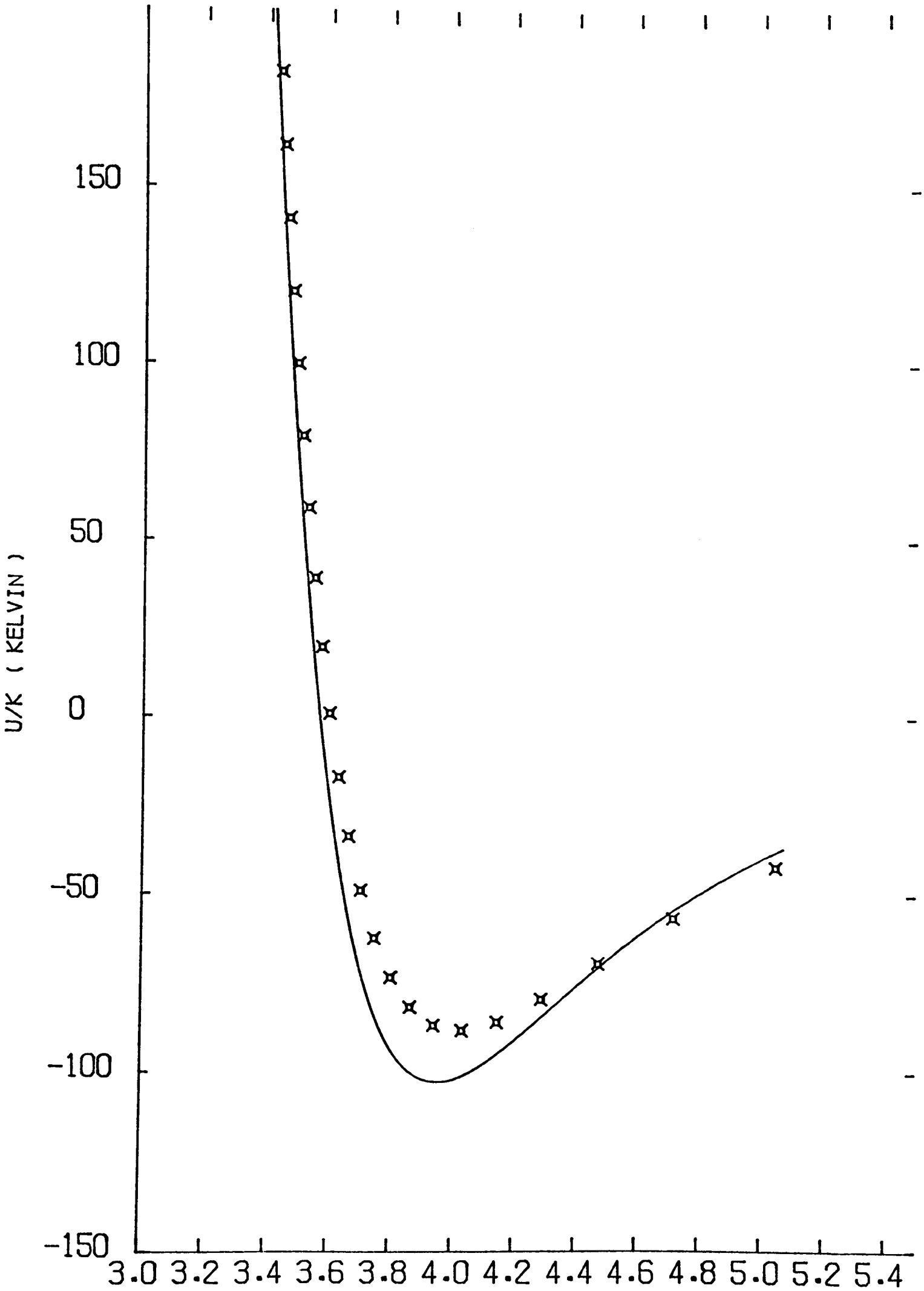


FIGURE 7.8 : Continuous line is the potential which results from the inversion of second virial coefficients calculated from a di-Lennard-Jones potential with $\ell/\sigma = 0.3292$. ⌘ Indicates points from the averaging method at fixed orientation (Figure 7.6).



(f) Conclusions

The fact that there exists one effective potential which reproduces a wide range of properties over a large temperature range is very interesting. It is also, at the moment, unexplained. Two methods of averaging the anisotropic potential to give the "effective" isotropic potential have been tried. The first, at fixed separation proved to be unsatisfactory since the effective temperature used in the averaging was so sensitive to the final potential and could not be predicted in any straightforward manner.

The second method of averaging which we attempted did seem to produce a potential which, at modest degrees of anisotropy, could both reproduce the second virial coefficients and also could be related to the potential produced on inversion. However, this method also proved to be unsatisfactory as the degree of anisotropy as increased, although there does appear to be some evidence that it does reproduce the repulsive portion of the "effective" potential.

The observation that the potential produced on averaging does give reasonable virial coefficients and transport properties although different in shape to that of "effective" potential produced on inversion may suggest that there are several potentials which are able to produce satisfactory properties and the potentials

produced on inversion of these anisotropic properties are not necessarily unique.

The inversion of properties from *isotropic* potentials is, in principle, unable to produce a unique potential, but this is achieved in practice (see Chapter 4) due to the restrictions imposed by the inversion method which requires a continuous function and continuous first derivative. It may be the case with the properties from anisotropic potentials that this restriction imposed by the inversion method is less severe and so a unique potential does not result from the inversion.

There is always the possibility that the reproduction of both second virial coefficients and transport properties may be fortuitous and depend on the assumption of the Mason and Monchick approximation since this results in both the second virial coefficients and transport coefficients being evaluated by the same average of angle dependent properties P (T) over all space.

In summary, therefore, the problem of anisotropy is only just beginning to be investigated. The preliminary results, however, of this work in the field seems to suggest though it is a complex phenomenon whose precise nature is not fully understood, that there are underlying principles which could be of immense value in the future in the study of anisotropic molecules.

REFERENCES

CHAPTER ONE

1. R. Clausius, Ann. Phys. 100 (1857) 353.
2. J.C. Maxwell, Phil. Mag. 19 (1860) 19.
3. J.C. Maxwell, Phil. Mag. 20 (1860) 21.
4. J.C. Maxwell, Phil. Trans. Roy. Soc. 157 (1867) 49.
5. L. Boltzmann,Sitz. Akad. Wiss., Wein 66 (1872) 275.
6. J.D. Van der Waals, Doctorial Dissertation, Leiden (1873).
7. J.E. Lennard-Jones, Proc.Roy.Soc.(Lond.) A169 (1939) 317.
8. J.E. Lennard-Jones & A.F. Devonshire, Proc.Roy.Soc. (Lond.) A106, (1924), 441, 463.
9. M. Born & J.R. Oppenheimer, Ann.Phys. 84 (1927) 457.
10. L. Wolniewiez, J.Chem.Phys. 45 (1966) 515.
11. B.M. Axilrod & E. Teller, J.Chem.Phys. 11 (1943) 299.
12. P.E. Phillipson, Phys.Rev. 125 (1962) 1981.
13. G.H. Matsumoto, G.F. Bender & E.R.Davidson, J.Chem.Phys. 46 (1967) 402.
14. P. Bertoncini & A.C. Wahl, J.Chem.Phys. 58 (1973) 1259.
15. D.R. McLaughlin & H.F. Schaefer, Chem.Phys.Lett. 12 (1971) 244.
16. T.L. Gilbert & A.C. Wahl, J.Chem.Phys. 47 (1967) 3425.
17. R.L. Matcha & R.K. Nesbet, Phys.Rev. 160 (1967) 72.
18. K.B. Hathaway & J.A. Krumhansl, J.Chem.Phys. 63 (1975) 4308.
19. B. Tsapline & W. Kutzelnigg, Chem.Phys.Lett. 23 (1973) 173.
20. C.R.A. Catlow, A.H. Harker & M.R. Hayns, J.Chem.Soc. Faraday Trans II, 71 (1975) 275.
21. G.C. Maitland, M. Rigby, E.B. Smith & W.A. Wakeham,

"Intermolecular Forces - Their Origin and Determination", 1981, OUP (Oxford), Chapter 1, page 13.

22. F. London, Z. Phys.Chem. (B) 11 (1930) 222.

23. Ref. 21, Chapter 1, page 16 and section.

24. J.C. Slater & J.G. Kirkwood, Phys.Rev. 37 (1931) 682.

25. J.G. Kirkwood, Physik, Zeit., 33 (1932) 57.

26. A. Muller, Proc. Roy. Soc. 154A (1936) 624.

27. A. Dalgarno & A.E. Kingston, Proc.Phys.Soc. 78 (1961) 607.

28. R.J. Bell, Proc.Phys.Soc. 86 (1965) 17.

29. H.B.G. Casimir & D. Polder, Phys.Rev. 73 (1948) 360.

30. Ref. 21, Chapter 2, page 71.

31. P.W. Langhoff & M. Karplus, J.Chem.Phys. 53 (1970) 233.

32. G. Starkschall & R.G. Gordon, J.Chem.Phys. 54 (1971) 663.

33. R.W. Langhoff, R.G. Gordon & M. Karplus, J.Chem.Phys. 55 (1971) 2126.

34. D.A. McQuarrie, J.Terebey & J.J. Shire, J.Chem.Phys. 51 (1969) 4683.

35. P.R. Certain & L.W. Bruch, M.T.P. Int.Rev.Sci.Phys. Chem.I 1 (1972) 113.

36. J.N. Murrell & A.J.C. Varandas, Mol. Phys. 30 (1975) 223.

37. A.A. Abrahamson, Phys.Rev. 130 (1963) 692.

38. V.I. Gaydaenko & V.K. Nikulin, Chem.Phys.Lett. 7 (1970) 360.

39. R.G. Gordon & Y.S. Kim, J.Chem.Phys. 56 (1972) 3122.

40. A.I.M. Rae, Chem.Phys.Lett. 18 (1973) 574.

41. B. Schneider, J.Chem.Phys. 58 (1973) 4447.

42. Y.S. Kim, J.Chem.Phys. 68 (1978) 5001.

43. S.Lee & Y.S. Kim, J.Chem.Phys. 70 (1979) 4856.

44. H.E.Cox, F.W. Crawford, E.B. Smith & A.R. Tindell, Mol. Phys. 40 (1980) 705.

45. E.B. Smith, A.R. Tindell, B.H. Wells & F.W. Crawford, Mol. Phys. 42 (1981) 937.

46. R. DiPippo & J. Kestin, Proc. 4th Symp. Thermophys. Props. A.S.M.E., New York, 304 (1968).

47. F.A. Guevara, B.B. McInteer & W.E. Wageman, Phys. Fluids 12 (1969) 2493.

48. R.A. Dawe & E.B. Smith, J.Chem.Phys. 52 (1970) 693.

49. e.g. H.J.M. Hanley & G.E. Childs, Science 159 (1968) 1114.

50. H.J.M. Hanley & M. Klein, Nat.Bur.Stand.Tech.Note No. 360 (1967) and Trans. Faraday Soc. 64 (1968) 2927.

51. J.H. Dymond, J.Chem.Phys. 49 (1968) 3673.

52. D.W. Gough, G.C. Maitland & E.B. Smith, Mol. Phys. 24 (1972) 151.

53. G.S. Springer & E.M. Wingeier, J.Chem.Phys. 59 (1973) 2747 and references therein.

54. P. Clancy & E.B. Smith, Physica 83C (1976) 231.

55. E.B.Smith, A.R. Tindell, B.H. Wells & J.L. Brun, Physica 106C (1981) 117.

56. J.M. Hanley & M.Klein, J.Chem.Phys. 50 (1969) 4765; J. Phys.Chem. 76 (1972) 1743.

57. Y. Tanaka & K. Yoshino, J.Chem.Phys. 57 (1972) 2964.

58. Y. Tanaka & K. Yoshino, J.Chem.Phys. 53 (1970) 2012.

59. Y. Tanaka, K. Yoshino & D.E. Freeman, J.Chem.Phys. 59 (1973) 5160.

60. D.E. Freeman, K. Yoshino & Y. Tanaka, J.Chem.Phys. 61 (1974) 4880.

61. R.T. Birge & H. Sponer, Phys.Rev. 28 (1926) 259.

62. R.J. LeRoy & R.B. Bernstein, Chem.Phys.Lett. 5 (1970) 42 ; J.Chem.Phys. 52 (1970) 3869.

63. R.J. LeRoy, in Molecular Spectroscopy I (ed. R.F. Barrow, D.A. Long and D.J. Millen) p.113, Specialist Periodical Report of Chem.Soc. (1973).

64. R.J. LeRoy, J.Chem.Phys. 57 (1972) 573.

65. G.C. Maitland & E.B. Smith, Mol.Phys. 22 (1971) 861.

66. J.M. Parson, P.E. Siska & Y.T. Lee, J.Chem.Phys. 56 (1972) 1511.

67. J.A. Barker, R.A. Fisher & R.O. Watts, Mol. Phys. 21 (1971) 657.

68. E.A. Colbourne & A.E. Douglas, J.Chem.Phys. 65 (1976) 1741.

69. S.E. Novick, K.C. Janda, S.L. Holmgren, M. Waldman & W. Klemperer, J.Chem.Phys. 65 (1976) 1114.

70. D.H. Rank, W.A. Glickman & T.A. Wiggins, J.Chem.Phys. 43 (1965) 1304 and references therein.

71. A.R.W. McKellar & H.L. Welsh, J.Chem.Phys. 55 (1971) 595.

72. G.E. Ewing, Acc.Chem.Res. 8 (1975) 185.

73. R.J. LeRoy & J. Van Kranendonk, J.Chem.Phys. 61 (1974) 4750.

74. G. Henderson & G.E. Ewing, J.Chem.Phys. 59 (1973) 2280.

75. G. Henderson & G.E. Ewing, Mol.Phys. 27 (1974) 903.

76. Ref. 21, Chapter 4.

77. B. Baratz & R.P. Andres, J.Chem.Phys. 52 (1970) 6145.

78. R.B. Bernstein & R.A. LaBudde, J.Chem.Phys., 58 (1973) 1109.

79. E.F. Greene & E.A. Mann, J.Chem.Phys. 58 (1973) 2651.

80. M. Cavallini, G. Callinaro, L. Meneghetti, G. Scoles & U. Valbusa, Chem.Phys.Lett. 7 (1970) 303.

81. C.Y. Ng, Y.T. Lee & J.A.Barker, J.Chem.Phys. 61 (1974) 1996.

82. C.H. Chen, P.E. Siska & Y.T. Lee, J.Chem.Phys. 59 (1973) 601.

83. J.M. Parson, T.P. Schafer, F.P. Tully, P.E. Siska, Y.C. Wong & Y.T. Lee, J.Chem.Phys. 53 (1970) 2123.

84. Idem, ibid, 53 (1970) 3755.

85. U. Buck, M.G. Dondi, U. Valbusa, M.L. Klein & G. Scholes, Phys.Rev. A8 (1973) 2409.

86. e.g. J. Corner, Trans. Faraday Soc. 35 (1939) 711; 44 (1948) 914.

87. Ref. 21, Chapter 1, p.41.

88. E.A. Guggenheim & M.L. McGlashan, Proc.Roy.Soc. A255, (1960) 456.

89. F.J. Smith, E.A. Mason & R.J. Munn, J.Chem.Phys. 42 (1965) 1334.

90. S.D. Hamann & J.A. Lambert, Austral.J.Chem. 7 (1954) 1.

91. J.H. Dymond, M. Rigby & E.B. Smith, Phys.Fluids. 9 (1966) 1222.

92. R.A. Buckingham & J. Corner, Proc.Roy.Soc. A189 (1947) 118.

93. T. Kihara, Rev.Mod.Phys. 25 (1953) 831.

94. A.N. Dufty, G.P. Matthews & E.B. Smith, Chem.Phys. Lett. 26 (1974) 108.

95. J.A. Barker & A. Pompe, Austral. J. Chem. 21 (1968) 1683.

96. G.C. Maitland & E.B. Smith, Chem.Phys.Lett. 22 (1973) 443.

CHAPTER TWO

1. J.H. Ferziger & H.G. Kaper, "The Mathematical Theory of Transport Processes in Gases", Chapter 13 (1972) North-Holland, Amsterdam.
2. Ref. 1, Chapter 3, p.27.
3. S. Chapman, Phil. Trans. 211A (1912) 433.
4. D. Enskog, Physik, Zeit., 12 (1911) 56, 533.
5. G.C. Maitland, M. Rigby, E.B. Smith & W.A. Wakeham, "Intermolecular Forces - Their Origin and Determination" Chapter 5, p.288-296, (1981) OUP Oxford.
6. F. Wigner, Phys.Rev. 40 (1932) 749.
7. R.F. Snider, J.Chem.Phys. 32 (1960) 1051.
8. L.Z. Walderman, Naturforsch, 13a (1958) 609.
9. F.R. McCourt & R.F. Snider, J.Chem.Phys. 41 (1964) 3185; 43 (1965) 2276.
10. R.F. Snider, Physica, 78 (1974) 387.
11. H. Moraal & R.F. Snider, Chem.Phys.Lett. 9 (1971) 401.
12. N. Taxman, Phys.Rev. 110 (1958) 1235.
13. C.S. Wang Chang, G.E. Uhlenbeck & J. de Boer, "Studies in Statistical Mechanics" Vol. 2., Part C (1964), (ed. J. de Boer & G.E. Uhlenbeck), North-Holland, Amsterdam.
14. S.I. Sandler & J.S. Dahler, J.Chem.Phys. 44 (1966) 1229.
15. E.A. Mason & L. Monchick, J.Chem.Phys. 36 (1962) 1662.
16. Ref. 5, Chapter 4.
17. M.S. Child, "Molecular Collision Theory", Academic Press, London and New York.

18. S. Iman-Rahajoe, C.F. Curtiss & R.B. Bernstein, J. Chem.Phys. 42 (1965) 530.

19. R.J. Munn, F.J. Smith, E.A. Mason & L. Monchick, J.Chem.Phys. 42 (1965) 537.

CHAPTER THREE

1. J.A. Bearden, Phys.Rev. 56 (1939) 1023.

2. G.C. Maitland & E.B. Smith, J.Chem.Eng.Data. 17 (1972) 150.

3. J. Kestin, H.E. Khalifa, S.T. Ro & W.A. Wakeham, Physica 88A (1978) 242 and references therein, Erratum Physica 97A (1979) 466.

4. F.A. Guevara, B.B. McInteer & W.E. Wageman, Phys. Fluids, 12 (1969) 2493.

5. J.R. Partington, "An Advanced Treatise on Physical Chemistry", Longmans, London (1949) 1 833.

6. R.D. Present, "Kinetic Theory of Gases", McGraw-Hill (1958).

7. D.E. Meyer, Pogg.Ann. 127 (1866) 253.

8. J.C. Maxwell, Collected Works, Vol. II, Cambridge University Press 1890.

9. M. Knudsen, Ann.Physik, 28 (1909) 75.

10. G.M. Freyer, Proc.Roy.Soc. A293 (1966) 329.

11. S. Albertoni, C. Cercignani & L. Gotusso, Phys. Fluids, 6 (1963) 993.

12. R.M. Barrer & D. Nicholson, Can.J.Chem. 43 (1965) 896.

13. R.A. Dawe, Rev.Sci.Instr. 44 (1973) 1231.

14. D.W. Gough, D.Phil. Thesis, Oxford University, 1974.

15. C.G. Maitland & E.B. Smith, J.Chem.Soc. Faraday I, 70 (1974) 1191.

16. J. Kestin, M. Sokolov & W.A. Wakeham, Appl.Sci.Res. 27 (1973) 241.

17. W.R. Dean, Phil. Mag., 4 (1927) 208, 5, 673.

18. C.M. White, Proc. Roy.Soc. 123A (1929) 645.

19. A.G. Clarke, Part II Thesis, Oxford University, 1966.

20. J. Larrain & C.F. Bonilla, Trans.Soc.Rheol. 14 (1970) 135.

21. J.P. McCullough & D.W. Scott, "Experimental Thermodynamics", Vol. 1, Butterworths, London, 1968, p. 116.

CHAPTER FOUR

1. D.W. Gough, G.C. Maitland & E.B. Smith, Molec. Phys. 24 (1972) 151.

2. G.C. Maitland, M. Rigby, E.B. Smith & W.A. Wakeham, "Intermolecular Forces - Their Origin and Determination", Chapter 5, Appendix 5.2, (1981) OUP, Oxford.

3. Ref. 2, Chapter 5, p.300.

4. J.O. Hirschfelder & M.A. Eliason, Ann.N.Y.Acad.Sci. 67 (1957) 451.

5. J.H. Dymond, J.Chem.Phys. 49 (1968) 3673.

6. J.O. Hirschfelder, C.F. Curtiss & R.B. Bird "Molecular Theory of Gases and Liquids", Wiley, New York (1964) p.528.

7. G.C. Miatland & E.B. Smith, Molec. Phys. 22 (1971) 861.

8. J.A. Barker, R.A. Fisher & R.O. Watts, Molec. Phys. 21 (1971) 657.

9. J.M. Parson, P.E. Siska & Y.T. Lee, J.Chem.Phys. 56 (1972) 1511.

10. Ref. 2, Chapter 3, p.109-111.

11. J.B. Keller & B. Zumino, J.Chem.Phys. 30 (1959) 1351.

12. H.L. Frisch & E. Helfand, J.Chem.Phys. 32 (1960) 269.

13. D.A. Jonah & J.S. Rowlinson, Trans. Faraday Soc. 62 (1966) 1067.

14. G.C. Maitland & E.B. Smith, Molec.Phys. 24 (1972) 1185.

15. J.D. Dymond & E.B. Smith, "The Virial Coefficients of Pure Gases and Mixtures", 1980, OUP Oxford.

16. H.E. Cox, F.W. Crawford, E.B. Smith & A.R. Tindell, Molec. Phys. 40 (1980) 705.

17. E.B. Smith, A.R. Tindell, B.H. Wells & F.W. Crawford, Molec. Phys. 42 (1981) 937.

18. F.W. Crawford, E.J.R. Harris & E.B. Smith, Molec. Phys. 37 (1979) 1323.

19. E.B. Smith, A.R. Tindell, B.H. Wells & D.J. Tildesley, Molec. Phys. 40 (1980) 997.

20. A. Bousheri, L.A. Viehland & E.A. Mason, Physica 91A (1978) 424.

21. G.C. Maitland & W.A. Wakeham, Molec. Phys. 35 (1978) 1429.

22. Ref. 2, Chapter 2, p. 114-115.

23. E.B. Smith, A.R. Tindell, B.H. Wells & J.L. Brun, Physica 106C (1981) 117.

24. J.M. Hanley & M. Klein, J.Chem.Phys. 50 (1969) 4765; J.Phys.Chem. 76 (1972) 1743.

25. P. Clancy & E.B. Smith, Physica 83C (1976) 231.

26. S. Chapman, Phil. Trans.Roy.Soc. (London), A211 (1912) 433; A216 (1916) 279; A217 (1918) 115.

27. D. Enskog, Physik, Z. 12 (1911) 56, 533.

28. S.C. Saxena & E.A. Mason, J. Chem.Phys. 28 (1958) 623.

29. E.R.S. Winter, Trans. Faraday Soc. 46 (1950) 81.

30. W.L. Taylor & S. Weissman, J.Chem.Phys. 59 (1973) 1190.

31. D.W. Gough, G.C. Maitland & E.B. Smith, Molec. Phys. 27 (1974) 867.

32. E.A. Mason & L. Monchick, Chem. Phys.Lett. 34 (1975) 427.

33. Y. Tanaka & K. Yoshino, J.Chem.Phys. 53 (1970) 2012.

34. D.E. Freeman, K. Yoshino & Y. Tanaka, J.Chem.Phys. 59 (1973) 5160.

35. R.A. Aziz & H.H. Chen, J.Chem.Phys. 67 (1977) 5719.

CHAPTER FIVE

1. I.A. Barr, G.P. Matthews, E.B. Smith & A.R. Tindell, J.Phys.Chem. (1981) in the press.

2. J.D. Dymond & E.B. Smith, "The Virial Coefficients of Pure Gases and Mixtures", 1980, OUP Oxford.

3. R.A. Dawe & E.B. Smith, J.Chem.Phys. 52 (1969) 693.

4. D.W. Gough, G.P. Matthews & E.B.Smith, J.Chem.Soc. Faraday Trans. I, 72 (1976) 645.

5. G.C. Maitland & E.B. Smith, J.Chem.Soc. Faraday Trans. I, 70 (1974) 1191.

6. I.A. Barr, Part II Thesis, Oxford University 1979.

7. E.J. Harris, Part II Thesis, Oxford University 1978.

8. S. Weissman & E.A. Mason, J.Chem.Phys. 37 (1962) 1289.

9. B.E.F. Fender & G.D. Halsey, J.Chem.Phys. 36 (1962) 1881.

10. G.P. Matthews, D.Phil. Thesis, Oxford University 1976.

11. J. Kestin, H.E. Khalifa & W.A. Wakeham, Physica 90A (1978) 215.

CHAPTER SIX

1. G.C. Maitland & E.B. Smith, Mol. Phys. 22 (1971) 861.

2. J.D. Dymond & E.B. Smith, "The Virial Coefficients of Pure Gases and Mixtures", OUP Oxford, 1980.

3. E.A. Mason & T.R. Marrero, Adv.At.Mol.Phys. 6 (1970) 156.

4. T.S. Storvick & E.A. Mason, J.Chem.Phys. 45 (1966) 3752.

5. J.M. Parson, T.P. Schafer, P.E. Siska, F.P. Tully, T.C. Wong & Y.T. Lee, J.Chem.Phys. 53 (1970) 3755.

6. M.V. Bobetic & J.A. Barker, J.Chem.Phys. 64 (1966) 2367.

7. J.A. Barker & A. Pompe, Austral.J.Chem.Phys. 21 (1968) 1683.

8. J.K. Lee, D. Henderson & J.A. Barker, Mol. Phys. 29 (1974) 429.

9. B. Schneider, J.Chem.Phys. 58 (1973) 4447.

10. G.C. Maitland & W.A. Wakeham, Mol.Phys. 35 (1978) 1443.

11. J.J.H. van den Biesen, F.A. Stokvis, E.H. van Veen & C.J.N. van den Meijdenberg, Physica 100A (1980) 375.

12. M. Klein & H.J.M. Hanley, J.Chem.Phys. 53 (1970) 4722.

13. D.C. Berthelot, R. Hebd.Seanc.Acad.Sci. (Paris) 126 (1898) 1703, 1857.

14. G.H. Hudson & J.C. McCoubrey, Trans. Faraday Soc. 56 (1960) 761.

15. P.L. Church & M.L. Parusnitz, Ind.Eng.Chem.Fundamental Quart. 6 (1967) 492.

16. B.E.F. Fender & G.D. Halsey, J.Chem.Phys. 36 (1962) 1881.

17. J.G. Kirkwood, Physik,Zeit. 33 (1932) 57.

18. A. Muller, Proc.Roy.Soc. 154A (1936) 624.

19. e.g. G.C. Maitland, M. Rigby, E.B. Smith & W.A. Wakeham, "Intermolecular Forces - Their Origin and Determination" 1981, OUP Oxford, p. 520.

20. J.A. Barker, R.O. Watts, J.K. Lee, T.P. Schafer, Y.T. Lee J.Chem.Phys. 61 (1974) 3081.

21. E.B. Smith, D.J. Tildesley, A.R. Tindell & S.L. Price, Chem.Phys. Lett. 74 (1980) 193.

22. G.P. Matthews, H. Schofield, E.B. Smith & A.R. Tindell, to be published.

23. G.P. Matthews, D.Phil. Thesis, Oxford University, 1976.

24. H. Schofield, Part II Thesis, Oxford University, 1981.

25. J. Hellemans, J. Kestin & S.T. Ro, J.Chem.Phys. 57 (1972) 4036.

26. R. DiPippo, J. Kestin & K. Oguchi, J.Chem.Phys. 46 (1967) 4758.

27. T.R. Marrero & E.A. Mason, J. Phys. & Chem. Ref. Data 1 (1972) 3.

28. Y.S. Kim, J.Chem.Phys. 68 (1978) 5001.

29. S. Lee & Y.S. Kim, J.Chem.Phys. 70 (1979) 4856.

30. F.P. Tully & Y.. Lee, J.Chem.Phys. 57 (1972) 866.

31. K.G. Anlauf, R.W. Bickes & R.B. Bernstein, J.Chem.Phys. 54 (1971) 3647.

CHAPTER SEVEN

1. G.C. Maitland, V. Vesovic & W.A. Wakeham, to be published.
2. G.A. Parker & R.T. Pack, J.Chem.Phys. 68 (1978) 1585.
3. H.E. Cox, F.W. Crawford, E.B. Smith & A.R. Tindell, Mol. Phys. 40 (1980) 705.
4. P.S.Y. Cheung & J.G. Powles, Mol. Phys. 32 (1976) 1383.
5. T.L. Hill, "Introduction to Statistical Mechanics", Addison-Wesley, Reading, Massachusetts (1960); Statistical Mechanics, McGraw-Hill, New York (1956).
6. A.H. Stroud, "Approximate Calculation of Multiple Integrals", Prentice-Hall, New Jersey (1971).
7. L. Monchick & E.A. Mason, J.Chem.Phys. 35 (1961) 1676.
8. S.L. Price, Chem.Phys.Lett. 79 (1981) 553.
9. G.C. Maitland & E.B. Smith, Mol. Phys. 22 (1971) 861.
10. E.B. Smith, D.J. Tildesley, A.R. Tindell & S.L. Price, Chem.Phys.Lett. 74 (1980) 193.